NTNU – Trondheim
Norwegian University of
Science and Technology

Slip Prediction Based on Manipulator Motion

Arne Ranvik

Master of Science in Engineering Cybernetics (2 year))
Submission date: June 2014
Supervisor: Anton Shiriaev, ITK

Norwegian University of Science and Technology
Department of Engineering Cybernetics

Norwegian University of Science and Technology

Master Thesis

Slip Prediction Based on Manipulator Motion

Author:
Arne Ranvik

Supervisor:
Prof. Anton Shiriaev

A thesis submitted in fulfilment of the requirements

for the degree of Master of Science

in the

Department of Engineering Cybernetics

June 2014

Norwegian University of Science and Technology

Abstract

Faculty of Information Technology, Mathematics and Electrical Engineering
Department of Engineering Cybernetics

Master of Science

Slip Prediction Based on Manipulator Motion

by Arne Ranvik

Predicting slip during robotic manipulation is of interest for a variety of applications. Especially applications where weak grasps are applied. In this thesis, a model for predicting slip for a two fingered grasping scenario is considered. Other than model parameters, the only measurements or sensor information assumed is of the manipulator joints. Soft objects that deform substantially under applied forces are especially interesting in terms of frictional behaviour. A soft ball was used as a test object and parameters for friction and deformation was experimentally determined. By grasping and moving the ball with an industrial manipulator, slip and object loss was induced in order to compare these observations against model predictions.

It was found that the models prediction of slip was reasonable when compared to the observations. However, the model could not be fully tested and validated because the simple geometry of the test object did not excite any frictional behaviour from the soft characteristics.

Acknowledgements

I would like to thank my supervisor, Professor Anton Shiriaev, for his support, encouragement and valuable input during this semester. I would also like to express my gratitude to Postdoctoral Fellow Leonid Paramonov for his useful critiques. Thanks are also in order for the assistance and guidance provided by Anton Pyrkin, Sergey Kolyubin and Stepan Pchelkin during my time at the robotics laboratory.

I would like to offer my special thanks to Senior Engineer Trond Auestad from the Department of Structural Engineering for helping me with force-displacement measurements.

Contents

List of Figures

List of Tables

Dedicated to my siblings, Carita and Joakim

Chapter 1

Introduction

Grasping using robotic manipulators is, in general, a wide area of research due to the possible combinations of different grippers, objects and research goals. This thesis will focus on two-fingered grasping of soft, deformable, objects. The goal is to formulate a model that may estimate and predict grasp behaviour during manipulator motions. More specifically, given joint motions of a manipulator, we seek to predict whether object slip will occur or not. Also, a measure of how "safe" the grasp is, is also sought after.

A grasping model may be used to optimize the grasping tightness while moving an object, or optimize the motion itself, depending on certain limitations or goals put forth by the user. For example, some soft objects like fruits and vegetables can not be gripped too hard during manipulation in pick and place tasks. And by having a sufficiently accurate model one may find a compromise between gentle handling and speed. This thesis will not address that of optimization, but rather only the modelling and testing of the proposed model in order to investigate its usefulness.

Estimated grasp maintenance will be based on computed contact forces between gripper fingers and the object, and whether they violate the frictional limitations at the contact patches. Using available robots and equipment (Section 1.4), some experimental motions are conducted in order to test the proposed model. During experimentation, the goal is to induce object slip and compare observations with simulations. Direct measurement of the contact forces was not possible due to the lack of sensors.

1.1 Background

Robotic grasping is an area of research that can be traced back to the late 1800s where restraining objects using fixtures and jigs were studied [Bicchi and Kumar, 2000]. However, the modern era of grasping began in the late '70s, early '80s, when research teams started to build multi-fingered robotic hands [Mason and Salisbury Jr, 1985]. One of the most simple designs of robotic grippers is the two-fingered parallel gripper where finger motion is symmetric. This one degree of freedom gripper is extensively used in both industry and research. This gripper design will be used when obtaining data and therefore also in much of the theoretical work in this thesis.

In grasping, there are multiple elements that affect the total behaviour during manipulation tasks. One important element being what type of object that is being handled. Especially soft and easily deformable objects present challenges for predicting behaviour. Before we discuss that of grasping with soft materials involved, an introduction to grasping in general is in order.

Grasps are usually described by forces and torques so that one may investigate force equilibria. The task of a gripper is usually to restrain the object against external influences, or induce some desired motion of the object. The grasps ability to reject disturbances can be determined based on its *closure properties* [Bicchi and Kumar, 2000, Howard and Kumar, 1996, Suárez et al., 2006]. Two types of grasp definitions have become popular:

- **Form-closure:** The positions of the fingers ensure object immobility. Only the normal components of the contact *wrenches*(Section 2.1.4) may interact with the object. Friction is in this case a moot subject because the contacts does not exert tangential restraint.
- **Force-closure:** A weaker condition than form-closure where the fingers may also exert frictional forces in order to restrict the object. In this case, additional conditions must be placed upon the contact forces due to the limitations of friction.

Grasps with many contacts may often be proved to be form-closed while grasps with fewer contacts may satisfy force-closure in stead. The two definitions may be

used in order to further characterize the grasp. Force-closure will be discussed in greater detail when mathematical background and models have been established.

When the resultant of forces and torques applied by the fingers and other externals (gravity etc.) are zero, the grasp is considered to be an *equilibrium grasp*. Furthermore, a grasp is considered as a *stable grasp* if any perturbation away from an equilibrium configuration, caused by some disturbance, disappears in time after the disturbance is removed. The prevalent definitions of grasp equilibrium and stability is based on a quasi-static assumption, i.e. that the parts of the grasping system moves at low velocities so that inertial effects may be neglected. Due to the dynamics of forces in high acceleration manipulator motions, stability in its strictest sense will not be addressed in this thesis. We will in stead rely on force-closure properties alone in order to state a quantitative measure of the quality of two-fingered grasps during manipulator motions.

The approximation that contact with an object may be described by point contacts leads to the topic of *contact modelling* where one determines which forces and torques are transferred between the fingers and the object. The most basic contact is the frictionless point contact, used in form-closure, where the contact only transmits a normal force. Frictional contacts may also transmit tangential forces. The most restricting contact is the so-called *soft contact* that, in addition to normal and tangential forces, may also exhibit a pure torsional moment about the contact normal which is due to the substantial area of contact. Soft contacts and the frictional behaviour will be discussed in detail later in this thesis. For more about soft contacts, see Barbagli et al. [2004], Ciocarlie et al. [2007], Li and Kao [2001].

The rigid-body assumption for bodies in contact leads to the *static-indeterminacy problem* [Bicchi, 1994], so that one can not predict the force distribution for the contacts. By introducing compliance at the contacts, the static indeterminacy problem may be removed. In this thesis, a *quasi-rigid-body* approach will be applied where contact area grows with applied normal force as well as a model for normal force due to one-dimensional object deformation.

There are several approaches to how one quantifies the quality of grasps, Suárez et al. [2006] provides an extensive review on the subject and mentions two groups of such quality measures:

1: Measures associated with the positions of the contacts.

2: Measures associated with the configuration of the hand, or manipulator.

The quality measure of grasps in this thesis comes directly from how "secure" the grasp is in terms of friction. Other considerations such as power consumption or optimal manipulator configuration is not considered. In more than two fingered grasping, the area of grasp quality becomes more involved due to the possible ways of placing the contacts and how to restrict the object.

The prevalent mathematical modelling of grasping relies on the assumption of point contacts and several textbooks provides the material and procedures involved [Murray et al., 1994, Siciliano and Khatib, 2008]. The idea is to consider two separate dynamics, the object and the manipulator dynamics, and tie them together with constraints. The constraints may be evaluated from two different perspectives, velocities and forces/torques. These relations exist at the points of contact and guarantees that the object and the gripper fingers are constrained together. During a manipulator motion, due to gravity and inertial forces, constraint forces must occur at the contacts and the mathematical model may be used in order to find them.

Slip detection and prevention usually relies heavily on force, acceleration and/or tactile sensors [Song et al., 2012]. Song et al. [2012] developed an efficient prediction method using the LuGre friction model [De Wit et al., 1995]. In the absence of such sensors, and for both off-line and on-line considerations, determining whether manipulator motions results in slip is also of interest. This thesis will address this issue for the case of two-fingered grasps of soft, deformable, objects.

1.2 Problem Statement

This thesis focuses on three main questions:

1. *How can one predict whether a given manipulator motion will result in object slip and possibly loss of the object entirely?*
2. *For two-fingered grasping scenarios with soft, deformable, objects, is there some quantitative measure of grasp maintenance?*

1.2.1 Limitations and Assumptions

The two-fingered gripping tool has fingers that may be assumed to be rigid, only the object itself is deformable. Also, the manipulator links are assumed to be rigid.

Objects under consideration may deform under applied force. However, object dynamics are assumed negligibly fast, i.e. compressed objects regain its initial shape instantaneously. Without this assumption, a bound must be placed upon gripper finger acceleration (and possibly higher derivatives). Otherwise, the gripper might lose contact with the object during finger repositioning.

1.3 Software

MATLAB®
Is used for all calculations, simulations and measurement processing. The software package is a powerful mathematical tool with high-level programming, numerical computation and visualization capabilities [The MathWorks, Inc., 2012].

RobotStudio
This is the software for supervision, control and programming of the industrial robots manufactured by ABB. The programming language, also made by ABB, is RAPID. All experiments were realized with this software. It should be noted that realizing predefined trajectories, complete with position, velocity and acceleration

profiles, are not supported by the built-in commands in RAPID. RAPID is however, together with the IRC5 controller, a powerful tool in creating accurate linear and point-to-point motions [ABB, 2014b].

LabVIEW

A product by National Instruments that provides the means of sampling and logging sensor measurements. LabVIEW is used in a range of different areas, especially when it comes to control systems and signal processing [National Instruments Corp., 2013]. In this thesis, LabVIEW was used for obtaining estimation data for model parameters, see Chapter 4. Other products by National Instruments were used in conjunction with LabVIEW, see Section 1.4.

1.4 Lab Equipment

ABB IRB 140 Robot

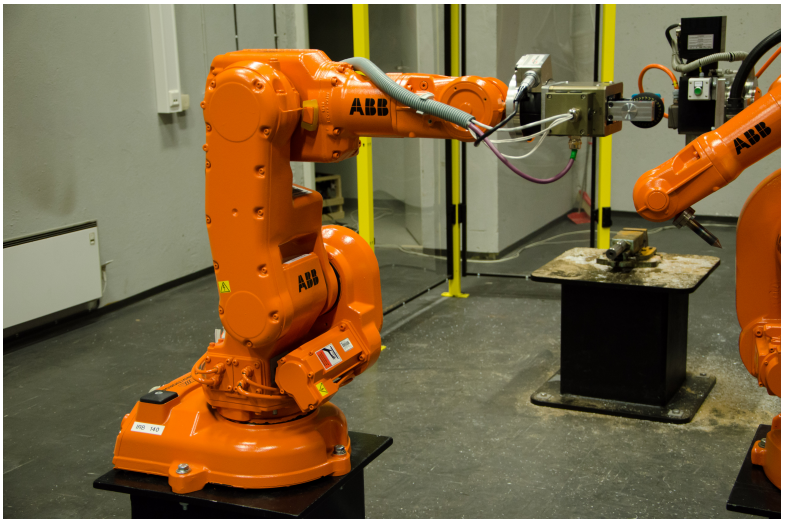

FIGURE 1.1: Picture of the ABB IRB 140, taken at the robotic laboratory of the Department of Engineering Cybernetics.

This fast and powerful industrial robot have six axes and can reach up to 810 [mm] (without end-effector) [ABB, 2014a].

Schunk PG 70 Gripper

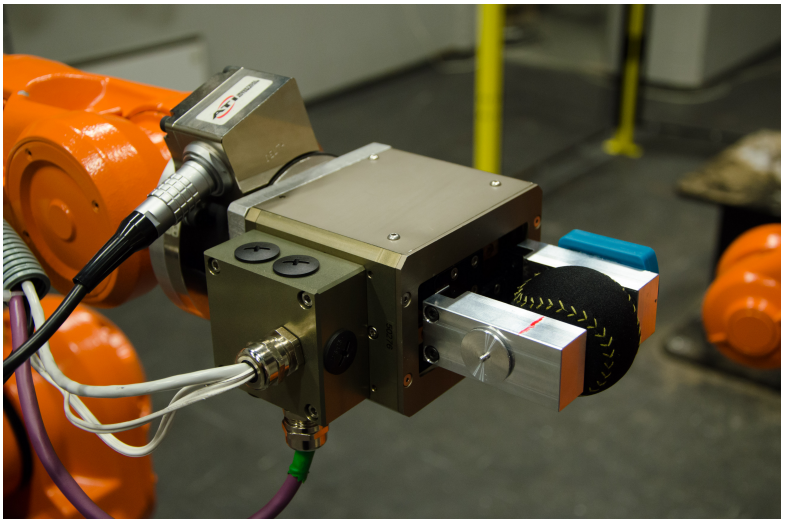

FIGURE 1.2: Picture of the Schunk gripper tool.

A parallel two-fingered gripper with symmetric motion of the two fingers [SCHUNK GmbH and Co. KG, 2014].

Futek LSB200 Miniature Load Cells

Two highly sensitive compression and tension sensors. One is calibrated to compression and can take loads up to 44 [N]. The other is calibrated for tension with a capacity of 22 [N] [FUTEK Advanced Sensor Technology, Inc., 2014]. The sensors were used in order to identify model parameters for test objects and frictional characteristics.

Data Acquisition with NI

A 4-channel NI 9237 Bridge analog input module, capable of sampling all channels at 50 000 times per second, mounted in a cDAQ-9171 compactDAQ chassis. This equipment is used to process the raw voltage readings from the force sensors.

1.5 Thesis Outline

Chapter 2 gives the reader necessary mathematical background that is applied in Chapter 3 where the grasping model is introduced. Chapter 3 also establishes frictional theory as well as how the mathematical grasping model is implemented in MATLAB®. The grasping model requires some parameters, these are experimentally found in Chapter 4. In Chapter 5 the results and observations from some experimental motions are presented. The experiments were set up in order to induce slip and object loss. Chapter 6 presents the simulated motions of the previous chapter and discusses and compares these simulations against the observations. The final conclusions can be found in Chapter 7.

Chapter 2

Mathematical Preliminaries

This chapter will give the reader a short and concise overview of the mathematical concepts used throughout the thesis.

2.1 Rigid Body Motion and Dynamics

As mentioned in Chapter 1, even though we are dealing with deformable bodies, we will assume that the bodies can, in general, be treated as rigid bodies. The deformation will be accounted for as variable body inertia, yet the dynamics of this deformation will not be considered. Other flexible body effects such as internal motion of the CoM will be assumed negligible due to the relatively small size, small mass and high stiffness of the test objects under consideration.

2.1.1 Rigid Bodies and Position

The position of a particle, $\vec{p}$, in Euclidean space can be given as a triple $(x, y, z) \in \mathbb{R}^3$ relative to an inertial Cartesian coordinate frame. The coordinates can be functions of time which gives rise to a continuous motion of the particle. A system of several particles are collectively termed as a *rigid body* if every particle pair $(\vec{p}, \vec{q})$ satisfies the constraint

$$\|\vec{p}(t) - \vec{q}(t)\| = \|\vec{p}(0) - \vec{q}(0)\| = constant$$

[Murray et al., 1994, p. 20] defines a *rigid motion* as: *"A rigid motion of an object is a continuous movement of the particles in the object such that the distance between any two particles remains fixed at all times.*

Another rigid body concept important to note is a rigid displacement. According to Chasles' Theorem [Chasles, 1830][Siciliano and Khatib, 2008, p. 14], which dates back to 1830, the most general rigid displacement can be characterized by a translation along a line, and a rotation about that line. The line is called the screw axis of the displacement, screws will be further discussed when twists and wrenches are introduced later in this chapter.

2.1.2 Orientation

The orientation of rigid bodies and coordinate frames, relative to both an inertial frame of reference and other non-inertial frames of references, can be described in several ways. In this thesis we have made use of rotation matrices and unit quaternions.

Rotation Matrices

A rotation of a Cartesian coordinate frame $\mathcal{O}_1 x_1 y_1 z_1$, projected onto another frame $\mathcal{O}_0 x_0 y_0 z_0$, can be represented by a 3×3 matrix called a rotation matrix. Our treatment of homogeneous transformations and rotation matrices is condensed from Chapter 2 in [Spong et al., 2006]. This thesis will follow the same notation as in Spong when we are referring to coordinate axes and their associated unit vectors. However, in all equations the unit vectors will be bold. In text, when we are referring to coordinate axes, but not specifically the unit vectors along those axes, we will not use boldface characters.

$$\mathbf{R}_1^0 = \begin{bmatrix} r_{11} & r_{12} & r_{13} \\ r_{21} & r_{22} & r_{23} \\ r_{31} & r_{32} & r_{33} \end{bmatrix} = \begin{bmatrix} \mathbf{x}_1 \cdot \mathbf{x}_0 & \mathbf{y}_1 \cdot \mathbf{x}_0 & \mathbf{z}_1 \cdot \mathbf{x}_0 \\ \mathbf{x}_1 \cdot \mathbf{y}_0 & \mathbf{y}_1 \cdot \mathbf{y}_0 & \mathbf{z}_1 \cdot \mathbf{y}_0 \\ \mathbf{x}_1 \cdot \mathbf{z}_0 & \mathbf{y}_1 \cdot \mathbf{z}_0 & \mathbf{z}_1 \cdot \mathbf{z}_0 \end{bmatrix} = \begin{bmatrix} \mathbf{x}_1^0 | \mathbf{y}_1^0 | \mathbf{z}_1^0 \end{bmatrix}$$

We say that $\mathbf{R}_1^0$ is the rotation *from* frame $\mathcal{O}_0 x_0 y_0 z_0$ *to* frame $\mathcal{O}_1 x_1 y_1 z_1$. The unit vectors $\mathbf{x}_1^0, \mathbf{y}_1^0, \mathbf{z}_1^0$, are the coordinates in frame 0 of the unit vectors $\mathbf{x}_1, \mathbf{y}_1, \mathbf{z}_1$.

The inverse rotation, i.e. the rotation from frame 1 to frame 0, is obtained by

$$\mathbf{R}_0^1 = \left(\mathbf{R}_1^0\right)^T$$

Since coordinate axes in Cartesian coordinate frames are mutually orthogonal, the transpose operation is identical to the inverse operation. Furthermore, rotation matrices belong to the *Special Orthogonal* group of order 3. To summarize, for any $\mathbf{R} \in SO(n)$ the following holds:

- $\mathbf{R}^T = \mathbf{R}^{-1} \in SO(n)$
- The columns (and therefore the rows) of $\mathbf{R}$ are mutually orthogonal
- Each column (and therefore each row) of $\mathbf{R}$ is a unit vector
- $\det \mathbf{R} = 1$

A composition of rotations can be obtained by matrix multiplication, where the order of multiplication varies according to which frame the rotation is performed with respect to.

$$\mathbf{R}_2^0 = \mathbf{R}_1^0\mathbf{R}, \quad \text{If } \mathbf{R} \text{ is performed relative to current frame}$$
$$\mathbf{R}_2^0 = \mathbf{R}\mathbf{R}_1^0, \quad \text{If } \mathbf{R} \text{ is performed relative to fixed (or initial) frame}$$

Rotation matrices are a good way to represent orientations of rigid bodies, relative to an inertial frame. However, there are a number of different ways to parametrize these rotations. *Euler angles* for example, parametrize a rotation using three quantities (as few as possible) where an arbitrary rotation is obtained by three consecutive rotations. This method, and other similar ones, suffer from singularities when the first and last rotation occur about the same axis, leaving some rotation angles as undefined [Siciliano and Khatib, 2008, p. 12]. Since we are dealing with body orientations that change with time and need to relate angular velocities to orientation parameters, we are motivated to find another way to represent and parametrize orientations.

Unit Quaternions

Unit quaternions provide an alternative way to represent orientation and does not suffer from singularities like the Euler angle representation does [Siciliano and Khatib, 2008, p. 13], they give a global parametrization of $SO(3)$. Quaternions are an interesting topic, they are in fact a generalization of complex numbers [Murray et al., 1994, p. 33]. However, we will only explore their significance regarding spatial rotations.

A quaternion can be represented as a vector quantity of the form

$$\boldsymbol{\epsilon} = \epsilon_0 + \epsilon_1 \mathbf{i} + \epsilon_2 \mathbf{j} + \epsilon_3 \mathbf{k}$$

where $\epsilon_0, \epsilon_1, \epsilon_2, \epsilon_3 \in \mathbb{R}$ are scalar quantities and $\mathbf{i}, \mathbf{j}, \mathbf{k}$ are the standard basis vectors that are mutually orthogonal. We will often refer to a quaternion as having one scalar quantity ϵ_0 and a vector quantity $\mathbf{v}_\epsilon = [\epsilon_1, \epsilon_2, \epsilon_3]^T$ so that

$$\boldsymbol{\epsilon} = \begin{bmatrix} \epsilon_0 \\ \mathbf{v}_\epsilon \end{bmatrix}$$

Two quaternions can be multiplied together, forming a combined rotation, as

$$\mathbf{a} \otimes \mathbf{b} = \begin{bmatrix} a_0 \\ \mathbf{v}_a \end{bmatrix} \otimes \begin{bmatrix} b_0 \\ \mathbf{v}_b \end{bmatrix} = \begin{bmatrix} a_0 b_0 - \mathbf{v}_a \cdot \mathbf{v}_b \\ a_0 \mathbf{v}_b + b_0 \mathbf{v}_a + \mathbf{v}_a \times \mathbf{v}_b \end{bmatrix} \tag{2.1}$$

where the $\otimes$-symbol denotes quaternion multiplication, [Cline, 2002]. Quaternions that satisfy $\|\boldsymbol{\epsilon}\|^2 = 1$ can be used to represent rotations. While using unit quaternions numerically, one must therefore apply normalization (divide by magnitude) to guarantee that the quaternion does indeed represent a valid rotation. Once a quaternion representation exist, one can get the corresponding rotation matrix representation by

$$\mathbf{R} = \begin{bmatrix} 1 - 2(\epsilon_2^2 + \epsilon_3^2) & 2(\epsilon_1\epsilon_2 - \epsilon_0\epsilon_3) & 2(\epsilon_1\epsilon_3 + \epsilon_0\epsilon_2) \\ 2(\epsilon_1\epsilon_2 + \epsilon_0\epsilon_3) & 1 - 2(\epsilon_1^2 + \epsilon_3^2) & 2(\epsilon_2\epsilon_3 - \epsilon_0\epsilon_1) \\ 2(\epsilon_1\epsilon_3 - \epsilon_0\epsilon_2) & 2(\epsilon_2\epsilon_3 + \epsilon_0\epsilon_1) & 1 - 2(\epsilon_1^2 + \epsilon_2^2) \end{bmatrix} \tag{2.2}$$

The operation of obtaining the quaternion from a rotation matrix is as follows

$$\begin{bmatrix} \epsilon_0 \\ \epsilon_1 \\ \epsilon_2 \\ \epsilon_3 \end{bmatrix} = \begin{bmatrix} \frac{1}{2}\sqrt{1 + r_{11} + r_{22} + r_{33}} \\ \frac{r_{32} - r_{23}}{4\epsilon_0} \\ \frac{r_{13} - r_{31}}{4\epsilon_0} \\ \frac{r_{21} - r_{12}}{4\epsilon_0} \end{bmatrix} \tag{2.3}$$

We are particularly interested in the relation between an angular velocity $\boldsymbol{\omega}$ and the quaternion derivative, which is described by

$$\dot{\boldsymbol{\epsilon}} = \frac{1}{2} \begin{bmatrix} 0 \\ \boldsymbol{\omega} \end{bmatrix} \otimes \boldsymbol{\epsilon} \tag{2.4}$$

[Cline, 2002, p. 12][Siciliano and Khatib, 2008, p. 13].

2.1.3 Homogeneous Transformations

To combine both translation and rotation into one representation for a general rigid body displacement, we use *homogeneous transformations*, [Spong et al., 2006, pp. 61-63]. Let us assume that a rigid body is rotated by $\mathbf{R}$ from its initial orientation and that it is translated by a distance $\mathbf{d}$ from its initial position, the total transformation can be now be represented by a 4×4 matrix as

$$\mathbf{H} = \begin{bmatrix} \mathbf{R} & \mathbf{d} \\ \mathbf{0} & 1 \end{bmatrix} \in SE(3), \quad \left(\mathbf{R} \in SO(3), \quad \mathbf{d} \in \mathbb{R}^3\right)$$

Like rotations, homogeneous transformations can be multiplied together to form compositions of rigid body transformations, they follow the same multiplicative rules as for rotations.

2.1.4 Twists and Wrenches

Due to Chasles', every rigid body motion can be obtained by a rotation about an axis while translating parallel to that axis. If one imagines the evolution of such a motion, any particle fixed to the body will trace out a helical path in space, i.e. a *screw motion* [Murray et al., 1994, pp. 45-50]. The axis of rotation and translation is called the *screw axis* and when we are talking about a continuous motion, the axis is called the *instantaneous screw axis*. One can characterize a screw motion by its axis, *pitch* and *magnitude*. However, this will not be strictly necessary for the scope of this thesis and readers are referred to Murray et al. [1994] for a more involved treatment of screws. Twists are related to screws in the sense that for every twist, one can also define the corresponding screw coordinates.

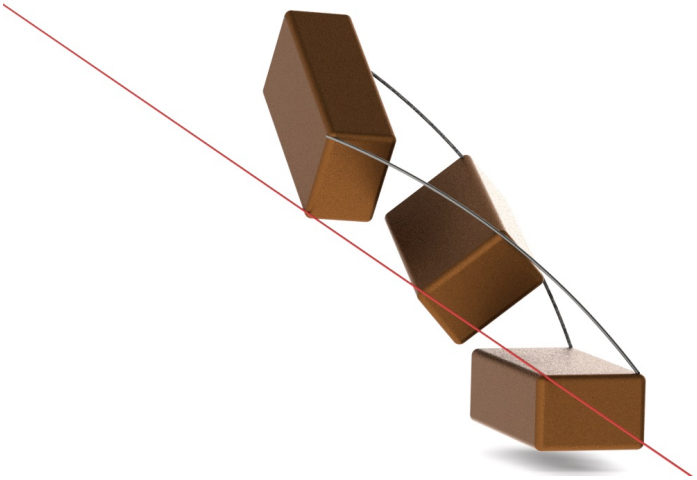

FIGURE 2.1: Illustration showing helical paths around the *ISA* of the object particles.

Twists

To properly define a twist we must first specify the frame in which the twist is expressed in. For now, let us express the twist in the $\mathcal{S}$-frame, which is a fixed frame in space with the origin $\mathcal{O}$. A body is moving in space, consider the velocity of a body-fixed point $\mathbf{p}^s$

$$\mathbf{v}_p^s = \mathbf{v}_O^s + \boldsymbol{\omega}^s \times \mathbf{p}^s = \mathbf{v}_O^s + [\boldsymbol{\omega}^s]\mathbf{p}^s \tag{2.5}$$

The point can be viewed as translating with a linear velocity and with an additional velocity due to the angular velocity of the body. One might wonder what $\mathbf{v}_O^s$

represents, which is somewhat unintuitive, $\mathbf{v}_O^s$ is the velocity of a body-fixed point currently at $\mathcal{O}$. The angular velocity vector, $\boldsymbol{\omega}^s$, passes through $\mathcal{O}$. See Figure 2.2 for an illustration of this scenario. To clarify, the velocity, $\mathbf{v}_O^s$, need not be parallel to $\boldsymbol{\omega}^s$ and twists should not be confused with screws.

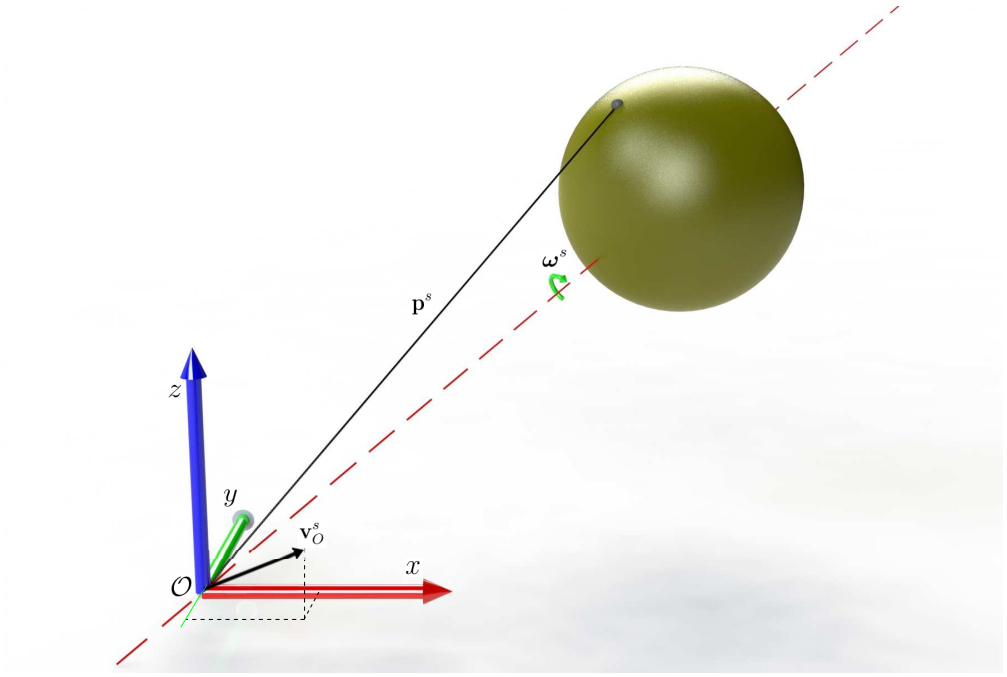

FIGURE 2.2: The velocity of a point attached to a rigid body, relative to a spatial frame.

The equation (2.5) is true for any point that is rigidly attached to the body, it can therefore be considered as a vector field, i.e. the velocity field of the body [Featherstone, 2008, p. 12]. In the rigid body dynamics literature, [Featherstone, 2008, Murray et al., 1994] and others, one usually refers to the fixed $\mathcal{S}$-frame as the *spatial frame*. The *spatial twist*, $\boldsymbol{\nu}^s$, can then be defined by the 6×1 vector

$$\boldsymbol{\nu}^s \triangleq \begin{bmatrix} \mathbf{v}_O^s \\ \boldsymbol{\omega}^s \end{bmatrix}$$

$\boldsymbol{\nu}^s$ is an example of a *spatial vector* and Featherstone [2008] provides an entire algebra that deals with such vectors.

Another important frame of reference is the body-frame, denote this frame as the $\mathcal{B}$-frame and note that its origin and axes are now fixed to the body and moving relative to the spatial frame. Again, consider the velocity of a point attached to the body, $\mathbf{p}^b$, but expressed in $\mathcal{B}$. Which means that $\mathbf{p}^b$ is the distance from the

$\mathcal{B}$-origin to the point.

$$\mathbf{v}_p^b = \mathbf{v}^b + [\boldsymbol{\omega}^b]\mathbf{p}^b \tag{2.6}$$

The interpretation of $\mathbf{v}^b$ is fairly straight forward, it is the velocity (relative to spatial frame) of the origin of the $\mathcal{B}$-frame, expressed in the $\mathcal{B}$-frame. The angular velocity vector, $\boldsymbol{\omega}^b$, passes now through the origin of the $\mathcal{B}$-frame, and all body-points that lie on this axis experience only the linear velocity component. The *body twist* can now be defined as

$$\boldsymbol{\nu}^b \triangleq \begin{bmatrix} \mathbf{v}^b \\ \boldsymbol{\omega}^b \end{bmatrix}$$

We have now discussed the two most popular frames of references. However, later on we will introduce one more body frame, one that is world aligned at all times and whose origin is body-fixed and coincident with the origin of the $\mathcal{B}$-frame. This convention is adopted from both Cline [2002] and [Siciliano and Khatib, 2008, Ch. 28], and simplifies the equations of motion for the body, as will be explained in section 2.1.5.

Wrenches

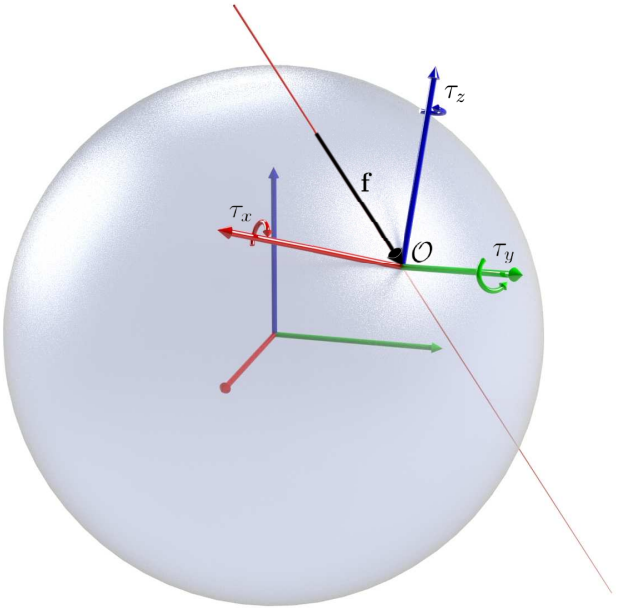

FIGURE 2.3: A wrench on a spherical object, applied at and about a point on the surface.

Like twists, wrenches are 6×1 spatial vectors and are composed of a linear force component, $\mathbf{f}$, and an angular torque component $\boldsymbol{\tau}$.

$$\mathbf{w} = \begin{bmatrix} \mathbf{f} \\ \boldsymbol{\tau} \end{bmatrix}$$

For wrenches it is important to note that the *point of application* is always at the origin of the frame in which the wrench is expressed in, and that the *line of application* passes through it. This is especially important when transforming wrenches from one coordinate frame to another, which will be explained shortly.

Adjoint Transformations

When transforming twists and wrenches between coordinate frames, one can not simply rotate the vectors, some transformation rules apply. Twists and wrenches also transform differently, first we will consider twist transformations.

Let us say that the homogeneous transformation from frame $\mathcal{A}$ to frame $\mathcal{B}$ is given by

$$\mathbf{H}_b^a = \begin{bmatrix} \mathbf{R}_b^a & \mathbf{d}_b^a \\ \mathbf{0} & 1 \end{bmatrix} \tag{2.7}$$

where $\mathbf{H}_b^a$ can also be time dependant. A twist, $\boldsymbol{\nu}^b$, expressed in frame $\mathcal{B}$ can then be expressed in frame $\mathcal{A}$ by using the *adjoint transformation* [Featherstone, 2008, pp. 20-23][Murray et al., 1994, p. 55], Ad_H, in the following manner

$$\boldsymbol{\nu}^a = \mathrm{Ad}_H \boldsymbol{\nu}^b = \begin{bmatrix} \mathbf{R}_b^a & [\mathbf{d}_b^a]\,\mathbf{R}_b^a \\ \mathbf{0} & \mathbf{R}_b^a \end{bmatrix} \boldsymbol{\nu}^b \tag{2.8}$$

The mapping, $\mathrm{Ad}_H : \mathbb{R}^6 \to \mathbb{R}^6$, will become important later in this thesis. Ad_H is invertible and can be used to obtain $\boldsymbol{\nu}^b$ given $\boldsymbol{\nu}^a$, the inverse is given by

$$\mathrm{Ad}_H^{-1} = \begin{bmatrix} (\mathbf{R}_b^a)^T & -(\mathbf{R}_b^a)^T\,[\mathbf{d}_b^a] \\ \mathbf{0} & (\mathbf{R}_b^a)^T \end{bmatrix} = \mathrm{Ad}_{H^{-1}} \tag{2.9}$$

For wrenches, if one considers the same homogeneous transformation, (2.7), one can obtain the *equivalent* wrench of $\mathbf{w}^a$ in frame $\mathcal{B}$ as

$$\mathbf{w}^b = \mathrm{Ad}_H^T \mathbf{w}^a = \begin{bmatrix} (\mathbf{R}_b^a)^T & \mathbf{0} \\ -(\mathbf{R}_b^a)^T [\mathbf{d}_b^a] & (\mathbf{R}_b^a)^T \end{bmatrix} \mathbf{w}^a \tag{2.10}$$

Conversely, $\mathbf{w}^a$ becomes

$$\mathbf{w}^a = \mathrm{Ad}_{H^{-1}}^T \mathbf{w}^b = \begin{bmatrix} \mathbf{R}_b^a & \mathbf{0} \\ [\mathbf{d}_b^a]\,\mathbf{R}_b^a & \mathbf{R}_b^a \end{bmatrix} \mathbf{w}^b \tag{2.11}$$

It is worth taking the time to really understand what this transformation does. The linear force vector, $\mathbf{f}^b$, is just rotated by $\mathbf{R}_b^a$ into frame $\mathcal{A}$. The torque vector on the other hand, now becomes

$$\boldsymbol{\tau}^a = [\mathbf{d}_b^a]\,\mathbf{R}_b^a \mathbf{f}^b + \mathbf{R}_b^a \boldsymbol{\tau}^b$$

The term, $[\mathbf{d}_b^a]\,\mathbf{R}_b^a \mathbf{f}^b$, compensates for the induced moment from moving the point and line of application for the wrench, making them *equivalent*. The wrench, $\boldsymbol{\tau}^a$, has the same effect as $\boldsymbol{\tau}^b$ on the body.

2.1.5 Newton-Euler Equations of Motion

One can write the Equations of Motion with respect to any convenient frame placed in space. However, to obtain EoM that are easy and intuitive to work with, we will introduce an intermediary body frame whose axes are aligned, at all times, with the world frame [Cline, 2002][Siciliano and Khatib, 2008, Ch. 28]. The origin of this world-aligned body frame is then fixed to the CoM, and we will keep track of its position with the position vector, $\mathbf{p}(t)$. The combined configuration of the body, i.e. its position and orientation, are stored in the 7×1 vector

$$\boldsymbol{\chi} = \begin{bmatrix} \mathbf{p} \\ \boldsymbol{\epsilon} \end{bmatrix} \tag{2.12}$$

From this vector, one can also obtain the homogeneous transformation between the $\mathcal{N}$-frame and the $\mathcal{B}$-frame by first using equation (2.2) to obtain the corresponding rotation matrix and then, together with the displacement $\mathbf{p}$, form the transformation.

From this point on we will refer to the inertial frame as the $\mathcal{N}$-frame, the world-aligned body frame as the $\mathcal{B}_{\mathcal{N}}$-frame and the body-fixed frame as the $\mathcal{B}$-frame. The twist, expressed in the $\mathcal{B}_{\mathcal{N}}$-frame, becomes

$$\boldsymbol{\nu} \triangleq \boldsymbol{\nu}^{bn} = \begin{bmatrix} \dot{\mathbf{p}} \\ \boldsymbol{\omega}^{bn} \end{bmatrix} \triangleq \begin{bmatrix} \mathbf{v} \\ \boldsymbol{\omega} \end{bmatrix} \tag{2.13}$$

The wrench, acting at and about the CoM, will be denoted by

$$\mathbf{w} \triangleq \mathbf{w}^{bn} \triangleq \begin{bmatrix} \mathbf{f} \\ \boldsymbol{\tau} \end{bmatrix} \tag{2.14}$$

For the motion of the CoM, we have by Newton's second law that the net force $\mathbf{f}$, acting on the CoM, is given by

$$\mathbf{f} = m_b \frac{d^2\mathbf{p}}{dt^2} = m_b \dot{\mathbf{v}} = m_b \mathbf{a} \tag{2.15}$$

where m_b is the entire mass of the body.

The net torque $\boldsymbol{\tau}$, acting on the body, is the rate of change of angular momentum, i.e.

$$\boldsymbol{\tau} = \frac{d}{dt}\left(\mathcal{I}\boldsymbol{\omega}\right) \tag{2.16}$$

where $\mathcal{I}$ is the *inertia tensor* [Spong et al., 2006, pp. 251-253], expressed in the $\mathcal{B}_{\mathcal{N}}$-frame. The inertia tensor can be found by the similarity transformation

$$\mathcal{I} = \mathbf{R}\mathbf{I}_b\mathbf{R}^T \tag{2.17}$$

where $\mathbf{I}_b$ is the body inertia, i.e. expressed in the $\mathcal{B}$-frame. $\mathbf{R}$ is the rotation matrix from the $\mathcal{B}_{\mathcal{N}}$-frame, and therefore also from the $\mathcal{N}$-frame, to the $\mathcal{B}$-frame.

Applying the product rule of differentiation, we have that

$$\begin{aligned} \boldsymbol{\tau} &= \frac{d}{dt}\left(\mathcal{I}\boldsymbol{\omega}\right) \\ &= \mathcal{I}\dot{\boldsymbol{\omega}} + \dot{\mathcal{I}}\boldsymbol{\omega} \\ &= \mathcal{I}\dot{\boldsymbol{\omega}} + \frac{d}{dt}\left(\mathbf{R}\mathbf{I}_b\mathbf{R}^T\right)\boldsymbol{\omega} \\ &= \mathcal{I}\dot{\boldsymbol{\omega}} + \left(\dot{\mathbf{R}}\mathbf{I}_b\mathbf{R}^T + \mathbf{R}\mathbf{I}_b\dot{\mathbf{R}}^T\right)\boldsymbol{\omega} \end{aligned}$$

From [Spong et al., 2006, p. 125], we know that $\dot{\mathbf{R}} = [\boldsymbol{\omega}]\mathbf{R}$, so

$$\begin{aligned}
\boldsymbol{\tau} &= \mathcal{I}\dot{\boldsymbol{\omega}} + \left([\boldsymbol{\omega}]\mathbf{R}\mathbf{I}_b\mathbf{R}^T + \mathbf{R}\mathbf{I}_b\left(-\mathbf{R}^T[\boldsymbol{\omega}]\right)\right)\boldsymbol{\omega} \\
&= \mathcal{I}\dot{\boldsymbol{\omega}} + [\boldsymbol{\omega}]\mathcal{I}\boldsymbol{\omega} - \mathcal{I}\left(\boldsymbol{\omega}\times\boldsymbol{\omega}\right) \\
&\left(\boldsymbol{\omega}\times\boldsymbol{\omega} = 0\right) \\
&\Downarrow \\
\boldsymbol{\tau} &= \mathcal{I}\dot{\boldsymbol{\omega}} + [\boldsymbol{\omega}]\mathcal{I}\boldsymbol{\omega}
\end{aligned}$$

These two Equations of Motion can now be expressed in terms of the twist and wrench (expressed in the $\mathcal{B}_\mathcal{N}$-frame, but **not** in the $\mathcal{N}$-frame) by setting up the matrix equivalent

$$\begin{bmatrix} m_b\mathbf{I} & \mathbf{0} \\ \mathbf{0} & \mathcal{I} \end{bmatrix}\begin{bmatrix} \dot{\mathbf{v}} \\ \dot{\boldsymbol{\omega}} \end{bmatrix} + \begin{bmatrix} \mathbf{0} & \mathbf{0} \\ \mathbf{0} & [\boldsymbol{\omega}]\mathcal{I} \end{bmatrix}\begin{bmatrix} \mathbf{v} \\ \boldsymbol{\omega} \end{bmatrix} = \begin{bmatrix} \mathbf{f} \\ \boldsymbol{\tau} \end{bmatrix}$$

$$\Downarrow$$

$$\mathbf{M}_b(\boldsymbol{\epsilon})\dot{\boldsymbol{\nu}} + \mathbf{C}_b(\boldsymbol{\epsilon},\boldsymbol{\omega})\boldsymbol{\nu} = \mathbf{w} \tag{2.18}$$

By using the relation (2.4), we can form the derivative $\dot{\boldsymbol{\chi}}$ as

$$\dot{\boldsymbol{\chi}} = \begin{bmatrix} \dot{\mathbf{p}} \\ \dot{\boldsymbol{\epsilon}} \end{bmatrix} = \begin{bmatrix} \mathbf{v} \\ \frac{1}{2}\begin{bmatrix} 0 \\ \boldsymbol{\omega} \end{bmatrix} \otimes \boldsymbol{\epsilon} \end{bmatrix} \tag{2.19}$$

2.2 Manipulator Kinematics

The kinematics of the robotic manipulator is an important part of this thesis because it allows us to construct the movement of the points of contact and the grasped object. This thesis uses an approach where velocities and accelerations are necessary in order to estimate contact forces, as will be explained in Chapter 3.

In Section 2.2.1 the forward kinematics of the ABB IRB 140 manipulator (Figure 2.4) will be derived, which may determine position and orientation of coordinate frames attached to it based on joint positions [Spong et al., 2006, Ch. 3]. Section 2.2.2 deals with the velocity kinematics and introduces a mapping between joint velocities and end-effector velocities.

2.2.1 Forward Kinematics

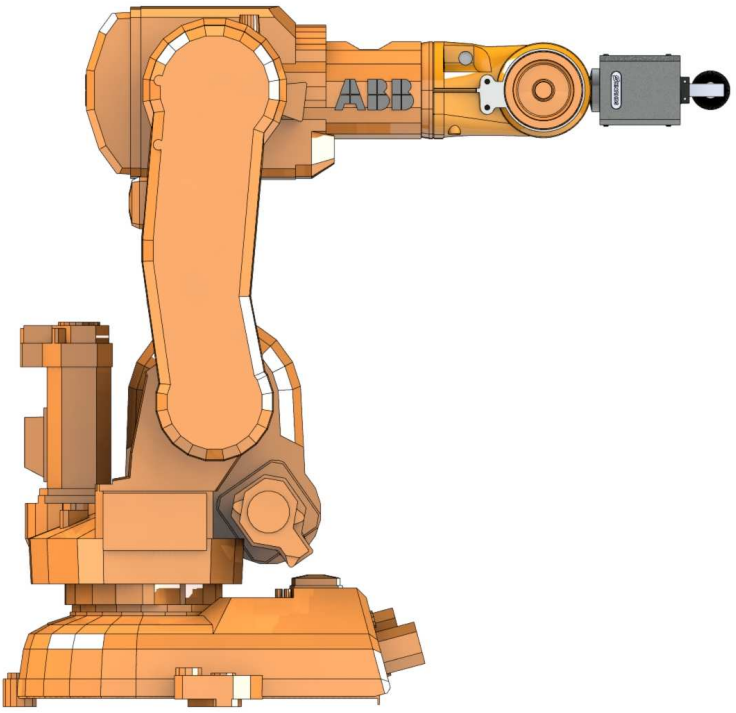

FIGURE 2.4: ABB IRB 140 Manipulator in its zero position.

Figure 2.4 shows the manipulator in its *zero position*, i.e. all joint positions are measured as zero. To establish the forward kinematics, we start by assigning coordinate frames to the links of the manipulator. The frame assignment follows the *Denavit-Hartenberg Convention* [Spong et al., 2006, Ch. 3], of which means that consecutive frames must satisfy two conditions

- The x_i axis must be perpendicular to the z_{i-1} axis.
- The x_i axis must intersect the z_{i-1} axis.

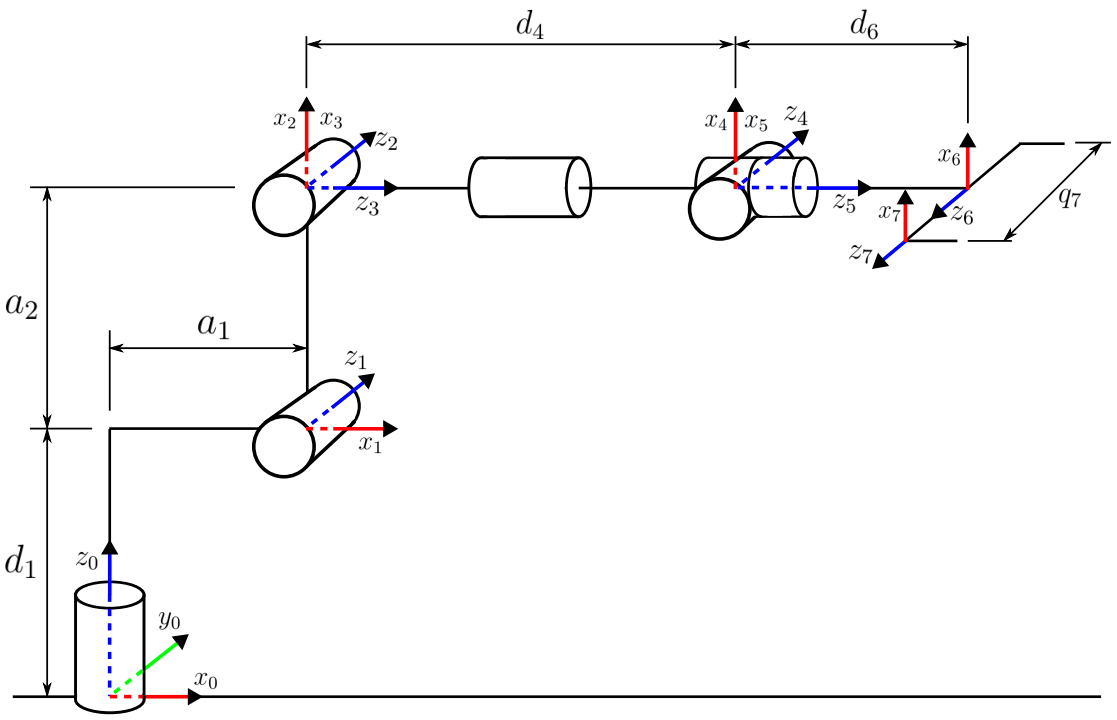

FIGURE 2.5: Frame assignment for IRB 140, including DoF for finger displacement.

In Figure 2.5, a simplified schematic of the manipulator with the assigned frames are shown. As the figure shows, a robotic gripper has been fitted as an end-effector where we have included the sliding freedom. With the DH convention, four parameters parametrize the homogeneous transformation between coordinate frames for each link, these are listed in Table 2.1. The four parameters for link i are named and described as

- **Link length** a_i: Distance along x_i from intersection of x_i and z_{i-1} to $\mathcal{O}_i$.
- **Link twist** α_i: Angle from z_{i-1} to z_i, measured about x_i.
- **Link offset** d_i: Distance along z_{i-1} from $\mathcal{O}_{i-1}$ to intersection of x_i and z_{i-1}. Variable if joint i prismatic.
- **Joint angle** θ_i: Angle from x_{i-1} to x_i, measured about z_{i-1}. Variable if joint i revolute.

Link	a_i	α_i	d_i	θ_i
1	a_1	$-\frac{\pi}{2}$	d_1	$\theta_1(t)$
2	a_2	0	0	$\theta_2(t) - \frac{\pi}{2}$
3	0	$-\frac{\pi}{2}$	0	$\theta_3(t)$
4	0	$\frac{\pi}{2}$	d_4	$\theta_4(t)$
5	0	$-\frac{\pi}{2}$	0	$\theta_5(t)$
6	0	$-\frac{\pi}{2}$	d_6	$\theta_6(t) + \theta_{off}$
7	0	0	$d_7 \triangleq \frac{1}{2}q_7(t)$	0

TABLE 2.1: DH-table for the IRB 140 manipulator with an attached gripper.

For the 6'th joint, an offset, θ_{off} was observed. In Chapter 3, Section 3.8, this table will be revisited and completed with numerical values.

Each row in Table 2.1 can be used to obtain the transformation matrix between the frames of each link. That is, frame i moves relative to frame $i-1$ due to link i and the transformation is given by

$$\mathbf{A}_i = \begin{bmatrix} c_{\theta_i} & -s_{\theta_i}c_{\alpha_i} & s_{\theta_i}s_{\alpha_i} & a_i c_{\theta_i} \\ s_{\theta_i} & c_{\theta_i}c_{\alpha_i} & -c_{\theta_i}s_{\alpha_i} & a_i s_{\theta_i} \\ 0 & s_{\alpha_i} & c_{\alpha_i} & d_i \\ 0 & 0 & 0 & 1 \end{bmatrix} \tag{2.20}$$

where $s_* \triangleq \sin(*)$ and $c_* \triangleq \cos(*)$ [Spong et al., 2006, p. 77]. The forward kinematics to any link frame can now be easily found by multiplying the $\mathbf{A}_i$ matrices consecutively together. For example, if one were to find the forward kinematics for the gripper frame 6, i.e. its position and orientation given all variables θ_{1-6}, it would be given by

$$\mathbf{T}_6^0 = \mathbf{A}_1\mathbf{A}_2\cdots\mathbf{A}_6$$

It is of course possible to attach frames to any part of the manipulator and find the forward kinematics, in Chapter 3 we will introduce contact frames that are attached to the gripper fingers, hence the necessity for including finger displacement freedom.

2.2.2 Manipulator Jacobian

The *manipulator Jacobian* relates linear and angular velocities, i.e. the twist, of the end-effector to the joint velocities [Spong et al., 2006, Ch. 4]. In Spong et al., *body velocity* is analogous to the twist of the rigid body attached to the end-effector frame. For an n-link manipulator, the Jacobian is a mapping such that

$$\boldsymbol{\nu}_n^0 = \mathcal{J}\dot{\mathbf{q}} \in \mathbb{R}^6 \tag{2.21}$$

where the Jacobian, $\mathcal{J} \in \mathbb{R}^{6\times n}$, can be expanded as

$$\begin{bmatrix} \mathbf{v}_n^0 \\ \boldsymbol{\omega}_n^0 \end{bmatrix} = \begin{bmatrix} \mathcal{J}_v \\ \mathcal{J}_\omega \end{bmatrix} \dot{\mathbf{q}}$$

Our approach to the Jacobian will differ slightly compared to [Spong et al., 2006] as we will develop the mapping for *any* frame attached to the end-effector body, as opposed to the end-effector frame *only*. The distance from the world origin to the origin of any end-effector frame will be denoted by $\mathbf{r}$, this origin point will be referred to as the *point of interest*. The reasoning behind this derivation will become apparent in Chapter 3 when the contact Jacobian is introduced.

Both linear and angular velocities of each link may be summed together to form the total velocity of the end-effector [Spong et al., 2006, pp. 130-131], therefore each 3×1 column in $\mathcal{J}_v$ and $\mathcal{J}_\omega$ is the relations to a single joint velocity. The determination of each $\mathcal{J}_{v_i}$ and $\mathcal{J}_{\omega_i}$, depends therefore on the type of link i. In the following derivation, we apply the *principle of superposition* at every joint and simultaneously keep all other joints stationary.

Prismatic Joints

For prismatic joints, the joint motion only contributes with a linear velocity so the angular Jacobian will be a zero column. The linear velocity will naturally be the prismatic joint velocity in the direction of actuation, i.e.

$$\mathbf{v}_r^0 = \mathbf{z}_{i-1}^0 \dot{q}_i$$
$$\Downarrow$$
$$\mathcal{J}_{v_i} = \mathbf{z}_{i-1} \tag{2.22a}$$
$$\mathcal{J}_{\omega_i} = \mathbf{0}_{3\times 1} \tag{2.22b}$$

Revolute Joints

With a revolute joint i, we have for the angular velocity that

$$\boldsymbol{\omega}_r^0 = \boldsymbol{\omega}_n^0 = \mathbf{z}_{i-1}^0 \dot{q}_i$$

The linear velocity due to joint i is dependant on the displacement between the frame attached to the point of interest and the frame $i-1$ as follows

$$\mathbf{v}_r^0 = \boldsymbol{\omega}_r^0 \times \mathbf{d} = \dot{q}_i \mathbf{z}_{i-1}^0 \times (\mathbf{r} - \mathcal{O}_{i-1})$$

Combining these two results for angular and linear velocity gives the Jacobian relations

$$\mathcal{J}_{v_i} = \mathbf{z}_{i-1} \times (\mathbf{r} - \mathcal{O}_{i-1}) \tag{2.23a}$$
$$\mathcal{J}_{\omega_i} = \mathbf{z}_{i-1} \tag{2.23b}$$

The Jacobian

Combining the results of (2.22) and (2.23), the final Jacobian for an n-link manipulator becomes

$$\mathcal{J} = [\mathcal{J}_1, \ldots, \mathcal{J}_n] \tag{2.24a}$$

$$\text{where} \quad \mathcal{J}_i = \begin{cases} \begin{bmatrix} \mathbf{z}_{i-1} \times (\mathbf{r} - \mathcal{O}_{i-1}) \\ \mathbf{z}_{i-1} \end{bmatrix} & \text{Joint } i \text{ revolute} \\ \begin{bmatrix} \mathbf{z}_{i-1} \\ \mathbf{0} \end{bmatrix} & \text{Joint } i \text{ prismatic} \end{cases} \tag{2.24b}$$

Comparing with [Spong et al., 2006, p. 133], the point of interest $\mathbf{r}$ is always the end-effector origin $\mathcal{O}_n$, in our case however the Jacobian will be used for other frames attached to the end-effector as well, see Section 3.4.

Chapter 3

Grasp and Friction Modelling

This Chapter will describe how the contact forces between the gripper fingers and the object are computed and also how slippage is predicted by use of a friction model.

The grasp of an object by use a robotic hand will be characterized by relations of the forces and torques involved. When the gripper fingers are in contact with an object, they actively restrict the motion of the object in space. The following sections will introduce the necessary quantities involved for defining this restricted motion and also a way of finding the constraint forces involved.

3.1 Definitions

The inertial frame of reference is conveniently placed at the base of the ABB IRB 140 manipulator and will also serve as the frame attached to the first link of the robot, making its z-axis the axis of revolution of the first joint. As in Section 2.1.5 of Chapter 2, the inertial frame will be referred to as the $\mathcal{N}$-frame. Joint displacements are contained in the vector $\mathbf{q} = [q_1, \ldots, q_7]^T$, where all but the last joint are revolute while the last represents finger displacement, i.e. a prismatic joint.

The position of the CoM of the object, or body, is denoted by $\mathbf{p} \in \mathbb{R}^3$. Again, as was discussed in Section 2.1.5, two frames are placed at $\mathbf{p}$, the body attached frame rotating with the body and a world aligned frame. These two will be referred to as the $\mathcal{B}$-frame and the $\mathcal{B}_\mathcal{N}$-frame, respectively. The orientation of $\mathcal{B}$, relative to

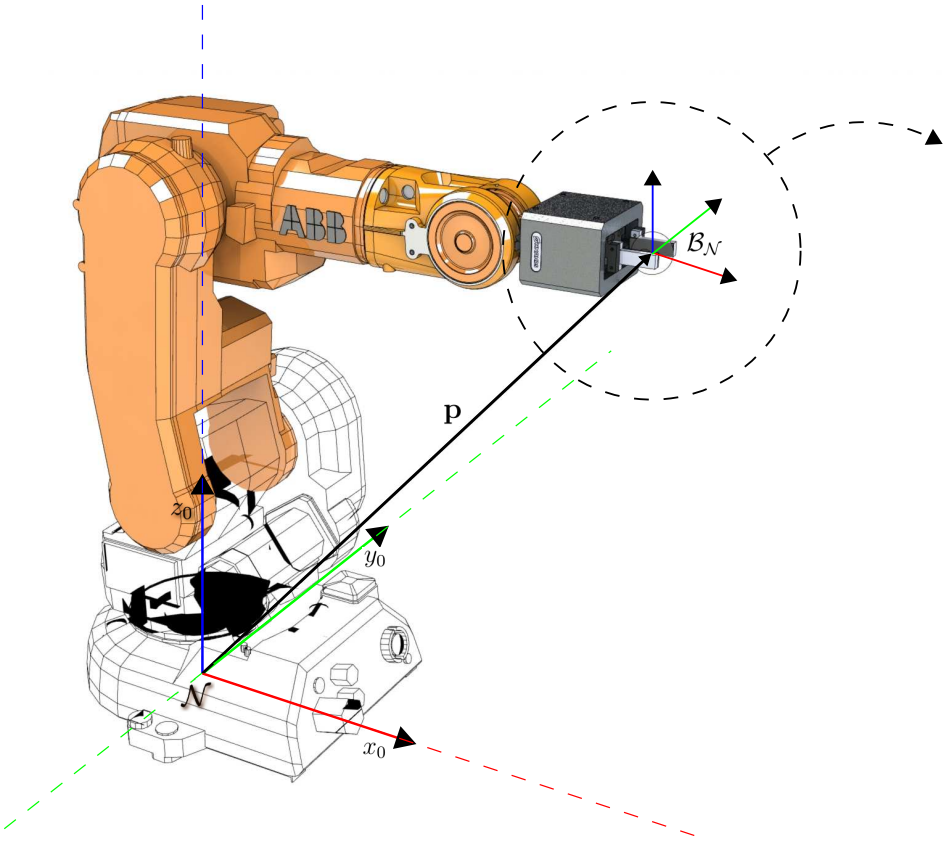

(A) Overview showing inertial frame and the position vector.

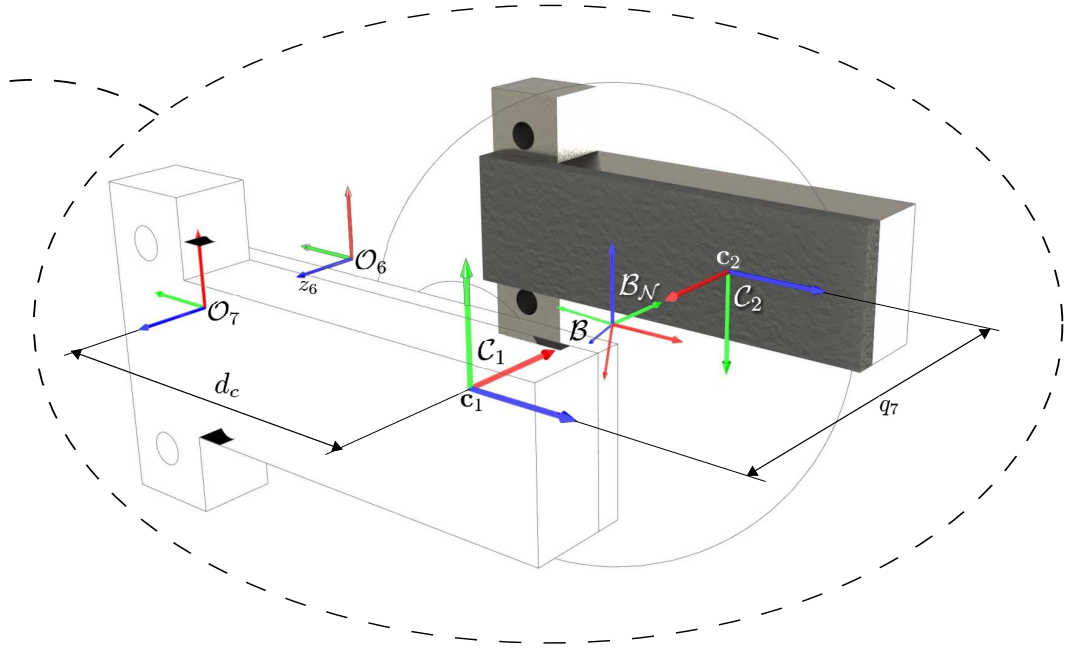

(B) Zoomed in view of the grasped object. Important coordinate frames are highlighted.

FIGURE 3.1: Some important vectors and frames used throughout the chapter.

$\mathcal{N}$ and $\mathcal{B}_{\mathcal{N}}$, are represented in quaternion form by the vector $\boldsymbol{\epsilon} = [\epsilon_0, \mathbf{v}_\epsilon{}^T]^T$. As equation (2.12), both position and orientation are combined into $\boldsymbol{\chi} = [\mathbf{p}^T, \boldsymbol{\epsilon}^T]^T$.

It will be assumed that the two fingers of the gripper will be in contact with the object making two points of contact where each will be regarded as a Center of Pressure (CoP) of a contact area. See Figure 3.1b for the placement of the two contact frames. The x-axis of a contact frame will always be normal to the finger surface and point towards the object, this is just a convention adopted from [Siciliano and Khatib, 2008, Ch. 28] and has no particular purpose other than being consistent. The z-axis will point in the *approach* direction of the gripper, as can be seen in Figure 3.1b. The contact frames are referred to as $\mathcal{C}_i$, where in our case $i = 1, 2$. The vector origins of the contact frames, relative to $\mathcal{N}$, will be denoted by $\mathbf{c}_i$.

3.2 Constrained Equations of Motion

An additional term can be added to the EoM (2.18) of Section 2.1.5 in order to include constraint forces due to interaction with the manipulator [Siciliano and Khatib, 2008, pp. 676-677].

$$\mathbf{M}_b(\boldsymbol{\epsilon})\dot{\boldsymbol{\nu}} + \mathbf{C}_b(\boldsymbol{\epsilon}, \boldsymbol{\omega})\boldsymbol{\nu} - \mathbf{G}\boldsymbol{\lambda} = \mathbf{w}_{app} \tag{3.1}$$

Where $\mathbf{w}_{app}$ is the applied wrench to the CoM, the only non-zero component being gravitational pull. $\boldsymbol{\lambda}$ is a vector of Lagrange multipliers and its physical interpretation will become apparent when the grasp matrix $\mathbf{G}$ is introduced in Section 3.3. Before we introduce the *constraint equation* that governs the motion of the object in space, an important concept must be discussed.

3.2.1 Transmitted Degrees of Freedom

When two separate objects are in contact, only some degrees of freedom (DoF) are transmitted depending on the type of contact. Consider, for example, the case where the contact area is so small that it can be considered as a point contact and that friction is negligible. In this case, the only transmitted DoF is the normal component of translational velocity and force, as seen in the respective contact

frame. This contact model, called the *point-contact-without-friction* [Siciliano and Khatib, 2008, p. 654], may not induce motion of an object in the tangential directions. From this it is easily understood that having point contacts without friction will require many contacts in order to be able to fully manipulate the object. In fact, [Siciliano and Khatib, 2008, p. 683] states that seven such contacts are necessary to fully constrain a three dimensional object.

The objects under consideration in this thesis are soft and deformable objects where contact introduces an area of contact. Friction will also play an important role and can not be ignored. Due to the relatively large area of contact, coupled with substantial friction between the surfaces, we will include *torsional friction* [Barbagli et al., 2004, Ciocarlie et al., 2007, Li and Kao, 2001, Xydas and Kao, 1999]. In relation to friction, this section will only concern itself with the transmitted DoFs. The grasping model will compute the necessary contact forces, whether the contact forces break frictional requirements will be handled separately, see Section 3.6 for more details on the friction models.

The gripper fingers of the experimental set-up are made of steel and can be regarded as rigid, or hard. However, the objects are soft and deformable and we will therefore apply the *soft finger* contact model [Siciliano and Khatib, 2008, Ch. 27-28]. We will however, refer to this model as the *soft contact* model, since the fingers are in fact rigid. A soft contact transmits all translational components of force and velocities, it also transmits an angular component about the contact normal. The contact model will be mathematically defined in the following subsection, in short, the idea is to select certain components of twists and/or wrenches that correspond to the transmitted DoFs.

3.2.2 Constraint Equation

To mathematically constrain the motion of the object, let us observe the fact that the points on the object, in contact with the gripper fingers, will be rigidly attached to the fingers during the motion. The origins of the contact frames, introduced in 3.1, represents the contact points both on the object and the fingers. At a velocity point of view, a contact point pair must have the same velocity at all times, which will ensure that their positions remain coincident. With this formulation one can consider the velocities of the contact frames from two perspectives, i.e. from the perspective of the manipulator and from the perspective of the object.

The general velocity, or twist, of the finger point at contact frame $\mathcal{C}_i$, due to the motion of the manipulator joints, are denoted by $\boldsymbol{\nu}_{i,arm}$. Similarly, the twist due to the motion of the object are denoted by $\boldsymbol{\nu}_{i,obj}$. Note that both of these are now expressed in their respective contact frame $\mathcal{C}_i$. A holonomic constraint that ensures that the object will remain rigidly attached to the gripper can *generally*, and without regard to the transmitted DoFs, be stated as

$$\begin{gathered}\boldsymbol{\nu}_{i,arm} = \boldsymbol{\nu}_{i,obj} \\ \Downarrow \\ \boldsymbol{\nu}_{i,arm} - \boldsymbol{\nu}_{i,obj} = \mathbf{0}, \quad i = 1, \ldots, n_c\end{gathered}$$

where n_c is the number of contacts between the object and the gripper fingers. In our case, $n_c = 2$. We must, however, include the contact model by selecting only the transmitted components of the twists. This can be realized with a selection matrix $\mathbf{S}_i$ [Siciliano and Khatib, 2008, p. 675]

$$\mathbf{S}_i(\boldsymbol{\nu}_{i,arm} - \boldsymbol{\nu}_{i,obj}) = \mathbf{0}, \quad i = 1, \ldots, n_c$$

where

$$\mathbf{S}_i = \begin{bmatrix} \mathbf{S}_{iF} & \mathbf{0} \\ \mathbf{0} & \mathbf{S}_{iM} \end{bmatrix} \overset{\text{Soft Contact}}{=} \begin{bmatrix} \mathbf{I}_{3\times 3} & \mathbf{0} \\ \mathbf{0} & [1\ 0\ 0] \end{bmatrix}$$

The sub-matrix, $\mathbf{S}_{iF}$, selects all translational components in a twist while $\mathbf{S}_{iM}$ only selects the angular component around the contact normal, i.e. given any twist, $\boldsymbol{\nu}$, we have that

$$\mathbf{S}_i\boldsymbol{\nu} = \begin{bmatrix} \mathbf{v} \\ \omega_x \end{bmatrix}$$

If one applies the selection matrix on a wrench $\mathbf{w}$, one obtains

$$\mathbf{S}_i\mathbf{w} = \begin{bmatrix} \mathbf{f} \\ \tau_x \end{bmatrix}$$

Hence, $\mathbf{S}_i$ reduces the dimensionality of twists and wrenches. A more convenient form is to gather all twists from all the contact frames into vectors so that

$$\begin{pmatrix} \mathbf{S}_1(\boldsymbol{\nu}_{1,arm} - \boldsymbol{\nu}_{1,obj}) \\ \vdots \\ \mathbf{S}_{n_c}(\boldsymbol{\nu}_{n_c,arm} - \boldsymbol{\nu}_{n_c,obj}) \end{pmatrix} = \mathbf{0}$$

$$\Downarrow$$

$$\mathbf{S}(\boldsymbol{\nu}_{c,arm} - \boldsymbol{\nu}_{c,obj}) = \mathbf{0} \tag{3.2}$$

where $\mathbf{S} = \text{Blkdiag}(\mathbf{S}_1, \ldots, \mathbf{S}_{n_c}) \in \mathbb{R}^{4n_c \times 6n_c}$ is a block diagonal matrix of selection matrices, assuming soft contact models for all contacts. Equation (3.2) represents the constraint equation that must be satisfied in order for the object to be rigidly attached to the gripper fingers. In fact, given the motion of the manipulator, one can describe the motion of the object by using this equation, this will become clear when the grasp matrix and contact Jacobian have been defined. The following sections will describe how $\boldsymbol{\nu}_{c,arm}$ and $\boldsymbol{\nu}_{c,obj}$ can be expressed in terms of joint motions and object motion, respectively.

3.3 The Grasp Map

Let us consider one of the object contact twists in $\boldsymbol{\nu}_{c,obj}$. Recall from Chapter 2, Section 2.1.4, that twists of a body can be transformed between any body-fixed frame with the use of adjoint transformations. The twist of the object, expressed in contact frame $\mathcal{C}_i$, can thus be related to the twist expressed in the $\mathcal{B}_\mathcal{N}$-frame, i.e. $\boldsymbol{\nu}$, by

$$\boldsymbol{\nu}_{i,obj} = \mathrm{Ad}_{T_{ci}}^{-1}\boldsymbol{\nu}$$

where

$$\mathbf{T}_{ci} \triangleq \mathbf{T}_{ci}^{bn} = \begin{bmatrix} \mathbf{R}_{ci}^{n} & (\mathbf{c}_i - \mathbf{p}) \\ \mathbf{0} & 1 \end{bmatrix} \tag{3.3}$$

is the homogeneous transformation from $\mathcal{B}_\mathcal{N}$ to $\mathcal{C}_i$. Note that since $\mathcal{B}_\mathcal{N}$ is aligned with $\mathcal{N}$, $\mathbf{R}_{ci}^{bn} = \mathbf{R}_{ci}^{n}$, we have that

$$\begin{aligned} \boldsymbol{\nu}_{i,obj} &= \begin{bmatrix} (\mathbf{R}_{ci}^{n})^T & -(\mathbf{R}_{ci}^{n})^T[\mathbf{c}_i - \mathbf{p}] \\ \mathbf{0} & (\mathbf{R}_{ci}^{n})^T \end{bmatrix} \boldsymbol{\nu} \\ &\triangleq \tilde{\mathbf{G}}_i^T \boldsymbol{\nu} \end{aligned}$$

where $\tilde{\mathbf{G}}_i^T$ is a *partial grasp matrix*, [Siciliano and Khatib, 2008, p. 673]. The *complete grasp matrix*, $\tilde{\mathbf{G}}^T$, is formed by combining all the partial grasp matrices into

$$\tilde{\mathbf{G}}^T = \begin{bmatrix} \tilde{\mathbf{G}}_1^T \\ \vdots \\ \tilde{\mathbf{G}}_{n_c}^T \end{bmatrix}$$

so that

$$\boldsymbol{\nu}_{c,obj} = \tilde{\mathbf{G}}^T \boldsymbol{\nu} \tag{3.4}$$

Inserting for $\boldsymbol{\nu}_{c,obj}$ from equation (3.4) into equation (3.2) yields

$$\mathbf{S}\boldsymbol{\nu}_{c,arm} - \mathbf{S}\tilde{\mathbf{G}}^T\boldsymbol{\nu} = \mathbf{0} \tag{3.5}$$

Finally, the *grasp matrix* is defined as

$$\mathbf{G}^T \triangleq \mathbf{S}\tilde{\mathbf{G}}^T \in \mathbb{R}^{4n_c \times 6} \tag{3.6}$$

The constraint term, $\mathbf{G}\boldsymbol{\lambda}$, represents the total wrench applied to and about the CoM of the grasped body, due to the interaction with the manipulator. The term

can be expanded into a sum of all the applied wrenches from all the contacts, for our case with two contacts this means that

$$\mathbf{G}\boldsymbol{\lambda} = \mathbf{G}_1\boldsymbol{\lambda}_1 + \mathbf{G}_2\boldsymbol{\lambda}_2$$

And by the definition of $\mathbf{G}_i$, which corresponds to a *selective* wrench transformation, the Lagrange multipliers may also be interpreted as wrenches, although with *reduced dimensionality*, i.e.

$$\boldsymbol{\lambda}_i = \mathbf{S}_i \begin{bmatrix} \mathbf{f}^{ci} \\ \boldsymbol{\tau}^{ci} \end{bmatrix} = \begin{bmatrix} f_x^{ci} \\ f_y^{ci} \\ f_z^{ci} \\ \tau_x^{ci} \end{bmatrix} \in \mathbb{R}^4$$

From this point on we will refer to the Lagrange multipliers as *local constraint wrenches*.

3.4 The Contact Jacobian

The combined twist vector, $\boldsymbol{\nu}_{c,arm}$, contains the translational and angular velocities of the origins of all $\mathcal{C}_i$, expressed in their respective contact frame. As we did for the grasp matrix, let us take one of the twists in $\boldsymbol{\nu}_{c,arm}$ as an example. Let us denote a twist, expressed in $\mathcal{N}$, as $\boldsymbol{\nu}^n_{i,arm}$. To find this velocity vector as a function of the joint velocities $\dot{\mathbf{q}}$, we can apply the Jacobian (2.24) from Section 2.2.2 with the *point of interest* as $\mathbf{c}_i$.

$$\boldsymbol{\nu}^n_{i,arm} = \mathcal{J}_i\dot{\mathbf{q}}$$

In the general case, where there might be joints that do not affect the contact and n_c contacts, readers are referred to [Siciliano and Khatib, 2008, p. 674] to find the appropriate $\mathcal{J}_i$ matrices. In our case however, all joints affect both contacts and the points of interest are $\mathbf{c}_1$ and $\mathbf{c}_2$.

Some special care must be applied at the last joint, the prismatic finger displacement, because of the symmetric motion of the fingers and because of our definition of q_7 as the total distance between the fingers. Recall that the gripper frame is placed exactly in the middle of the fingers, this makes the prismatic displacement from gripper frame to $\mathbf{c}_{1,2}$ as $\pm\frac{1}{2}q_7$. At the last joint we will define the linear

Jacobians as

$$\mathcal{J}_{1,v_7} = \frac{1}{2}\mathbf{z}_6$$
$$\mathcal{J}_{2,v_7} = -\frac{1}{2}\mathbf{z}_6$$

The linear Jacobian for contact frame two is negative because $\mathcal{C}_2$ is moving in the opposite direction of $\mathcal{C}_1$ (and the direction of z_6).

Now that $\boldsymbol{\nu}^n_{i,arm}$ has been obtained, one can express the vector in $\mathcal{C}_i$ in stead by rotating the two 3D vectors.

$$\begin{aligned}\boldsymbol{\nu}_{i,arm} \triangleq \boldsymbol{\nu}^{ci}_{i,arm} &= \begin{bmatrix}(\mathbf{R}^n_{ci})^T & \mathbf{0}\\ \mathbf{0} & (\mathbf{R}^n_{ci})^T\end{bmatrix}\boldsymbol{\nu}^n_{i,arm}\\ &= \begin{bmatrix}(\mathbf{R}^n_{ci})^T & \mathbf{0}\\ \mathbf{0} & (\mathbf{R}^n_{ci})^T\end{bmatrix}\mathcal{J}_i\dot{\mathbf{q}}\end{aligned}$$

And the *partial contact Jacobian* is defined as

$$\tilde{\mathbf{J}}_i \triangleq \begin{bmatrix}(\mathbf{R}^n_{ci})^T & \mathbf{0}\\ \mathbf{0} & (\mathbf{R}^n_{ci})^T\end{bmatrix}\mathcal{J}_i$$

Like we did for the grasp matrix, let us assemble all partial Jacobians into the *complete contact Jacobian*

$$\tilde{\mathbf{J}} \triangleq \begin{bmatrix}\tilde{\mathbf{J}}_1\\ \vdots\\ \tilde{\mathbf{J}}_{n_c}\end{bmatrix}$$

So that one can find $\boldsymbol{\nu}_{c,arm}$ by the equation

$$\boldsymbol{\nu}_{c,arm} = \tilde{\mathbf{J}}\dot{\mathbf{q}} \tag{3.7}$$

Inserting (3.7) and (3.4) into (3.2), yields

$$\mathbf{S}\tilde{\mathbf{J}}\dot{\mathbf{q}} - \mathbf{S}\tilde{\mathbf{G}}^T\boldsymbol{\nu} = \mathbf{0} \tag{3.8}$$

and by defining the *Contact Jacobian* as

$$\mathbf{J} \triangleq \mathbf{S}\tilde{\mathbf{J}} \tag{3.9}$$

we can rewrite the constraint equation (3.2) by using the definitions of contact Jacobian, (3.9), and grasp matrix, (3.6), so that

$$\mathbf{J}\dot{\mathbf{q}} - \mathbf{G}^T\boldsymbol{\nu} = \mathbf{0} \tag{3.10}$$

Equation (3.10) constitutes the final constraint equation that we will work with from this point on.

3.5 Finding the Local Constraint Wrenches

In order to predict whether a certain manipulator motion will induce a loss of an object, we must find a way to estimate the contact forces that occur at the contact points/patches. To begin with, we can consider the total contact wrench from interacting with the gripper fingers, $\mathbf{G}\boldsymbol{\lambda}$. This wrench is applied at the CoM of the body. Using equation (3.1), an expression for the total contact wrench can be found

$$\mathbf{G}\boldsymbol{\lambda} = \mathbf{M}_b(\boldsymbol{\epsilon})\dot{\boldsymbol{\nu}} + \mathbf{C}_b(\boldsymbol{\epsilon}, \boldsymbol{\omega})\boldsymbol{\nu} - \mathbf{w}_{app} \triangleq \mathbf{w} \tag{3.11}$$

Equation (3.11) requires the acceleration of the object, i.e. the twist derivative. The twist derivative can be obtained by differentiating the constraint equation (3.10)

$$\begin{aligned} &\frac{d}{dt}\left(\mathbf{J}\dot{\mathbf{q}} - \mathbf{G}^T\boldsymbol{\nu}\right) \\ &\quad = \mathbf{J}\ddot{\mathbf{q}} + \dot{\mathbf{J}}\dot{\mathbf{q}} - \mathbf{G}^T\dot{\boldsymbol{\nu}} - \dot{\mathbf{G}}^T\boldsymbol{\nu} = \mathbf{0} \\ &\quad \Downarrow \\ &\mathbf{G}^T\dot{\boldsymbol{\nu}} = \mathbf{J}\ddot{\mathbf{q}} + \dot{\mathbf{J}}\dot{\mathbf{q}} - \dot{\mathbf{G}}^T\boldsymbol{\nu} \end{aligned}$$

And by applying the generalized left inverse of $\mathbf{G}^T$, we have that

$$\dot{\boldsymbol{\nu}} = \mathbf{G}^{+L}\left(\mathbf{J}\ddot{\mathbf{q}} + \dot{\mathbf{J}}\dot{\mathbf{q}} - \dot{\mathbf{G}}^T\boldsymbol{\nu}\right) \tag{3.12}$$

where $\mathbf{G}^{+L} = \left(\mathbf{G}\mathbf{G}^T\right)^{-1}\mathbf{G}$ [Murray et al., 1994, p. 287]. This means that for a given motion of the manipulator joints, i.e. $\ddot{\mathbf{q}}$, $\dot{\mathbf{q}}$ and $\mathbf{q}$ known, equation (3.12) can be simulated by use of a numerical integration scheme. The implementation of this can be found in the attached files B and is discussed in Section 3.8.

By simulation of equation (3.12), the total contact wrench can be found by use of equation (3.11). However, we need to find the local constraint wrenches in $\boldsymbol{\lambda}$ in order to check them up against the friction models of Section 3.6. The solutions to the system of linear equations

$$\mathbf{G}\boldsymbol{\lambda} = \mathbf{w} \tag{3.13}$$

can not be trivially found by inverting $\mathbf{G}$ because it is not, generally speaking, a square matrix. Furthermore, utilizing the generalized right inverse of $\mathbf{G}$ to obtain the "best solution" in a *least squares sense* is also not applicable because there exist more constraints on the solutions of $\boldsymbol{\lambda}$. Specifically, the normal components of the local constraint wrenches $\boldsymbol{\lambda}_i$ may only exhibit non-negative values, i.e.

$$\lambda_{i,f_x} = f_x^{ci} \geq 0 \tag{3.14}$$

Physically, this means that contacts can not exhibit a sticking effect normal to the surface plane. In the tangential directions, *stiction* may occur [Wang et al., 2001].

Even for a grasping scenario with only two contacts, as in our case, there may exist an infinite solution set to equation (3.13). If we take our example, where it is assumed that the $x_{c_{1,2}}$-axes of their coordinate frames intersect each others origins, any positive value of a linear normal component may be counteracted by the other. And this will produce no net wrench, i.e. these solutions lie in the *null space* of $\mathbf{G}$.

Gauss's *principle of least forcing*, or *principle of least constraint* [Lanczos, 1970, pp. 107-110], must be taken into consideration to produce physically plausible solutions for $\boldsymbol{\lambda}$. The principle is equivalent to D'Alembert's principle, but is in stead a *minimum* formulation. Gauss defined the quantity to be minimized as

$$Z = \sum_{k=1}^{N} \frac{1}{2m_k} (\mathbf{F}_k - m_k \mathbf{a}_k)^2$$

where m_k, $\mathbf{F}_k$ and $\mathbf{a}_k$ is the mass, applied force and acceleration of the k'th particle of a system of N particles. Apart from the constant gravitational acceleration that all particles experience, the accelerations, $\mathbf{a}_k$, are dependant on the history of the applied forces $\mathbf{F}_k$. Therefore, this quantity is minimized by minimizing the forces of constraint, i.e. minimizing $\mathbf{F}_k$ for all k. For us, this translates into finding the minimal least squares solution for the forces and torques in $\boldsymbol{\lambda}$, subject to the

constraints (3.13) and (3.14). Torques are of course no exception to this principle because any torque can be described as a *pure force couple*.

3.5.1 Quadratic Optimization Problem

Minimizing the local constraint wrenches, subject to both equality constraints (3.13) and inequality constraints (3.14), can be formulated as a *quadratic programming problem*. The following quadratic program (QP) is proposed

$$\min_{\boldsymbol{\lambda}} \boldsymbol{\lambda}^T \boldsymbol{\lambda} \tag{3.15a}$$

$$\text{subject to : } \mathbf{G}\boldsymbol{\lambda} = \mathbf{w} \tag{3.15b}$$

$$\lambda_{i,f_x} \geq 0, \quad i = 1, \ldots, n_c \tag{3.15c}$$

The objective function, (3.15), is strictly convex since the *Hessian* [Wright and Nocedal, 1999] is positive definite, i.e.

$$\nabla^2(\boldsymbol{\lambda}^T \boldsymbol{\lambda}) = 2\mathbf{I} > 0$$

Furthermore, equality constraints are linear while the inequality constraints are concave (and convex), and the feasible set is therefore a convex hull. This type of QP is called a *convex* problem and any local solution will also be a global solution, for more about optimization, see [Wright and Nocedal, 1999]. Implementation is discussed in Section 3.8.

3.6 Soft Materials and Friction

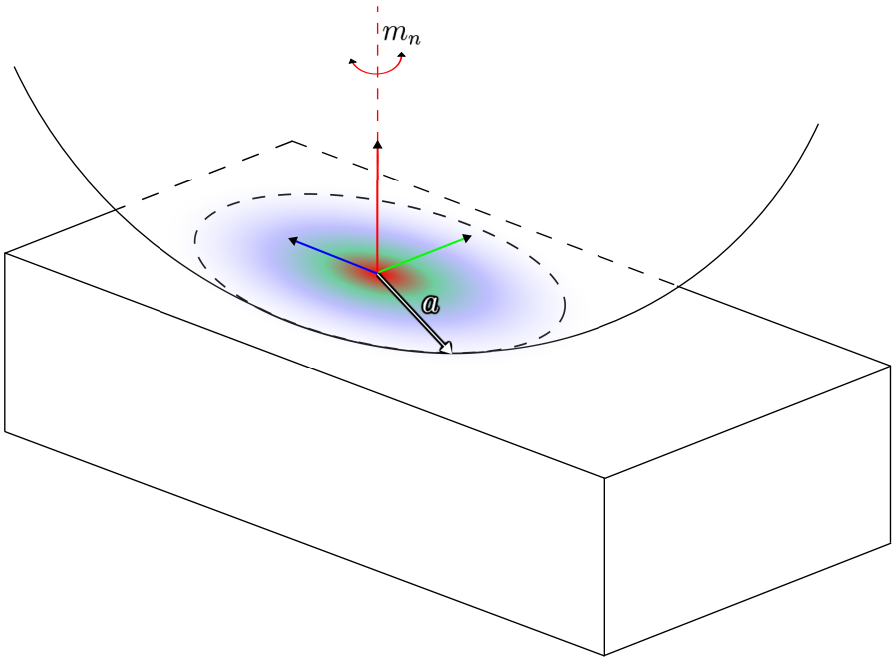

FIGURE 3.2: Soft round object pushed down on a hard surface, creating a circular contact patch.

In non-enveloping grasps, friction plays an important role in restraining an object. With soft and deformable objects, characterizing frictional contacts becomes challenging. As in many other areas of robotics, one ambition is to create human-like robotic hands that is able to function as highly as its human counterpart. And in the process of achieving this goal the grasping properties involving deformable materials with substantial frictional properties has been developed and is continuing to be developed [Barbagli et al., 2004, Bicchi and Kumar, 2000].

The treatment of friction in this thesis is strictly static, i.e. no relative movement between the contacting bodies. The goal is to develop a model for two-fingered grasping of soft objects where forces of constraint are estimated and checked against frictional limits. The models prediction of slip and loss of object will be compared to actual experiments where the occurrence of slip is recorded. The approach to friction chosen here is point-based, although with contact area considerations.

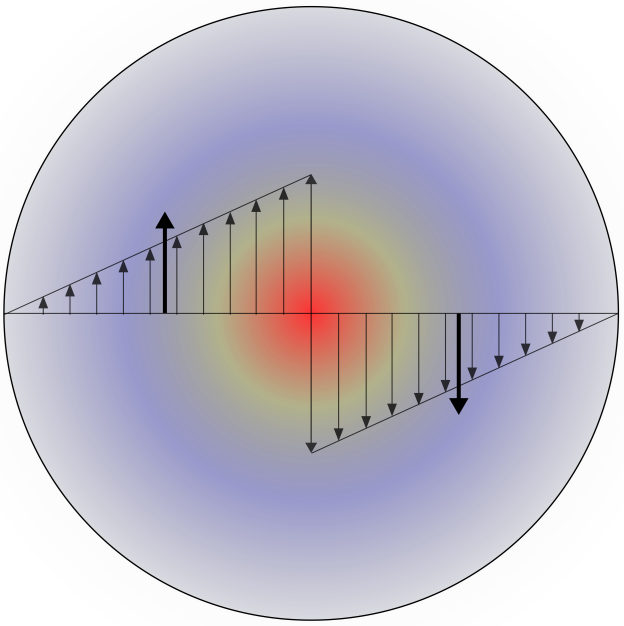

FIGURE 3.3: Torsional stiction.

For objects in contact where relatively large areas are in contact and where the surfaces show considerable friction, use of *only* the standard Coulomb model is rendered inappropriate. When the area of contact becomes large enough, a frictional moment will become substantial. This is basically due to the fact that an area introduces a mean moment arm. In Figure 3.3, a circular contact profile is shown with, for simplicity sake, a linear pressure distribution. For some mean moment arm from the CoP, a pure force couple can be applied without sliding occurring. For the force couple, one can apply Coulomb's friction model with an appropriate friction coefficient. However, the torsional friction coefficient is highly dependant on the radius of contact as well as the pressure distribution of the contact. This will be explored further in Section 3.6.2.

For the combined frictional limit, a model including a coupling between tangential and torsional friction will be used, see Section 3.6.1.

3.6.1 The Friction Ellipse

For object interactions where the contacts experience both shear and torsion, experiments have shown that the two are coupled [Howe et al., 1988]. It has been shown that an elliptical approximation to this coupling is sufficiently accurate for most applications [Xydas and Kao, 1999], this thesis will make use of the elliptical model. In the tangential directions, if one does not consider the frictional moment, Coulomb's model may be used without regard for the area of contact. The maximum tangential force, in all tangential directions, that may be applied before sliding occurs can therefore be modelled as

$$f_{t,max} = \mu N \tag{3.16}$$

while the maximum moment, when no tangential force is applied, is denoted by $m_{n,max}$. The elliptical model can thus be stated as

$$\left(\frac{f_t}{f_{t,max}}\right)^2 + \left(\frac{m_n}{m_{n,max}}\right)^2 = 1 \tag{3.17}$$

where

$$f_t = \|[f_{t,y}\ f_{t,z}]\| = \|[f_y^{ci}\ f_z^{ci}]\| = \sqrt{\left(f_y^{ci}\right)^2 + \left(f_z^{ci}\right)^2}$$
$$m_n = \tau_x^{ci}$$

are the tangential contact force and normal contact moment, respectively [Li and Kao, 2001, Xydas and Kao, 1999]. In Figure 3.4, the geometric interpretation of equation (3.17) is illustrated.

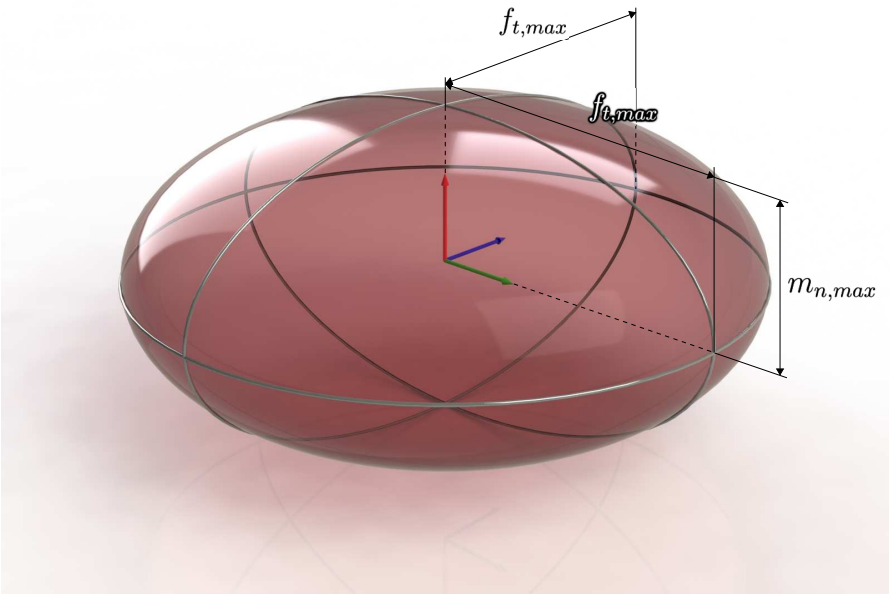

FIGURE 3.4: Ellipsoidal friction limit surface.

If, during simulation, a local constraint wrench fall outside this friction ellipsoid, the model predicts a slip event. In the next section, an expression for the maximum frictional moment will be discussed. The ellipsoid in Figure 3.4 is an example of a *friction limit surface*, comparable to the more known *friction cone* [Siciliano and Khatib, 2008, Ch. 27].

3.6.2 Contact Area and Torsional Friction

The maximum amount of frictional moment, $m_{n,max}$, is dependant on the size of the contact area. A lot of research has been done for circular contact profiles, [Howe and Cutkosky, 1996, Howe et al., 1988, Xydas and Kao, 1999] and others. The test objects under consideration are spheres and will produce circular contacts and we will therefore apply this to our modelling. [Xydas and Kao, 1999] built upon the work by [Hertz, 1882] and generalized his linear elastic model to also include non-linear elastic materials. The general model was coined as the *Power Law*

$$a = cN^{\gamma} \tag{3.18}$$

where

a : Radius of contact area

c : Proportionality constant

N : Applied normal force

$\gamma = \dfrac{n}{2n+1}$: Normal force exponent where n is the strain hardening factor

Estimates of the two parameters, c and γ, will be experimentally found in Section 4.

A general pressure distribution for circular contact area with radius a is given by

$$p(r) = C_k \frac{N}{\pi a^2} \left[1 - \left(\frac{r}{a}\right)^k\right]^{\frac{1}{k}} \tag{3.19}$$

where

k : Number, usually an integer, that determines shape of pressure profile

r : Radius, $0 \leq r \leq a$

C_k : Coefficient adjusted to satisfy equilibrium condition : $\int_A p(r)dA = N$

[Siciliano and Khatib, 2008, Ch. 27][Xydas and Kao, 1999]. Higher values of k leads to more uniform pressure distributions. A linear distribution corresponds to $k = 1$, also called a triangular distribution. Linear elastic materials have parabolic distributions ($k = 2$), while hyper elastic materials, as our test objects are assumed to be made of, have more uniform distributions with higher values of k [Xydas and Kao, 1999]. It can be shown that the maximum amount of frictional moment can be found as

$$m_{n,max} = \int_A \mu |r| p(r) dA = \int_A \mu |r| C_k \frac{N}{\pi a^2} \left[1 - \left(\frac{r}{a}\right)^k\right]^{\frac{1}{k}} dA \tag{3.20}$$

The pressure profile for our test objects remains unknown and its determination could not be realized with the lab equipment at hand. A quadruple distribution ($k = 4$) was therefore assumed due to the hyper elastic nature of the objects. Carrying out the definite integral in equation (3.20) over the entire contact region

yields

$$\begin{aligned}
&\int_A \mu|r|C_4\frac{N}{\pi a^2}\left[1-\left(\frac{r}{a}\right)^4\right]^{\frac{1}{4}} dA \\
&= \mu C_4\frac{N}{\pi a^2}\int_0^{2\pi}\int_0^a r^2\left[1-\left(\frac{r}{a}\right)^4\right]^{\frac{1}{4}} dr d\phi \\
&= \mu C_4\frac{N}{\pi a^2}\int_0^{2\pi}\frac{\pi a^3}{8\sqrt{2}}d\phi \\
&= \mu C_4 a\frac{N}{8\sqrt{2}}\cdot 2\pi \\
&= \mu C_4\pi a\frac{N}{4\sqrt{2}}
\end{aligned}$$

The equilibrium constant, with $k = 4$, becomes $C_4 = 1.1441$ [Xydas and Kao, 1999], so the maximum frictional moment may be evaluated by the following equation

$$m_{n,max} \approx 0.635\mu a N \tag{3.21}$$

Equation (3.21) and (3.16) may then be used to generate the friction ellipsoid.

The friction ellipsoids may be used to obtain a measure of how secure the grasp is, i.e. how far a contact wrench is from breaking its limitation.

$$Q_i(N) \triangleq \left(\frac{f_{i,t}}{f_{it,max}(N)}\right)^2 + \left(\frac{m_{i,n}}{m_{in,max}(N)}\right)^2, \quad i = 1,\ldots,n_c \tag{3.22}$$

The amount every Q_i is less than 1 indicate more secure grasps.

3.7 Force-Closure and Object Slip

Adopting the definition of force-closure from Bicchi and Kumar [2000], Howard and Kumar [1996] and others, we define the following:

Definition 3.1. Force-Closure
Consider a grasp of n_c contacts with the grasp matrix $\mathbf{G}$ and the combined constraint wrench $\boldsymbol{\lambda}$. Furthermore, normal force components in all local constraint wrenches, $\lambda_{i,n}$, are lower bounded by

$$\lambda_{i,n} \geq 0, \quad i = 1, \ldots, n_c \tag{3.23}$$

While all other components in $\boldsymbol{\lambda}$ are both upper and lower bounded by given frictional limitations. The grasp is defined as a force-closed grasp if and only if

$$\mathbf{G}\boldsymbol{\lambda} = \mathbf{w} \tag{3.24}$$

where $\mathbf{w}$ is any arbitrary wrench and $\boldsymbol{\lambda}$ satisfies the aforementioned constraints.

During the motion of the manipulator, solutions to $\boldsymbol{\lambda}$ are numerically calculated. A slip event will be recorded whenever force-closure can not be guaranteed with the frictional limitations put forth in Section 3.6. That is, computed contact wrenches must be within their respective frictional ellipsoids

$$\left(\frac{f_{i,t}}{f_{it,max}}\right)^2 + \left(\frac{m_{i,n}}{m_{in,max}}\right)^2 < 1, \quad i = 1, \ldots, n_c$$

3.8 MATLAB Implementation

MATLAB® is used in order to simulate and compare model against observations (Section 6). This section will explain how the model is implemented. The model needs to be supplied certain parameters in order to calculate contact forces, object forces and frictional ellipsoids. These are listed and described in the following table.

Parameter	Description	Units
`mu`	Static friction coefficient	Unitless
`Cpwr`	Proportional constant in Power Law model	$\left[\frac{\mathrm{m}}{\mathrm{N}}\right]$
`gamma`	Normal force exponent in Power Law model	Unitless
`mb`	Object mass	[kg]
`De`	Equilibrium diameter of object	[m]
`P`	Coefficients for object model	Vector of $\left[\frac{\mathrm{N}}{\mathrm{m^P}}\right]$

TABLE 3.1: Model parameters.

In addition to the model parameters, there are some simulation parameters like gravity, simulation step length etc. that must be set.

The user may specify whether the simulation is to rely on either user-defined functions or actual measurements for the joint variables (position, speed and acceleration) through the *bool* parameter `UseJfuns`. If measurements are to be used, the data must be interpolated in order to be used with the simulation and its user specified step length, `h`, see Section 3.8.1.

The simulation of the objects movement in space is realized, numerically, by an explicit *Runge-Kutta method* of order 4 [Egeland and Gravdahl, 2002, Sec. 14.4]. It is possible to use a different order by changing the *Butcher array* [Egeland and Gravdahl, 2002, p. 527] in the main script `RUN`. Due to numerical errors during simulation, the velocity constraint (3.10) will not be upheld by using Equation (3.12) as it is. This requires a stabilizing modification, see Section 3.8.3. Particulars regarding grasp quantities and their derivatives, as well as the forward kinematics, can be found in Section 3.8.2.

For each time step, the local contact wrenches for both contacts are computed, see Section 3.8.4. Based on finger displacement, the added normal force due to object compression is added on top of the normal components of both local contact wrenches and then checked against frictional ellipsoids. Object slip is detected in the subroutine `CheckFriction`. Finally, one can view an animation of the movement by running the `Animate` script after `RUN` has been executed, see Section 3.8.5.

3.8.1 Data Interpolation

There was technical difficulties in obtaining good and accurate measurements of joint speeds and accelerations, only joint positions could be measured. This limitation led the author to seek alternative methods of obtaining necessary "measurements" of speed and acceleration. Numerical differentiation of position data is highly noisy and would lead to unrealistic high peaks of accelerations and forces. As an alternative, fitting a *B-spline* to the position data makes it possible to obtain continuous approximations of the trajectories.

B-spline functions are representations of *piecewise polynomials* [Robertson, 2013]. There are several applications of B-splines, our usage is restricted to that of generating continuous approximations to sampled data. The MATLAB® function `spaps` returns the B-form of a cubic *smoothing spline* to the supplied data points. The tolerance input, `TOL`, determines how much the function should adhere to the data points. By relaxing the tolerance input to `spaps`, one can get a high degree of smoothness on the resulting function. `spaps` does this by penalizing the magnitude of the second derivative of the function. Of course, one should exercise restraint when setting this tolerance so that the result does not deviate too much from the measured data.

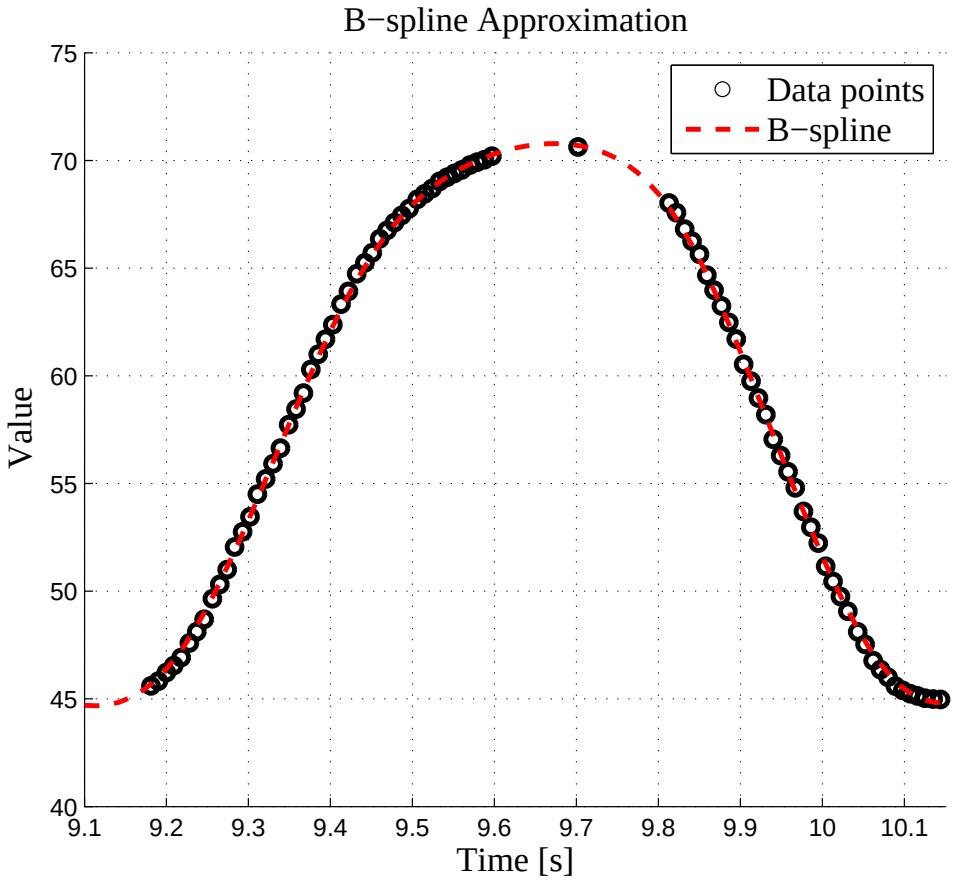

FIGURE 3.5: B-spline approximation to given data points.

Figure 3.5 illustrate how the B-spline approximation results in a continuous function given data points. For data with little noise, a low tolerance can be set. Therefore, the smaller the tolerance, the more confidence is given to the data points.

3.8.2 Forward Kinematics and Grasp Quantities

The forward kinematics requires the dimensions for the robot, specifically the distances between the axes, these are found in [ABB, 2014a]. Moreover, the gripper dimensions as well as the force/torque sensor dimensions affect the d_6 distance, which was measured to

$$d_6 = 65 \text{ [mm]} + 169.9 \text{ [mm]} = 234.9 \cdot 10^{-3} \text{ [m]}$$

It was observed that joint 6 measured an angle offset of $-26°$ away from its *defined* zero position, this is accounted for in Table 3.2. Inserting for all distances and measurements yields the final DH-table

Link	a_i	α_i	d_i	θ_i
1	$70 \cdot 10^{-3}$	$-\frac{\pi}{2}$	$352 \cdot 10^{-3}$	$q_1(t)$
2	$360 \cdot 10^{-3}$	0	0	$q_2(t) - \frac{\pi}{2}$
3	0	$-\frac{\pi}{2}$	0	$q_3(t)$
4	0	$\frac{\pi}{2}$	$380 \cdot 10^{-3}$	$q_4(t)$
5	0	$-\frac{\pi}{2}$	0	$q_5(t)$
6	0	$-\frac{\pi}{2}$	$234.9 \cdot 10^{-3}$	$q_6(t) + \frac{26° \pi}{180°}$
7	0	0	$\frac{1}{2} q_7(t)$	0

TABLE 3.2: DH-table for the IRB 140 manipulator with an attached gripper. Numerical values inserted.

This table can now be used to find forward kinematics to any frame attached to any part of the robot. The grasp quantities relies on the forward kinematics of the contact frames that are attached to the gripper fingers.

Grasp Quantities

Every partial grasp matrix is completely defined by the forward kinematics for the respective contact frame together with the position of the object. All the $\mathbf{A}_i$ matrices are given by the information in Table 3.2 along with the respective joint variable q_i. The forward kinematics for a contact frame i can then be found by

$$\begin{aligned}\mathbf{T}_{ci}^{n} &= \mathbf{A}_1\mathbf{A}_2\mathbf{A}_3\mathbf{A}_4\mathbf{A}_5\mathbf{A}_6\mathbf{A}_7\mathbf{H}_{ci}^{7} \\ &= \begin{bmatrix}\mathbf{R}_{ci}^{n} & \mathbf{c}_i \\ \mathbf{0} & 1\end{bmatrix}\end{aligned}$$

where $\mathbf{H}_{ci}^{7}$ is the transformation from gripper finger frame to contact frame i, i.e.

$$\mathbf{H}_{c1}^{7} = \begin{bmatrix}0 & 1 & 0 & 0 \\ 0 & 0 & -1 & -d_c \\ -1 & 0 & 0 & 0 \\ 0 & 0 & 0 & 1\end{bmatrix}$$

$$\mathbf{H}_{c2}^{7} = \begin{bmatrix}0 & -1 & 0 & 0 \\ 0 & 0 & -1 & -d_c \\ 1 & 0 & 0 & -q_7 \\ 0 & 0 & 0 & 1\end{bmatrix}$$

d_c is the position offset from $\mathcal{O}_7$ along $\mathbf{y}_7$, see Figure 3.1b. The transformation from $\mathcal{B}_{\mathcal{N}}$, in stead of $\mathcal{N}$, can now be found by Equation (3.3) and by using the remaining steps in Section 3.3, the grasp matrix may be formed.

Applying the rotation matrix $\mathbf{R}_{ci}^{n}$ in Section 3.4 and by following the procedures, the contact Jacobian may easily be found. The forward kinematics and both grasp quantities along with their derivatives were derived symbolically in the script `FK_IRB140`, which may be found in the attached files B.

3.8.3 Constraint Stabilization and Simulation

The constraint equation (3.10) is at a velocity/twist level, and by use of numerical integration of its derivative one can not guarantee that the original constraint is maintained. This manifests itself as an accumulating error for twist and consequently the configuration of the body itself and one will therefore observe drift. To counteract this one may apply a *constraint stabilization* technique. One popular and simple method is *Baumgarte stabilization* [Featherstone, 2008, pp. 145-148][Cline, 2002, p. 44]. The idea is to slightly modify the constraint equation under numerical integration so that it reacts and generate correctional terms. In fact, it behaves very much like a feedback loop. Consider the constraint (3.10)

$$\mathbf{J}\dot{\mathbf{q}} - \mathbf{G}^T\boldsymbol{\nu} \triangleq \mathbf{k} = \mathbf{0}$$

and let us now consider the constraint at acceleration level and add to it a term that reacts to error at twist level, i.e.

$$\dot{\mathbf{k}} + \alpha\mathbf{k} = \mathbf{0}, \quad \alpha > 0$$

Whenever the twist constraint isn't satisfied, the added stabilization term, $\alpha\mathbf{k}$, will correct the acceleration constraint. One can think of the scalar parameter as $\alpha = \frac{1}{T_{stab}}$ where T_{stab} is the time constant for desired decay of twist error. Choosing this time constant is not always that easy, choosing too large value results in bad stabilization while too small makes the differential equation unnecessary stiff. It depends on the frequency of which the system operates at, for example in our case, if a motion is fast with large variations in accelerations, a small time constant is needed. In any case, the stabilization will affect the acceleration and choosing a very small time constant will most likely lead to incorrect estimates of contact wrenches.

Variable Body Inertia

During compression of the object, the moment of inertia is varied as a function of finger displacement. Approximately, the ball has a spherical volume at equilibrium. It was observed that the ball did not maintain its volume when compressed. Therefore, we assume that the moment of inertia may be approximated to the moment of inertia of an ellipsoid where only one of the semi-principal axes change during compression. Furthermore, we assume that the material is homogeneous. Let us place the center of the ellipsoid at $\mathbf{p}$ and align it with the body $\mathcal{B}$-frame. The semi-axes a, b and c are now along the x, y and z-axes, respectively. Compression is defined to be along the y-axis, i.e. variable semi-axis b. The body moment of inertia tensor becomes

$$\mathbf{I}_b(q_7) = \begin{bmatrix} \frac{1}{5}m_b\left(\frac{1}{4}q_7^2 + x_e^2\right) & 0 & 0 \\ 0 & \frac{2}{5}m_b x_e^2 & 0 \\ 0 & 0 & \frac{1}{5}m_b\left(\frac{1}{4}q_7^2 + x_e^2\right) \end{bmatrix} \tag{3.25}$$

where $x_e = \frac{d_e}{2}$ is the equilibrium radius of the object.

Simulation

As mentioned, the object movement in space is simulated by use of the RK-4 numerical integration scheme which has the Butcher array

$\mathbf{c}$	$\mathbf{A}$
	$\mathbf{b}^T$

TABLE 3.3: Butcher array for numerical integration.

where

$$\mathbf{c} = \begin{bmatrix} 0 \\ \frac{1}{2} \\ \frac{1}{2} \\ 1 \end{bmatrix}, \quad \mathbf{A} = \begin{bmatrix} 0 & 0 & 0 & 0 \\ \frac{1}{2} & 0 & 0 & 0 \\ 0 & \frac{1}{2} & 0 & 0 \\ 0 & 0 & 1 & 0 \end{bmatrix}, \quad \mathbf{b} = \begin{bmatrix} \frac{1}{6} \\ \frac{2}{6} \\ \frac{2}{6} \\ \frac{1}{6} \end{bmatrix}$$

One may change this array if desired in the `RUN` script. The initial velocity, or twist, is assumed to be zero while the initial configuration of the object is supplied by the

user. Given initial conditions, the integration procedure can thus be summarized as

$$\dot{\mathbf{y}} \triangleq \mathbf{f}(\mathbf{y}, t)$$

is numerically integrated by

$$\mathbf{y}_{n+1} = \mathbf{y}_n + h\mathbf{K}\mathbf{b}$$

where

$$\begin{aligned}
&\mathbf{K} = [\mathbf{k}_1,\ \ldots,\ \mathbf{k}_4] \\
&\mathbf{k}_1 = \mathbf{f}(\mathbf{y}_n, t_n) \\
&\mathbf{k}_s = \mathbf{f}\left(\mathbf{y}_n + h(\mathbf{K}_{1:s-1}\mathbf{A}^T_{s,1:s-1}), t_n + hc_s\right), \quad s = 2, \ldots, 4
\end{aligned}$$

See the attached files B for actual implementation in MATLAB®. The entire derivative vector contains both $\dot{\boldsymbol{\chi}}$ and modified $\dot{\boldsymbol{\nu}}$ with constraint stabilization so that

$$\dot{\mathbf{y}} = \begin{bmatrix} \dot{\mathbf{p}} \\ \dot{\boldsymbol{\epsilon}} \\ \dot{\boldsymbol{\nu}} \end{bmatrix} = \begin{bmatrix} \mathbf{v} \\ \frac{1}{2}\begin{bmatrix} 0 \\ \boldsymbol{\omega} \end{bmatrix} \otimes \boldsymbol{\epsilon} \\ \mathbf{G}^{+L}\left(\mathbf{J}\ddot{\mathbf{q}} + \dot{\mathbf{J}}\dot{\mathbf{q}} - \dot{\mathbf{G}}^T\boldsymbol{\nu} + \alpha(\mathbf{J}\dot{\mathbf{q}} - \mathbf{G}^T\boldsymbol{\nu})\right) \end{bmatrix}$$

Note that the integration is for a time step *ahead*. At the *current* time step the rotation matrix for the body is obtained by use of the `Quat2Rot`($\boldsymbol{\epsilon}$) function, which corresponds to Equation (2.2), this is then used in conjunction with the current position $\mathbf{p}$ to form the complete transformation matrix for the object.

3.8.4 Computing Local Contact Wrenches

The quadratic program, (3.15), is solved by use of the built-in MATLAB® command `quadprog` where upper and lower bounds on the solutions of $\boldsymbol{\lambda}$ were set to

$$\text{Lower bounds} : lb = \begin{bmatrix} 0 \\ -\infty \\ -\infty \\ -\infty \\ 0 \\ -\infty \\ -\infty \\ -\infty \end{bmatrix}, \quad \text{Upper bounds} : ub = \begin{bmatrix} \infty \\ \infty \\ \infty \\ \infty \\ \infty \\ \infty \\ \infty \\ \infty \end{bmatrix}$$

Note that we do not wish to impose the frictional limitations here where it could render the QP as infeasible. In case the slip prediction is a false positive we wish that the simulation continues so that another instance of slip might be picked up later on. The actual test of whether or not friction is maintained is checked for separately.

Due to the simplicity of the QP as well as the known efficiency of *Active-set* methods for these types of problems [Wright and Nocedal, 1999, Ch. 16], the Active-set algorithm were specified as solver for `quadprog`. During simulation, (3.15) is solved for each time step and to further help the algorithm we store the solution and supply it as an initial guess of the solution for the next time step.

3.8.5 Visualization

In the visualization script one can choose the playing speed of the animation by changing the `capture` and `fps` parameters. Slowest possible capturing is the simulation step length, `h`, while "real-time" is $\frac{1}{\text{fps}}$. The renderer tries to play the animation with the assigned `fps` value. However, this is not guaranteed since the hardware may restrict rendering speed. As a consequence, "real-time" play speed is affected if renderer isn't actually playing at the assigned `fps`.

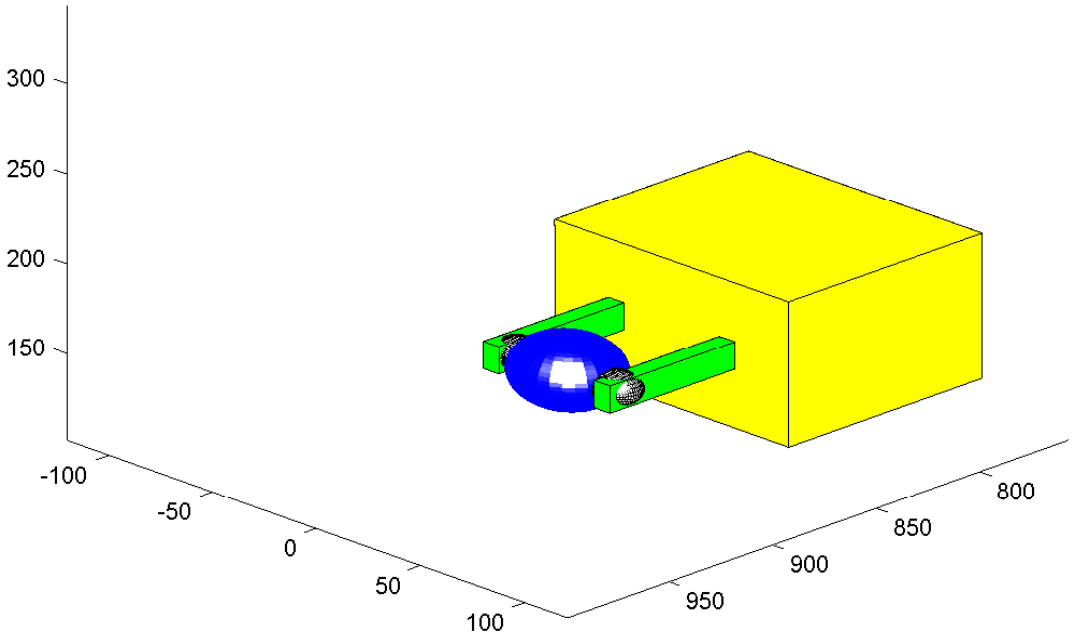

FIGURE 3.6: Snapshot during an animation of a simulated motion.

Figure 3.6 shows a snapshot during an animation. The small black ellipsoids represent frictional ellipsoids at the contacts, which are scaled by the normal forces at the contacts.

Chapter 4

Estimating Model Parameters

The model derived in Chapter 3 relies on some physical parameters regarding object mass, equilibrium size and frictional characteristics of finger-object interaction. This chapter describes the approach of finding estimates for these parameters using equipment available to the author. The parameters were found by a fairly limited amount of measurements. More measurements are necessary for stating them with statistical confidence. They should be regarded as rough estimates and treated as such. All MATLAB® scripts and raw data of all kinds, pertaining to this and other chapters, can be found in the attached files B.

4.1 Object Parameters

The following parameters are strictly related to the object.

4.1.1 Equilibrium Size

Equilibrium diameter is denoted by d_e. Diameter measured with a vernier caliper to

$$d_e \approx 52.7 \cdot 10^{-3} \text{ [m]}$$

4.1.2 Object Mass

The compression force sensor (Section 1.4) was used where the sensor was loaded with only the ball itself. The sample mean of this sensor reading was used so that

$$\bar{F} = 0.7870 \text{ [N]}, \text{ sample mean}$$

$$\Rightarrow m_b \approx \frac{\bar{F}}{g} = \frac{0.7870 \text{ [N]}}{9.81 \text{ [m/s}^2\text{]}} = 80.2 \cdot 10^{-3} \text{ [kg]}$$

4.1.3 Force and Displacement

With help from the Department of Structural Engineering at NTNU, a measurement series for the relationship between applied force and object displacement was obtained.

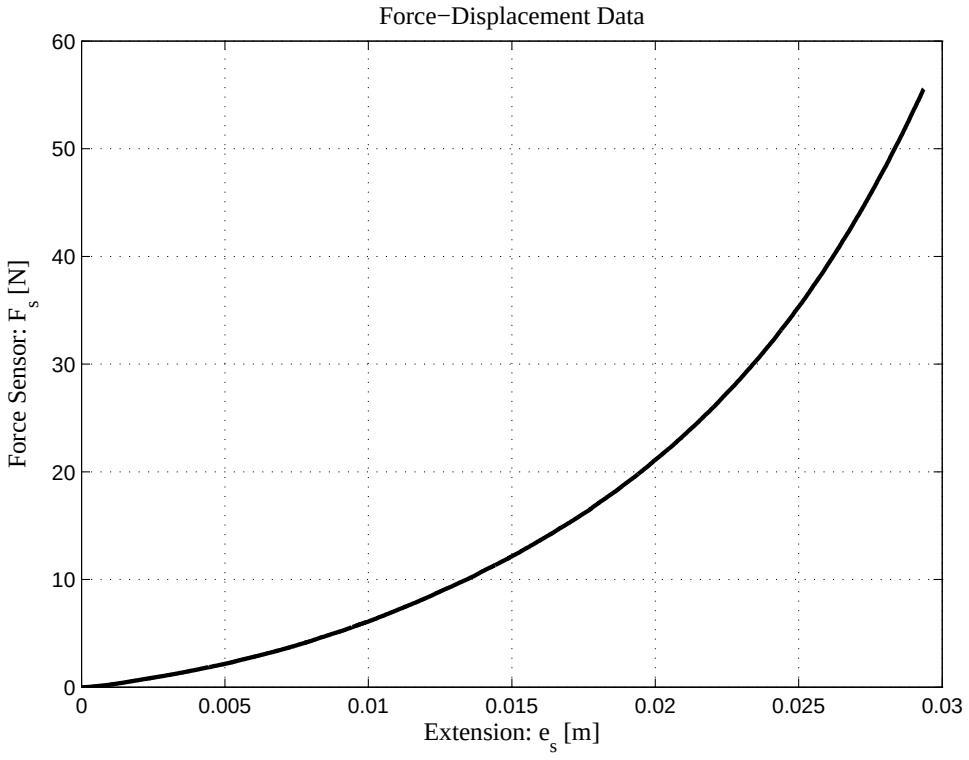

FIGURE 4.1: Measurements of applied force as a function of extension from initial position.

Based on first impressions of the raw data, seen in Figure 4.1, it was clear that some higher order polynomial is appropriate to model this relationship. Let us

denote the force from the object as F_{ob} and take this to be a function of object displacement, $\Delta d = d_e - d$, away from its equilibrium diameter. The measurements of force, F_s, are taken to be equal the force from the object. Furthermore, measurements of extension, e_s, are taken as Δd. It assumed that the object is symmetric and of homogeneous composition.

$$\begin{aligned} F_{ob}(\Delta d) \triangleq F_s(e_s) &\approx p_n \Delta d^n + p_{n-1}\Delta d^{n-1} + \cdots + p_1 \Delta d \\ &= \begin{bmatrix} p_n \\ p_{n-1} \\ \vdots \\ p_1 \end{bmatrix}^T \begin{bmatrix} \Delta d^n \\ \Delta d^{n-1} \\ \vdots \\ \Delta d \end{bmatrix} \\ &\triangleq y = \mathbf{p}_{ob}^T \boldsymbol{\phi} \end{aligned}$$

$\boldsymbol{\phi}$ is the *regression vector*, while $\mathbf{p}_{ob}$ is the *parameter vector* [Lennart, 1999]. Given polynomial degree n, these may be used in the *Least-Squares Algorithm* in order to find the best fit for the measurements of F_s and e_s. Lennart [1999] gives the following least-squares algorithm for N measurements

$$\hat{\mathbf{p}}_{ob,N}^{LS} = \left[\sum_{i=1}^{N} \boldsymbol{\phi}_i \boldsymbol{\phi}_i^T \right]^{-1} \left[\sum_{i=1}^{N} \boldsymbol{\phi}_i y_i \right]$$

where i is the measurement number. Let us combine all measurements of y and $\boldsymbol{\phi}$ into vectors so that

$$\begin{aligned} \sum_{i=1}^{N} \boldsymbol{\phi}_i \boldsymbol{\phi}_i^T = [\boldsymbol{\phi}_1, \ldots, \boldsymbol{\phi}_N] \begin{bmatrix} \boldsymbol{\phi}_1^T \\ \boldsymbol{\phi}_2^T \\ \vdots \\ \boldsymbol{\phi}_N^T \end{bmatrix} &= \boldsymbol{\Phi}^T \boldsymbol{\Phi} \\ &\triangleq \mathbf{A} \in \mathbb{R}^{n \times n} \end{aligned}$$

and

$$\sum_{i=1}^{N} \boldsymbol{\phi}_i y_i = [\boldsymbol{\phi}_1, \ldots, \boldsymbol{\phi}_N] \begin{bmatrix} y_1 \\ y_2 \\ \vdots \\ y_N \end{bmatrix} = \boldsymbol{\Phi}^T \mathbf{y}$$
$$\triangleq \mathbf{b} \in \mathbb{R}^{n \times 1}$$

The least-squares estimate may now be rewritten in a more compact form

$$\hat{\mathbf{p}}_{ob,N}^{LS} = \hat{\mathbf{p}}_{ob} = \mathbf{A}^{-1}\mathbf{b} \tag{4.1}$$

By trial-and-error it was found that a polynomial degree of $n = 4$ gave the most reasonable result in terms of error and polynomial degree. The parameter vector found is given by

$$\mathbf{p}_{ob} \approx \begin{bmatrix} 8.8273544 \cdot 10^7 \ [\frac{\mathrm{N}}{\mathrm{m}^4}] \\ -2.8474703 \cdot 10^6 \ [\frac{\mathrm{N}}{\mathrm{m}^3}] \\ 6.6616791 \cdot 10^4 \ [\frac{\mathrm{N}}{\mathrm{m}^2}] \\ 1.5130557 \cdot 10^2 \ [\frac{\mathrm{N}}{\mathrm{m}}] \end{bmatrix} \tag{4.2}$$

Figure 4.2 shows the function evaluations as well the error between the estimates and measured values. The MATLAB® script for this estimation procedure is named `FD_estimation`.

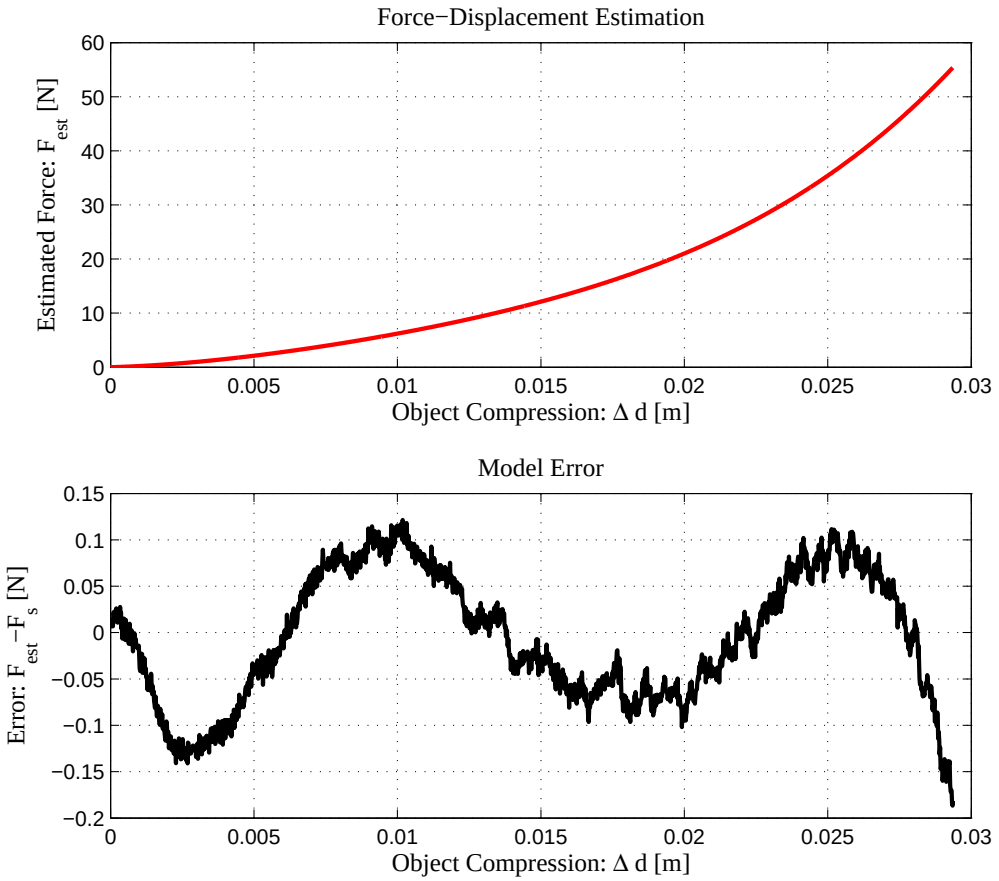

FIGURE 4.2: Least-squares polynomial fit of the force-displacement relationship of the object.

The object normal force due to object compression may now be approximated by the model

$$F_{ob}(\Delta d) \approx \hat{\mathbf{p}}_{ob}^{T} \begin{bmatrix} \Delta d^4 \\ \Delta d^3 \\ \Delta d^2 \\ \Delta d \end{bmatrix} \tag{4.3}$$

where $\hat{\mathbf{p}}_{ob}$ is given by Equation (4.2).

4.2 Frictional Parameters

4.2.1 Static Friction Coefficient

The static friction coefficient from Equation (3.16) must be determined. Figure 4.3 shows the concept of an experiment where the purpose is to obtain measurements necessary for estimation of this coefficient.

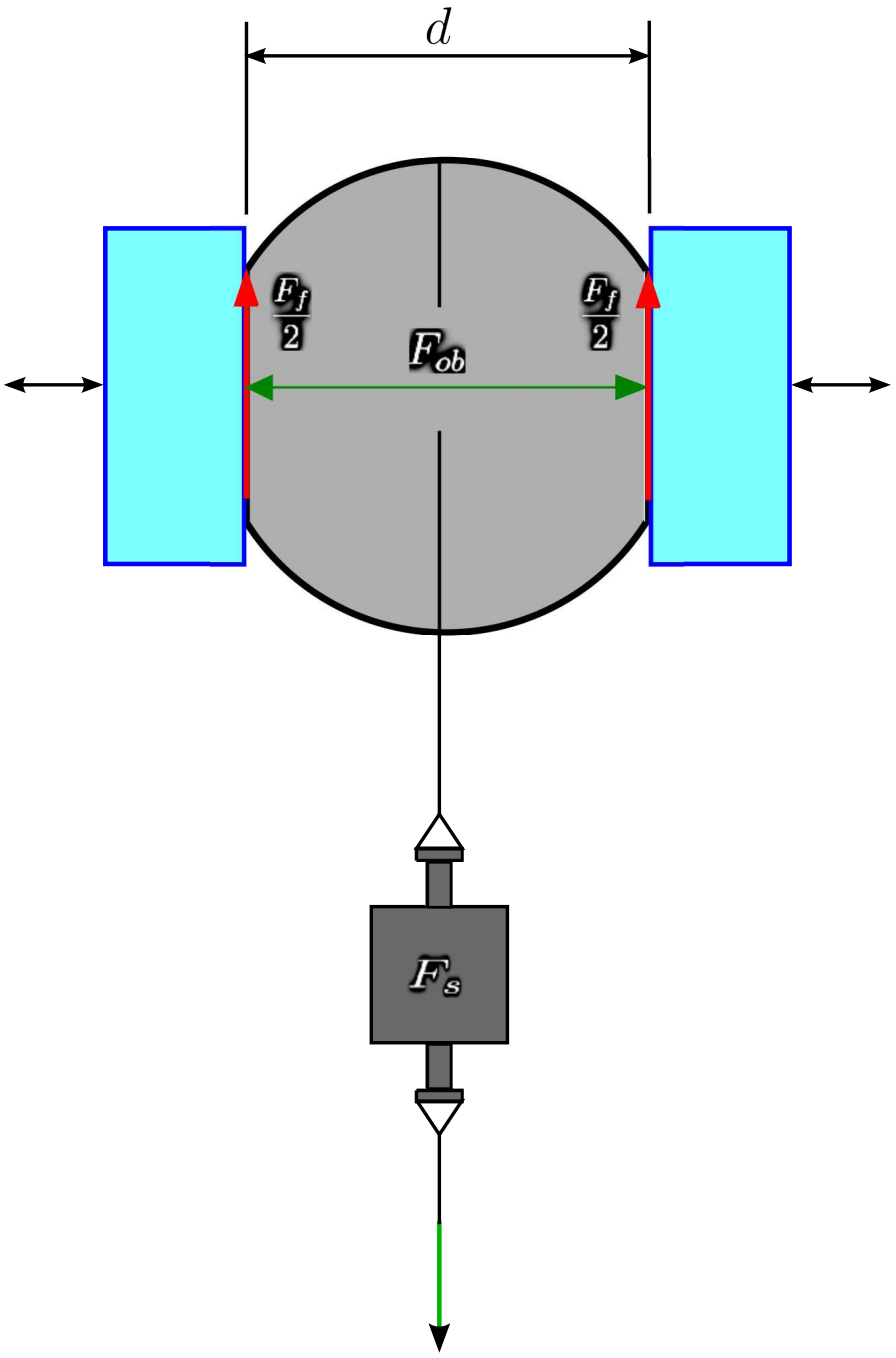

FIGURE 4.3: Experiment schematic for determining static friction coefficient.

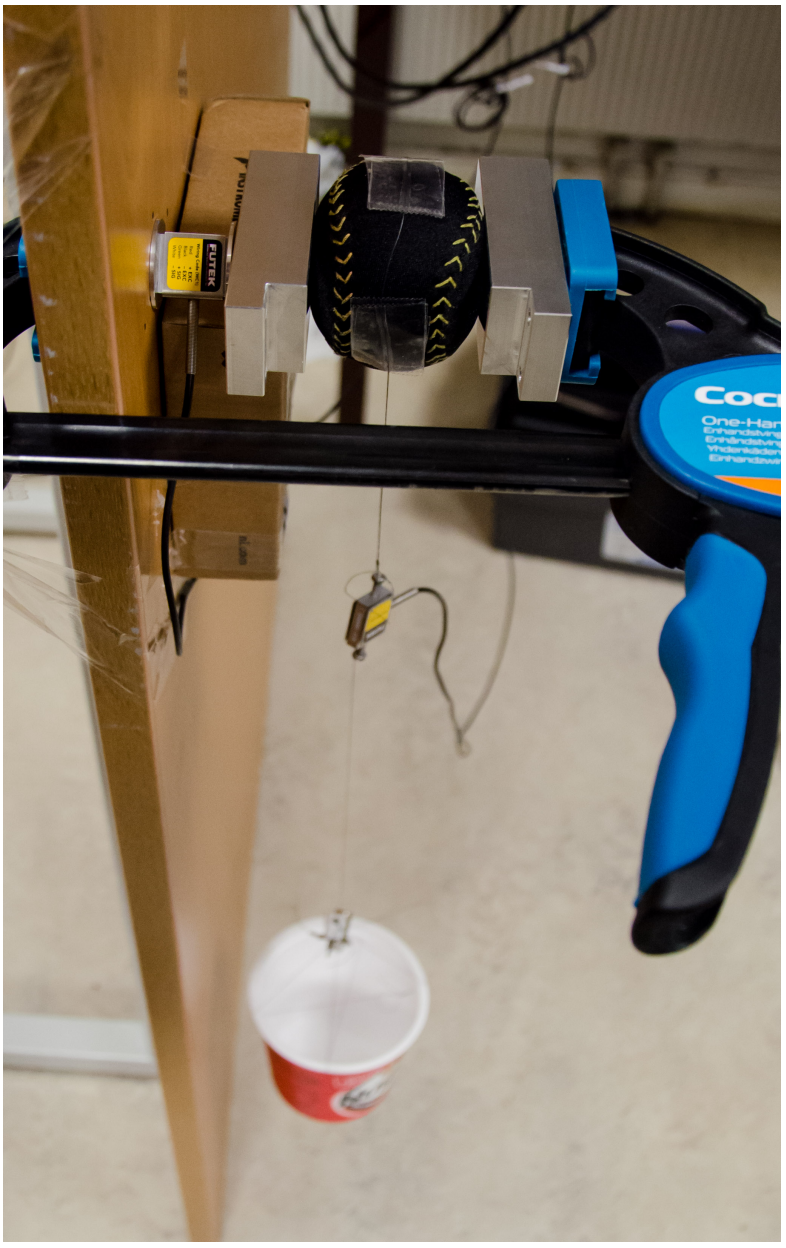

FIGURE 4.4: Actual set-up for determining static friction coefficient.

The actual set-up is shown in Figure 4.4. A string is tied around the object and fastened to the force sensor. On the underside, another piece of string is fastened to some load that may be varied. The idea is to slowly increase the load until the object starts to slide between the fingers. The object displacement is calculated from d and then supplied to the model (4.3) to get the object normal force F_{ob}. In addition, a force sensor is also placed behind one of the fingers so that a direct measurement may be obtained as well.

At the two contacts, it is assumed that equal frictional forces equilibrate the downwards force due to the weight of the object plus any additional load fastened to the sensor.

$$
\begin{aligned}
F_f &= G_{ob} + F_s \\
F_{f,1} = F_{f,2} &= \frac{F_f}{2} = \mu F_{ob}(\Delta d), \quad \Delta d = d_e - d \\
&\Downarrow \\
F_s &= 2\mu F_{ob}(\Delta d) - G_{ob}
\end{aligned}
$$

The friction coefficient is the slope of the assumed linear function for friction force. The constant weight term, G_{ob}, can therefore be ignored.

The measurements of F_s, d and normal force were obtained for a total of 12 measurements. Raw sensor readings from the tension sensor needed to be interpreted to get a value to work with. Sample mean of a short time interval of data right before slip was used. Figure 4.5 shows the friction-normal force relationship for both datasets, i.e. normal force from compression sensor and from diameter readings through object model (4.3).

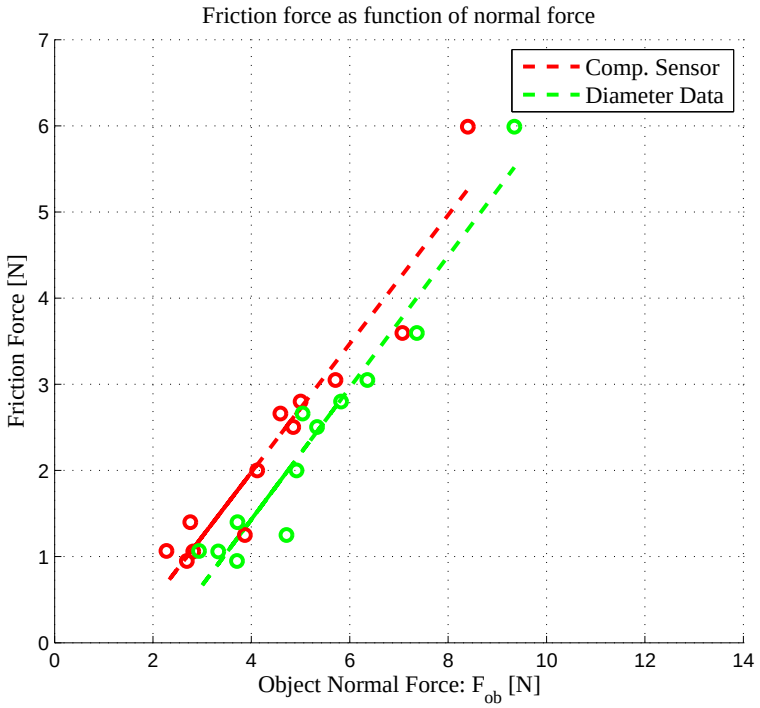

FIGURE 4.5: Measurement data and approximated functions. Normal force readings from the sensor (red) and those obtained by object model (4.3) (green) are displaced.

In Figure 4.5, a displacement can be observed between normal force readings. The cause for this displacement is thought to be from uncertainties regarding measurements of object diameters, d, obtained during the experiment. Also, the equilibrium diameter d_e also affects this outcome.

By halving the friction coefficients from those obtained directly from Figure 4.5, we find that

$$\mu_s \approx 0.373 \quad \text{From compression sensor}$$
$$\mu_d \approx 0.382 \quad \text{From diameter readings}$$

The similar values indicate that the object model for F_{ob} is a good approximation, at least for the domain in question. However, the constant displacement is some cause for worry because the normal force is directly responsible for scaling the friction ellipsoids. It was chosen to use the friction coefficient obtained from the sensor readings. However, readers are made aware that it was discovered that the sensor was sensitive for incorrect loading where, in addition to linear loading, it experience moments. This is the case in the experiment in Figure 4.4.

4.2.2 Contact Area and Normal Force

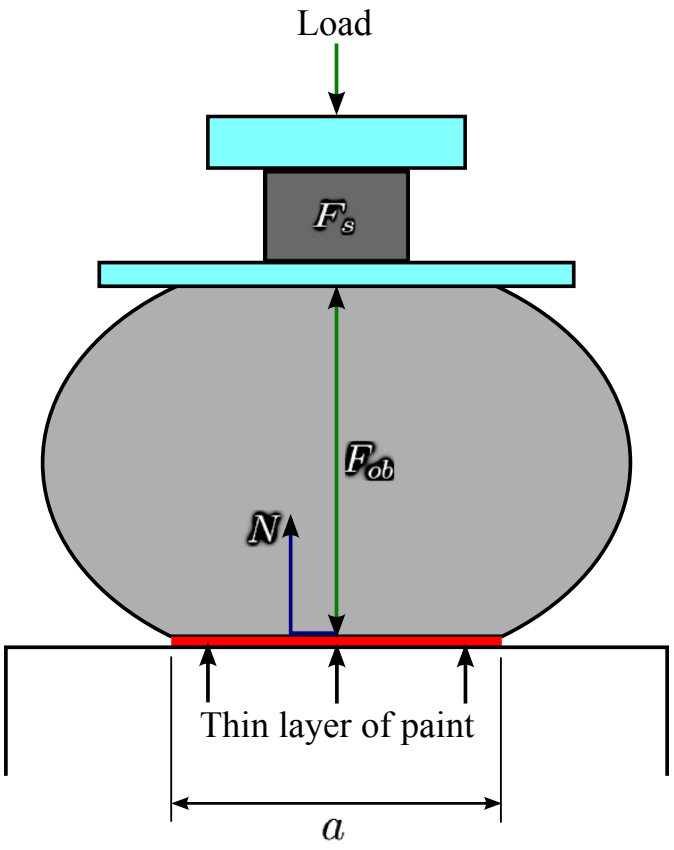

FIGURE 4.6: Experiment schematic for determining coefficients in the power-law model.

The power law model (3.18)

$$a = cN^{\gamma}$$

requires the two parameters c and γ. By measuring contact radius, a, and normal force, N, at different levels of loading, the parameters can be estimated using non-linear regression.

The sensor reading gives us the load while N must also account for the weight of the object, i.e.

$$N = G_{ob} + F_s = m_b g + F_s$$

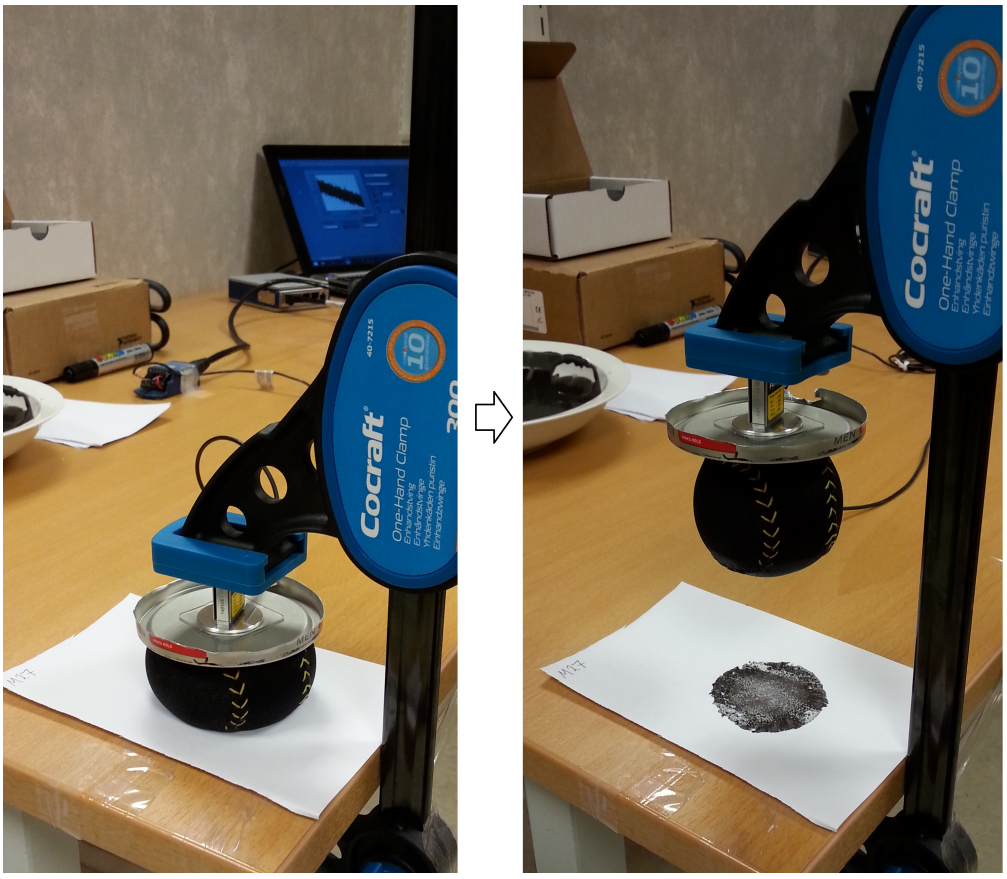

FIGURE 4.7: Actual set-up for determining parameters in power law model (3.18).

Pictures in Figure 4.7 show the actual set-up of the experiment. The picture on the left shows the compression phase, while the one on the right show how the paint imprint gives us the contact area. The paper sheets with contact area were scanned so that the digital copies could be treated with CAD software. For each measurement, the approximate center of the contact area were found and the distance to the uppermost edge of the "circle" was treated as the radius. Note that we did not find a mean radius, just radius measured in the same manner for all measurements.

It is suspected that the experimental set-up was not entirely rigid since it took some time before the reading settled to steady state. Indicating that there were slowly decaying dynamics in the set-up. After a load was applied and the sensor had reached steady state, sample mean of a short time interval was obtained and used further.

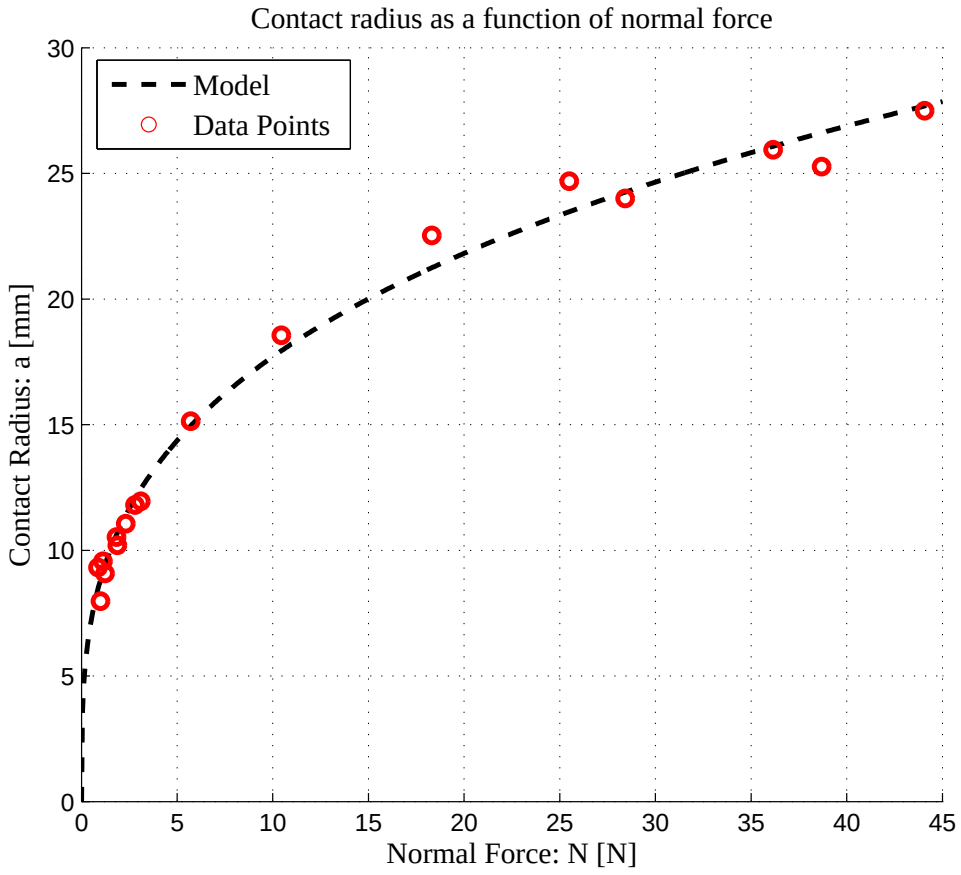

FIGURE 4.8: Plot of the relationship between contact radius and applied normal force. Dashed line represents power law model fit to the data-points (red).

Figure 4.8 shows the final results from the experiment, along with the model fitted to the data. The parameters were found by use of the MATLAB® function `fitnlm`. `fitnlm` fits models with parameters that appear non-linearly to given data. Estimates of c and γ were found to be

$$c \approx 8.8458815 \left[\frac{\text{mm}}{\text{N}}\right]$$
$$\gamma \approx 0.3013398$$

4.3 Summary

To summarize, the parameters found by experiments described in this chapter are given as

$$d_e = 52.7 \cdot 10^{-3} \text{ [m]} \tag{4.4}$$

$$m_b = 80.2 \cdot 10^{-3} \text{ [kg]} \tag{4.5}$$

$$\mathbf{p}_{ob} = \begin{bmatrix} 8.8273544 \cdot 10^{7} \ [\frac{\text{N}}{\text{m}^4}] \\ -2.8474703 \cdot 10^{6} \ [\frac{\text{N}}{\text{m}^3}] \\ 6.6616791 \cdot 10^{4} \ [\frac{\text{N}}{\text{m}^2}] \\ 1.5130557 \cdot 10^{2} \ [\frac{\text{N}}{\text{m}}] \end{bmatrix} \tag{4.6}$$

$$\mu = 0.373 \tag{4.7}$$

$$c = 8.8458815 \cdot 10^{-3} \ \left[\frac{\text{m}}{\text{N}}\right] \tag{4.8}$$

$$\gamma = 0.3013398 \tag{4.9}$$

Chapter 5

Results

This chapter presents observations from two experimental motions executed by the IRB 140 robot. Both motions are repeated for a number of times, with different grip forces. The observations are purely visual, based off on videos taken during the experiments. By analyzing the videos at crucial moments and noting both elapsed time and video-frame, it is possible to observe segments in which object slip has occurred. And of course, noting also when the object is lost by the gripper. For every experiment, the joint positions are measured. These will be applied in Chapter 6 to replicate the motions in simulations and predict contact forces. Sadly, due to technical difficulties, it was not possible to measure joint speeds, accelerations or forces. In all experiments, a synchronization movement was programmed so that the timing of the videos and the measurement data could be matched. All videos and data are supplied in the attached files B.

The first motion, presented in Section 5.1, is a simple repetitive linear motion in the world-frame. The second motion of Section 5.2 is a throwing motion, actuating only one joint. In both cases, the only forces most likely to occur at the contacts are tangential and normal forces, i.e. not torques and rotation about the contact normals. This is because the Center of Mass is located in the middle of the contact points. Therefore, none of the experiments will test the modelling of torsional friction. A suitable test-object with different geometry and CoM was not found and used in our case.

5.1 Linear Motion with Increasing Frequency

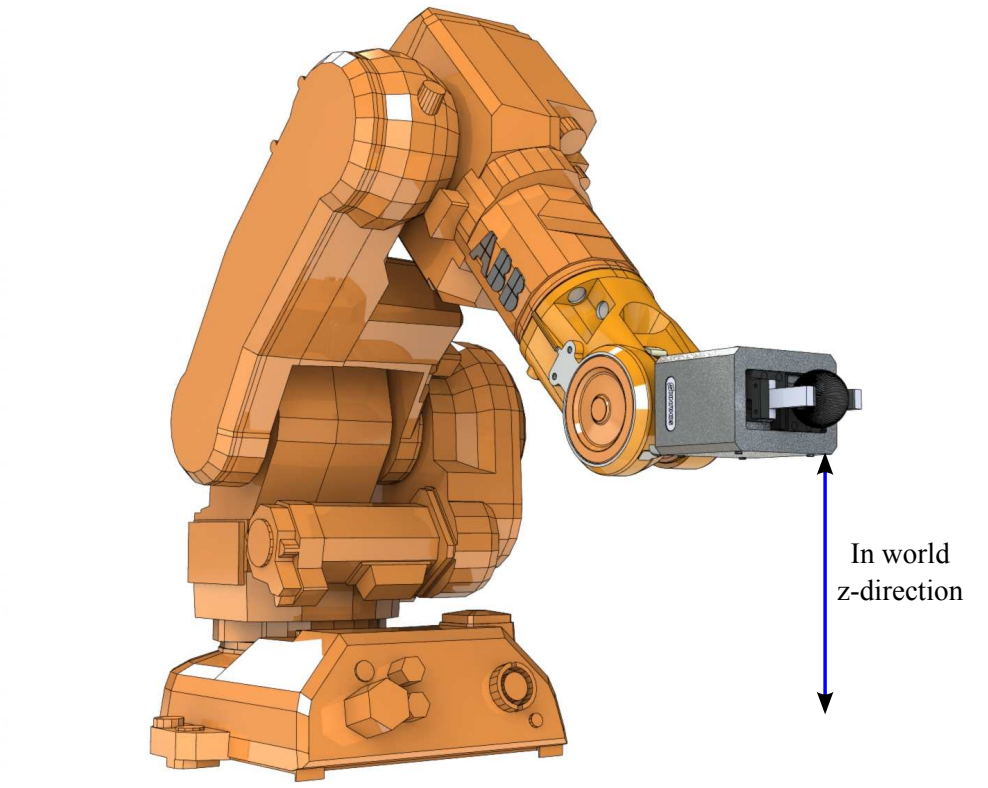

FIGURE 5.1: Illustration of the linear motion in world z-direction.

The first motion moves the gripper along the world z-axis only. Tangential contact forces in world z-direction is therefore expected. The gripper is kept level at all times during the motion and it is moved up and down repeatedly with an increase in frequency as time goes on. After about ten repetitions, the robot moves back into its zero-position.

Every time the gripper is at its lowest point, the video is investigated frame-by-frame to see if the ball has slipped since the previous time. If that is the case, then slip must have occurred in between these sightings. See the picture in Figure 5.2 for an illustration of this. For every experiment, the first and last (lost ball) slip occurrences are noted, these may be viewed in Table 5.1. The "Start" column gives the video time for when the actual motion starts. All the other times are relative to its respective start-time. The start-time is also used to synchronize the experiments with the simulations in Chapter 6. The last column gives the finger displacement, which is used to determine normal force due to object compression.

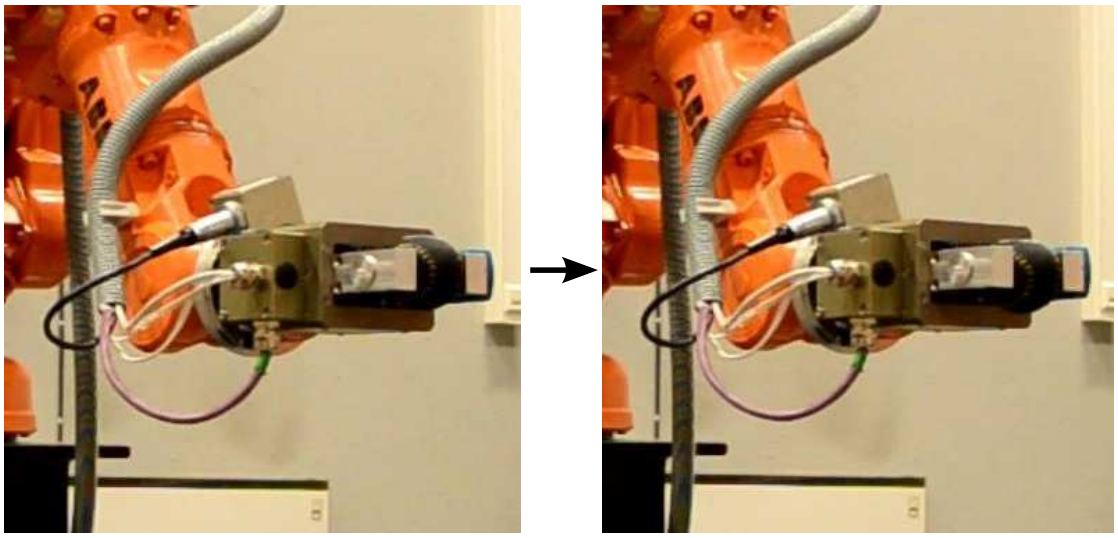

FIGURE 5.2: Illustrating the visual detection of object slip from video data.

#	Start	First Slide Segment	Object Lost	q_7 [mm]
1	47.91	5.60 → 7.00	9.45	48.75
2	24.62	-	-	45.70
3	15.28	10.72 → 11.35	11.91	45.70
4	16.92	11.58 → 12.35	-	45.70
5	14.21	10.85 → 11.41	11.98	45.70
6	18.49	8.98 → 9.80	10.95	47.65
7	16.39	10.80 → 11.41	11.89	47.65
8	12.88	10.25 → 12.08	-	47.65
9	15.22	9.03 → 9.85	10.44	47.65
10	17.45	-	-	43.65
11	12.55	-	-	43.65
12	13.25	-	-	43.65

TABLE 5.1: Table of slip detections based on videos from experiments. Linear motion with increasing frequency. Times are in seconds.

5.2 Throwing Motion

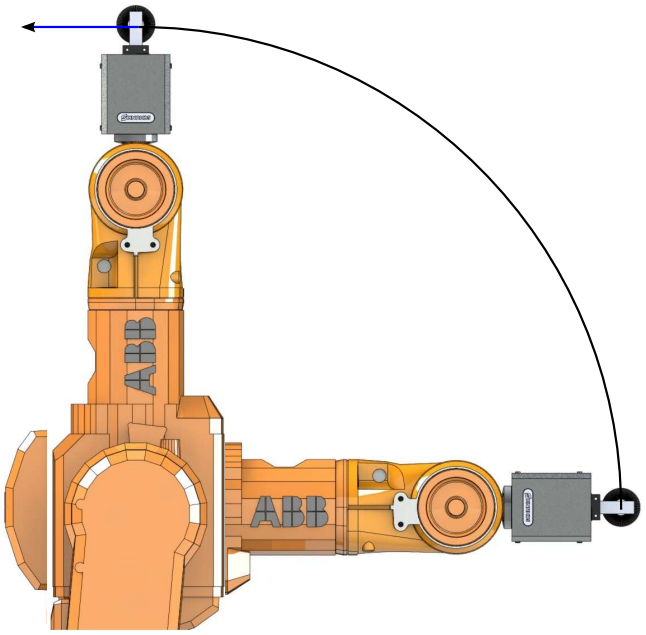

FIGURE 5.3: Illustration of the throwing motion by actuating only the third joint.

This motion moves the gripper in an arc, starting from its zero-position and stopping at $q_3 = -90°$, as Figure 5.3 shows. This allows us to get more distinct data, as opposed to the previous motion. The experiments have three possible outcomes: The ball might fly, slip, or stay firmly attached to the gripper. The observations for the total of 8 throwing experiments are listed in Table 5.2.

#	Start	Observation	q_7 [mm]
1	44.81	Loss	48.70
2	7.44	Loss	48.70
3	10.01	Loss	46.65
4	7.60	Small slip	46.65
5	6.44	Loss	46.65
6	6.68	Small slip	44.65
7	5.47	Medium slip	44.65
8	6.31	Large slip	44.65

TABLE 5.2: Table of slip detections based on videos from experiments. Throwing motion. Times are in seconds.

Chapter 6

Simulations and Discussion

This chapter aims to reproduce the motions of the previous chapter (5). This is realized by using B-splines to approximate joint position data obtained. The continuous spline functions, and their derivatives, for each joint and for each experiment are then used as inputs to the MATLAB® script `RUN`. The data interpolation method of B-splines is discussed in Section 3.8.1.

The angle measurements were pre-filtered with some unknown method by the ABB IRC5 controller. It was therefore practically no noise on the angle measurements. However, the sampling time varied throughout the logged data, ranging from 0.01 to 0.16 seconds. This caused some difficulties in terms of approximating B-splines to the data.

6.1 Linear Motion with Increasing Frequency

For these experiments, a tolerance of 0.002% of the respective joint angle range was chosen for the B-spline approximation. Such a strict tolerance was needed in order to capture the high acceleration peaks of the movement. Due to the horizontal orientation of the gripper, the only tangential contact forces generated was in the positive world z-direction. Furthermore, these contact forces were identical, as one would expect. We have therefore plotted the combined contact force in the z-direction and placed a horizontal blue line to represent the predicted friction limit. The red regions represent observational data of region of first slip and loss

of object while green represent simulated regions of slip. Figure 6.1 shows the simulation of experiment 5.

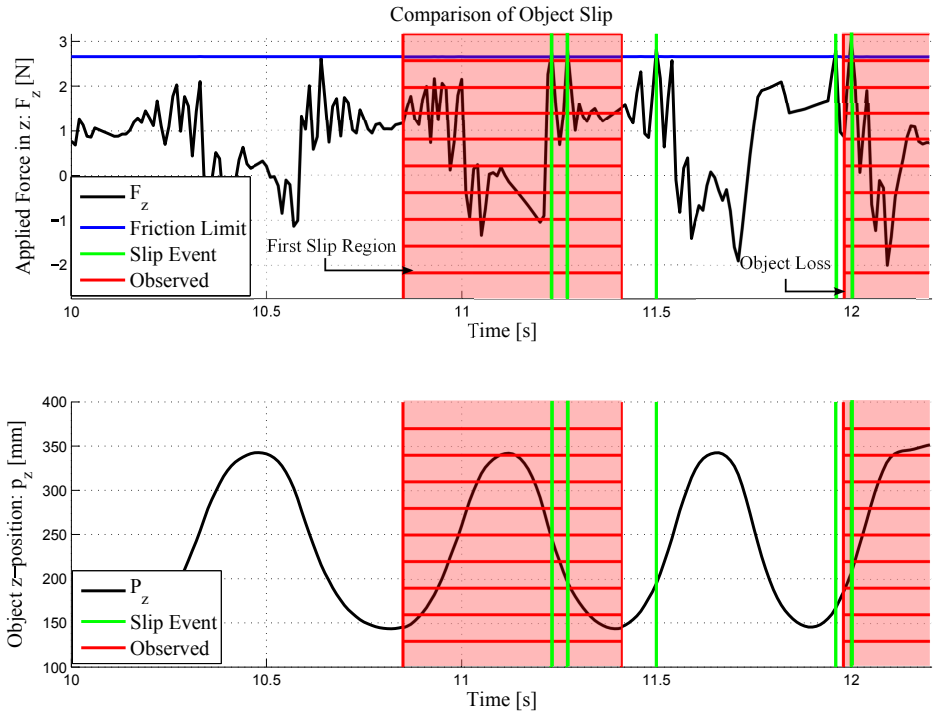

FIGURE 6.1: Plot showing simulated slip events (green) compared to observed first and last slip regions (red). Zoomed in view. Data from experiment 5.

In Figure 6.1 it is clearly seen where the slip events occur. If the motions were clean sinusoidal waves, one would expect that slip would most likely occur at the positions of maximum curvature, i.e. at the bottom of the position waves. However, this is not the case. The motion planner in the IRC5 controller always tries to minimize the movement time, unless told otherwise by use of `AccSet`. This is done by ramping up the acceleration as fast as possible to reach assigned speed, producing jerks. This change of acceleration occurs at the beginning of a movement command as well as right before it reaches the position when it needs to decelerate. It might actually be the case that this is captured by the simulation. The fact that observed and simulated object loss occurs at such an instant supports this. The phenomenon is a recurring theme among all the experiments.

Experiment 5 was a particularly nice example where first simulated slip occurred within observed region. This is not to be taken as representative for all the experiments. Plots for all the other experiments can be found in Appendix A.1. In

the experiments where slip and/or object loss took place, simulated slip occurred earlier than observed. However, it should be noted that small instances of slip might not have been observed due to the visual nature of the observations. Table 6.1 gives an overview of the key aspects about the simulations.

#	First Slip	Slip Within Observed	Slip at Object Loss	Comment
1	4.23	Yes	Yes	Many predictions before observed
2	10.91	-	-	Predicted, but not observed
3	10.58	Yes	Yes	-
4	-	No	-	Observed, but not predicted
5	11.23	Yes	Yes	Predicted within observed
6	4.42	Yes	Yes	Many predictions before observed
7	10.24	Yes	Yes	-
8	10.06	Yes	-	-
9	7.74	Yes	Yes	-
10	-	-	-	No prediction, no observation
11	-	-	-	No prediction, no observation
12	-	-	-	No prediction, no observation

TABLE 6.1: Summary of simulation results and their comparison against observations.

6.2 Throwing Motion

For the single joint motion, it was found that even tighter tolerance was needed for the B-spline approximation. Mainly because the spline approximation tended to easily smooth at the crucial stop moment. Tolerance was set to $5 \cdot 10^{-4}\%$ of joint data range. It was important to capture the high acceleration region. However, the success of this is debatable. One could treat every experiment individually and find a suitable tolerance for each, but that would be highly speculative and throw off any possible conclusions. In any case, using B-splines to obtain velocity and acceleration was a decision made in order to be able to compare simulations with at least some form of data.

Before we discuss the simulations, some remarks about the robot programming are needed. The throwing motion was realized by dividing the arc between 0° and 90° into three motion commands. The first being 30°, then 60° and the final stop at 90°. As can be seen in Figure 6.2, sharp bends are present at these degrees. This is due to the motion planner in the IRC5 controller. Note that angles are actually negative measured from the robot, this was changed for aesthetic reasons.

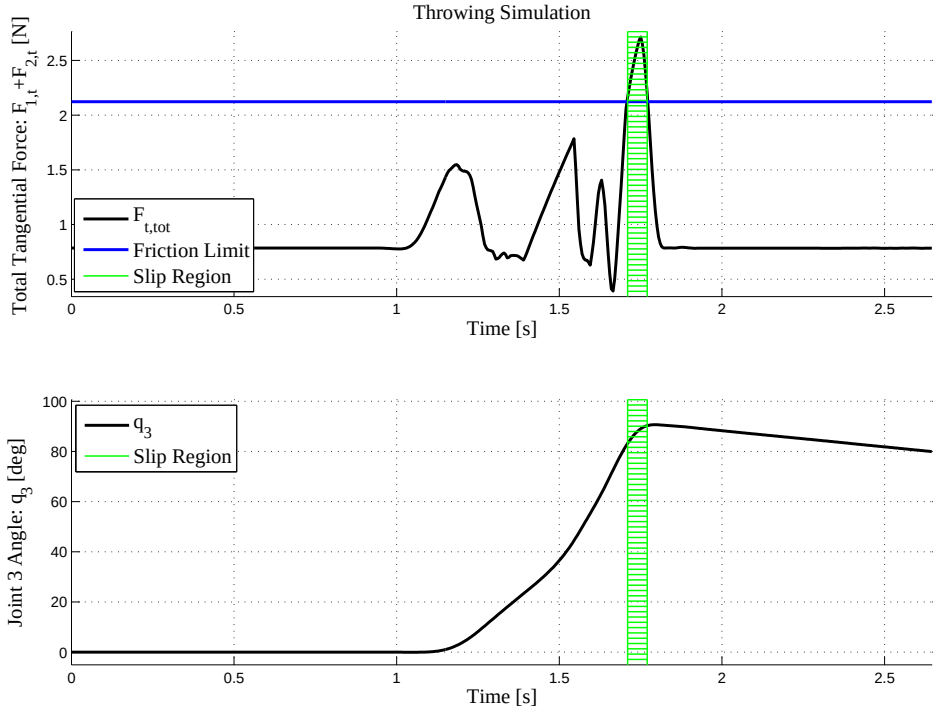

FIGURE 6.2: Plot of calculated combined tangential force with slip prediction regions in green. Joint data from experiment 5.

Again, as is expected for such a motion, the only substantial contact forces calculated were tangential contact forces. Some small amount of torque was generated at the contacts, this to change the angular orientation of the object. Both the tangential friction limits and the tangential forces were identical. The combined tangential force, i.e. the sum of the two, was plotted along with the combined friction limit.

In the experiments where grip force was low, especially 1 and 2, the slip prediction was sensitive. Several predictions were made at times when the robot was given a new motion command. Again, as was pointed out in the previous section, every time the robot executes a motion command, it ramps up the acceleration until target speed is obtained. These areas of jerking motion clearly affect the prediction of slip. All plots are found in Appendix A.2, but a summary may be found in the following table.

#	Slip Predicted	Observed	Comment
1	Yes	Loss	Predicted too early
2	Yes	Loss	Many predictions
3	Yes	Loss	Single prediction
4	No	Slip	Not close to limit
5	Yes	Loss	Single prediction
6	No	Small slip	Not close to limit
7	No	Medium slip	Close to limit
8	No	Large slip	Very close to limit

TABLE 6.2: Comparison of simulated throws versus observed behaviour.

The behaviour of the last three experiments was interesting. Jerk was limited by `AccSet` in the programming of experiments 6 and 7 to 20% and 50%, respectively. This is reflected in the contact force computations. In experiment 8 where jerk was 100%, the tangential force was extremely close to the friction limit.

The fact that slip was predicted every time the object was lost is truly an interesting result and worth noticing.

Chapter 7

Conclusions and Future Work

As previously noted, measurements from the experiments of Chapter 5 were scarce. However, by use of the B-spline approximation method, we were able to compare the simulations against the observations. Based on the simulations and discussions of Chapter 6, correlation between model predictions and observations are evident, at least to some degree. There were several false positive predictions, especially at low grasping forces where the model is sensitive for acceleration spikes. But most of the predictions lay within the expected and observed regions.

Parameters for the object and tangential friction directly affected the predictions. These predictions seems reasonable. However, the experimental motions did not yield any interesting results regarding the torsional friction modelling. We can therefore not conclude anything regarding that aspect of the grasping model. Although, in Chapter 4 the parameters for torsional friction were indeed identified from measurement data. In fact, it was found that measurements of growing contact area due to applied normal force followed that of the Power Law model [Xydas and Kao, 1999].

7.1 Main Conclusions

1. Slip Prediction from Manipulator Motions

The results of Chapters 5 and 6 show that the model introduced in Chapter 3, with the parameters of Chapter 4, produced reasonable predictions. A source of uncertainty are the B-spline approximation method used in order to obtain joint velocities and accelerations. The model parameters also carry with them uncertainty that influence the predictions. A statistical analysis was not conducted on estimation data and experimental data from the manipulator motions, as the limited amount of experimental time was concentrated at the end of the project period.

2. Grasp Quality Measure

It is believed that the quantity

$$Q \triangleq (1 - Q_1)(1 - Q_2) f(i_m|\Delta d|F_{ob}), \quad 0 \leq Q_{1,2} < 1 \tag{7.1}$$

where Q_1 and Q_2 are found by (3.22), may be used as a quality measure for the two fingered grasping scenario of this thesis. $f(i_m|\Delta d|F_{ob})$ is some function of either gripper current,object compression or object force that determines the tightness of the grasp. Larger values of Q indicate better grasps in terms of grasp tightness.

The experiments conducted in Chapter 5 could not shed light on the frictional modelling regarding soft object properties which are part of the quality measure. However, based on the works of Xydas and Kao [1999], it is assumed that given correct parameters, the elliptical model may be utilized.

7.2 Future Work

First and foremost, the torsional friction modelling should be investigated more closely. Test objects that may be grasped so that the CoM does not lie between the contact points should be used. During motion, this will ensure that frictional torque are induced at the contacts. It was assumed that the gripper fingers and the object produced circular contacts, the model should be modified in order to support non-circular contacts as well. The assumption that the locations of the Centers of Pressure are fixed on the finger surfaces is a weakness of the model. Sometimes, this might not be the case and the CoP's may vary locally from their initial position.

The grasping model was only tested as an off-line application, on-line implementation should be explored. For on-line application, the grasp quality measure (7.1) from frictional ellipsoids could be used in order to vary the grasping force applied. This could lead to a more gentle handling of objects during motion.

Instead of using joint measurements to reproduce the motion of the gripper and the grasped object, using acceleration sensors attached to the gripper could result in more reliable measurements. This could be used to further test the grasping model of Chapter 3 and its prediction of slip.

Appendix A

Additional Figures

A.1 Simulation: Linear Motion

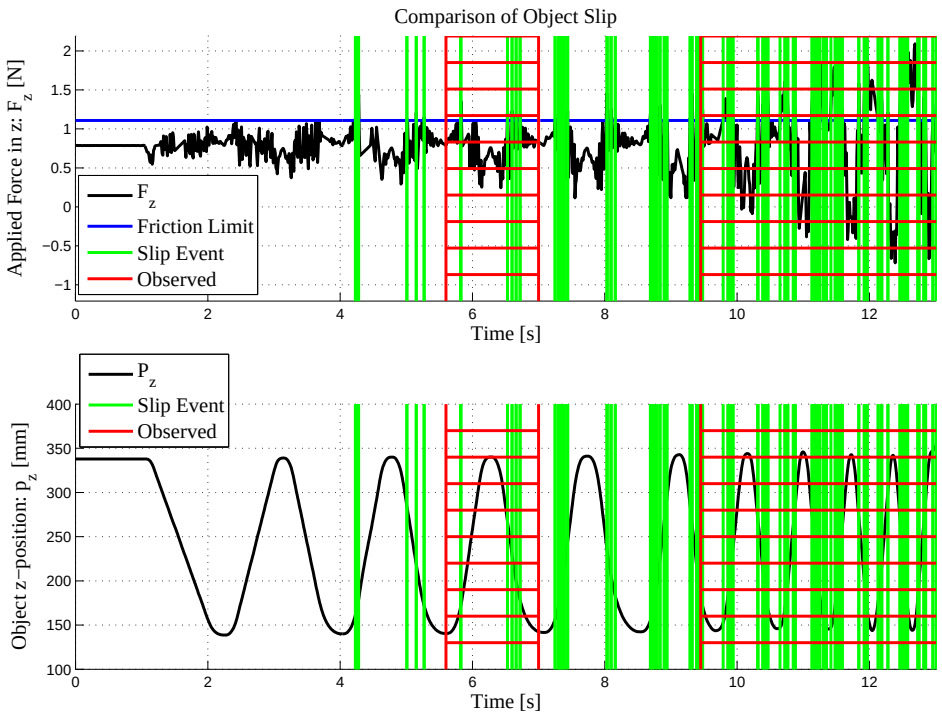

FIGURE A.1: Simulation plot of experiment UD-1.

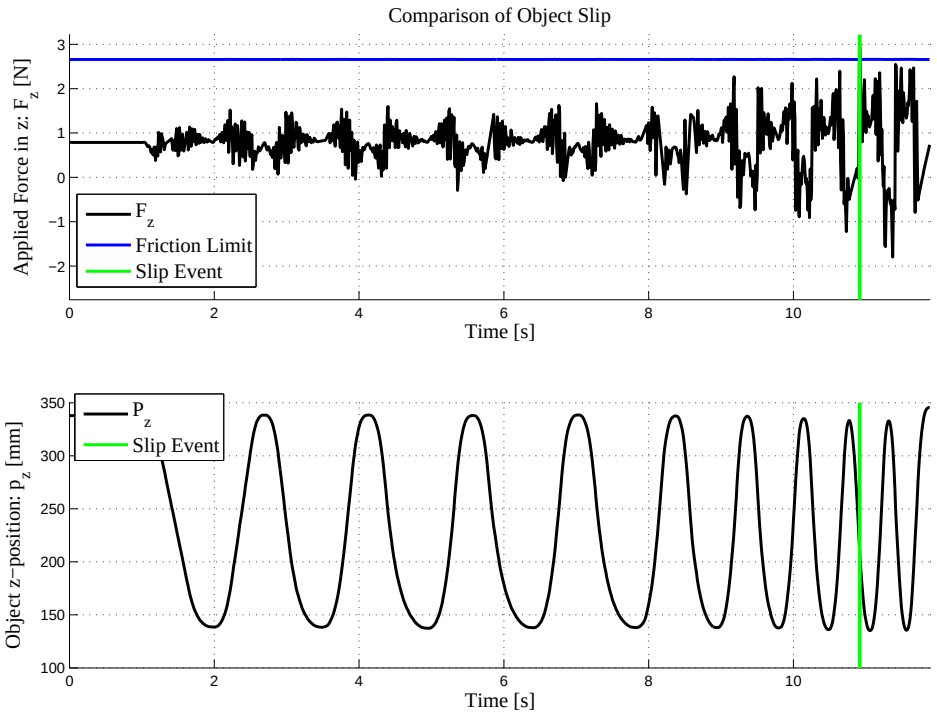

FIGURE A.2: Simulation plot of experiment UD-2.

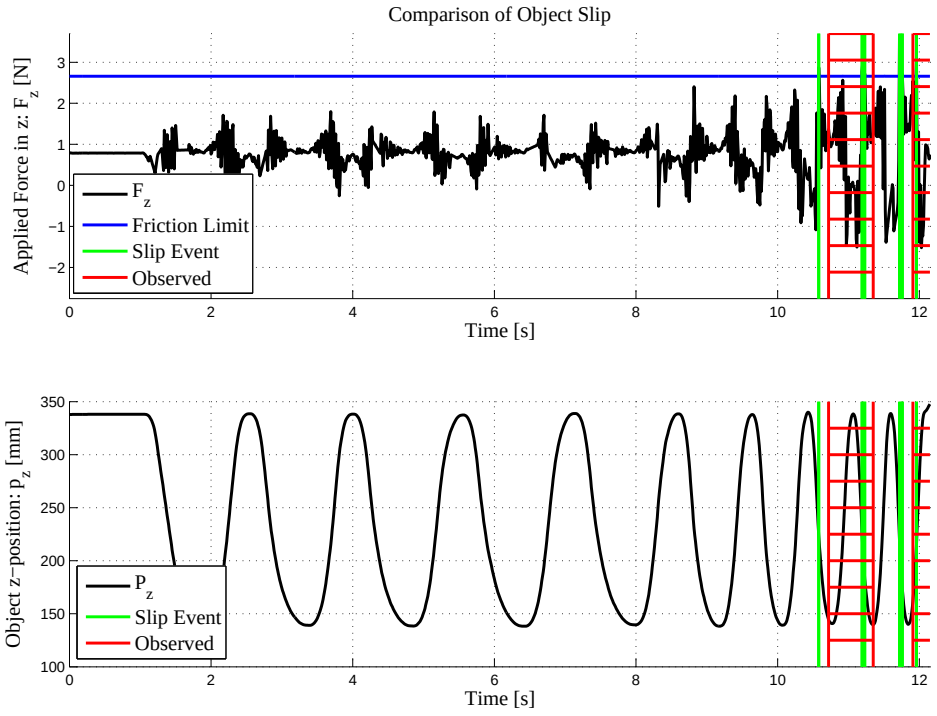

FIGURE A.3: Simulation plot of experiment UD-3.

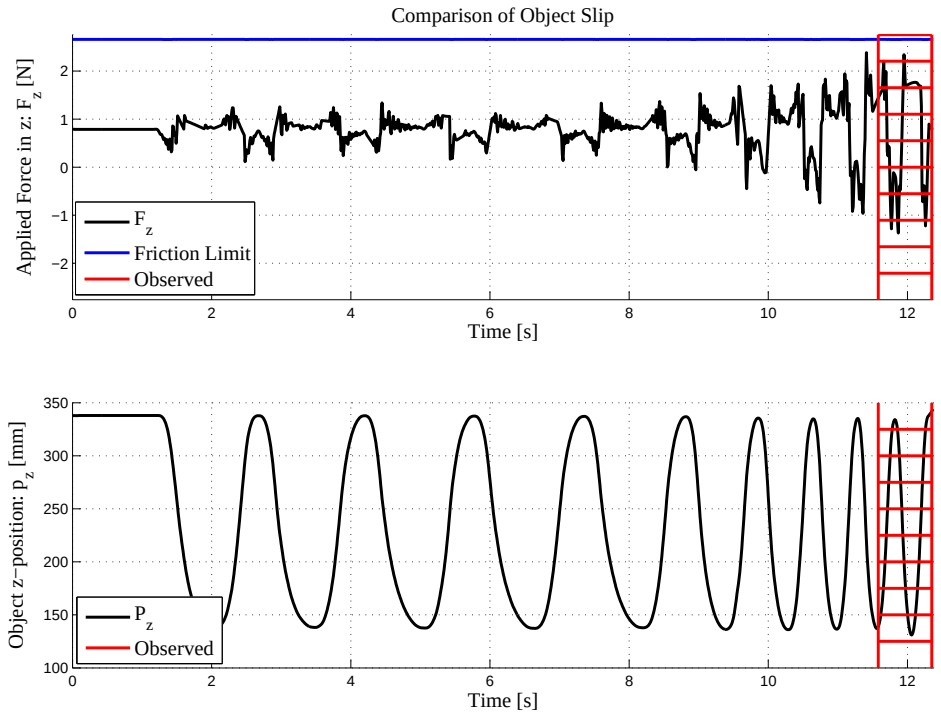

FIGURE A.4: Simulation plot of experiment UD-4.

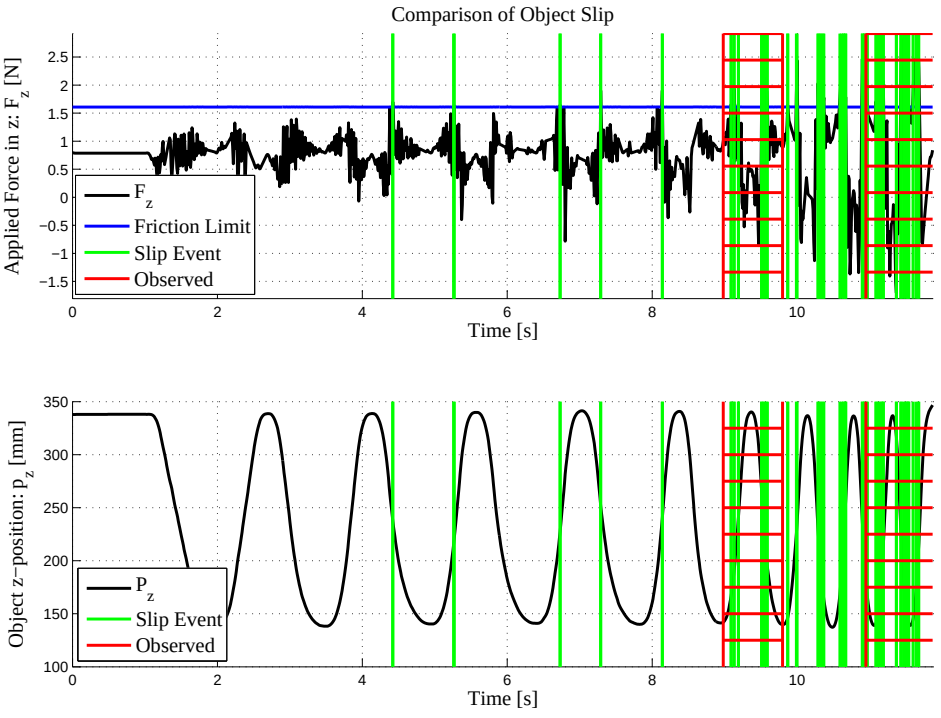

FIGURE A.5: Simulation plot of experiment UD-6.

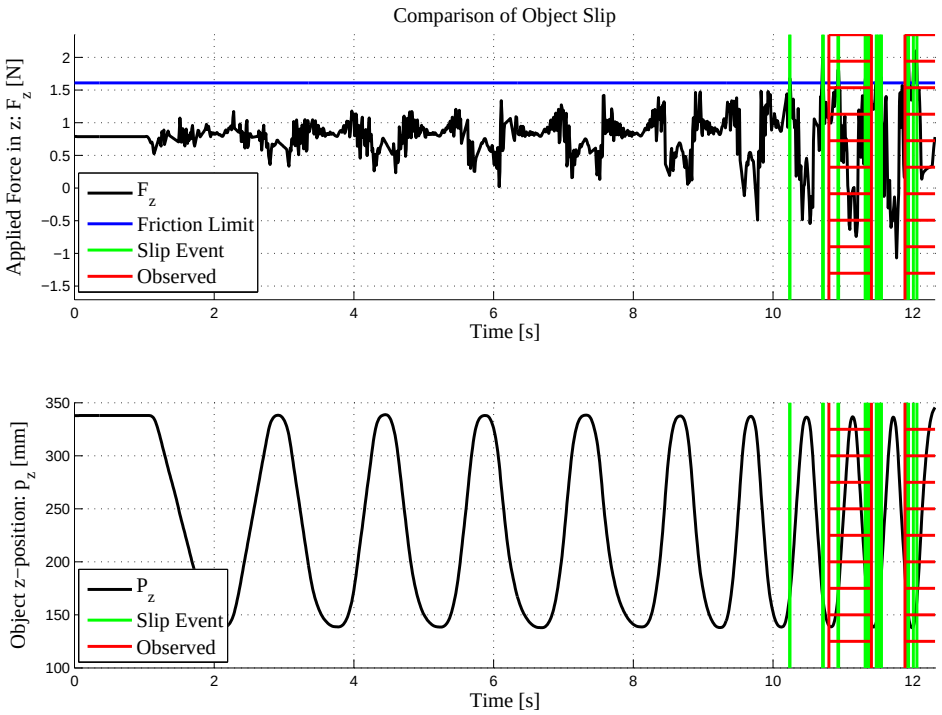

FIGURE A.6: Simulation plot of experiment UD-7.

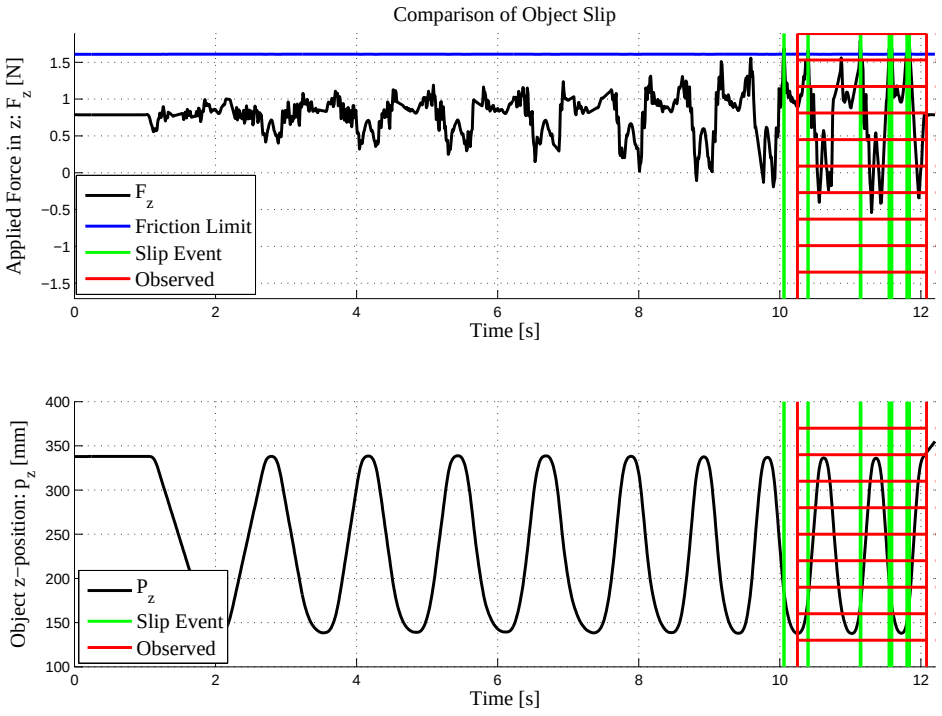

FIGURE A.7: Simulation plot of experiment UD-8.

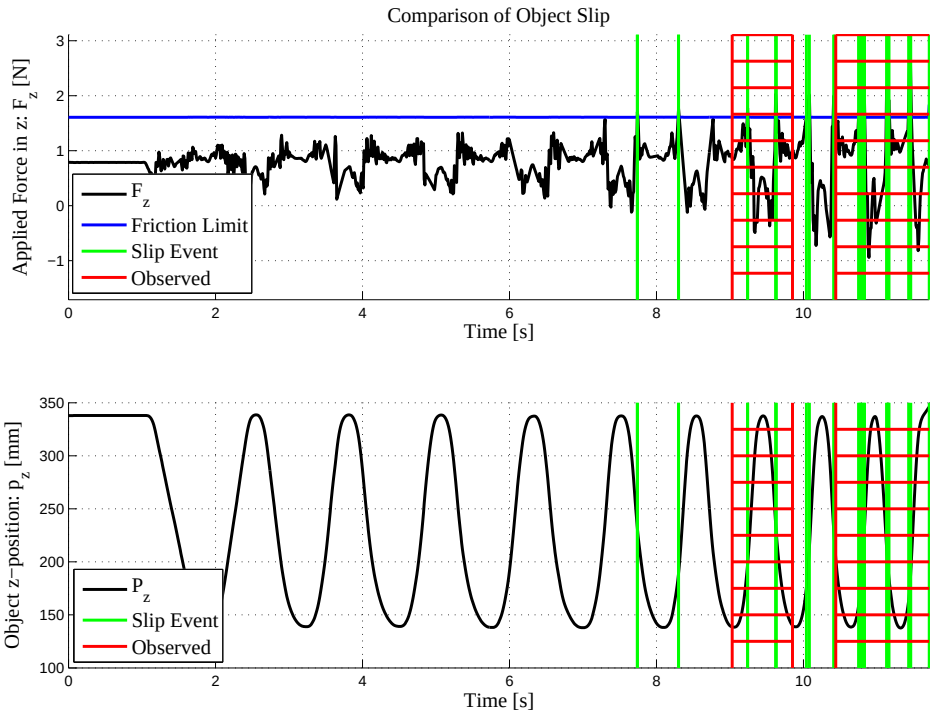

FIGURE A.8: Simulation plot of experiment UD-9.

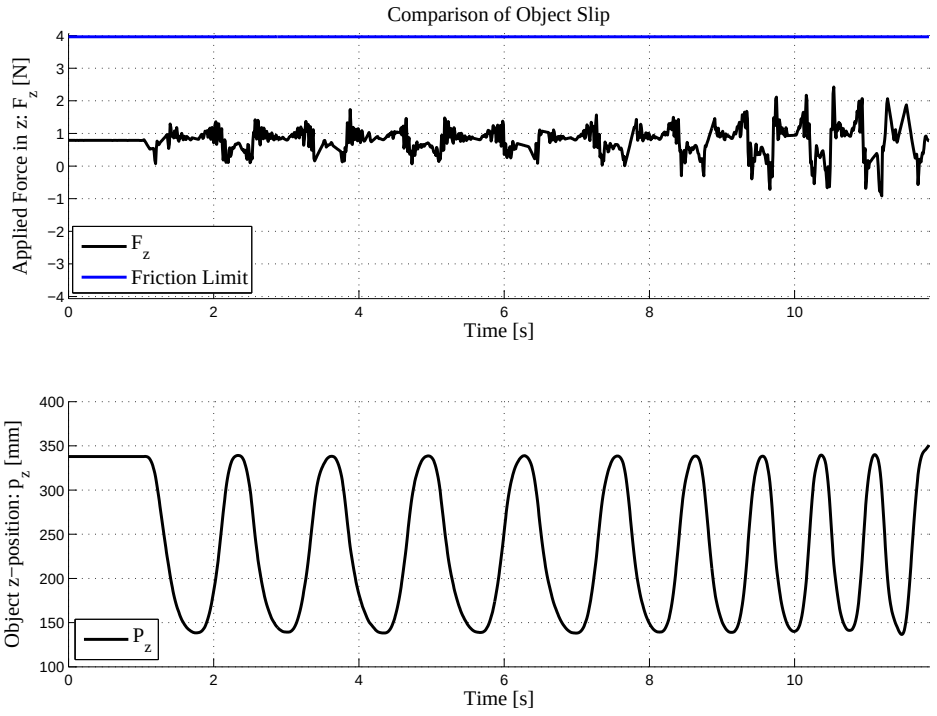

FIGURE A.9: Simulation plot of experiment UD-10.

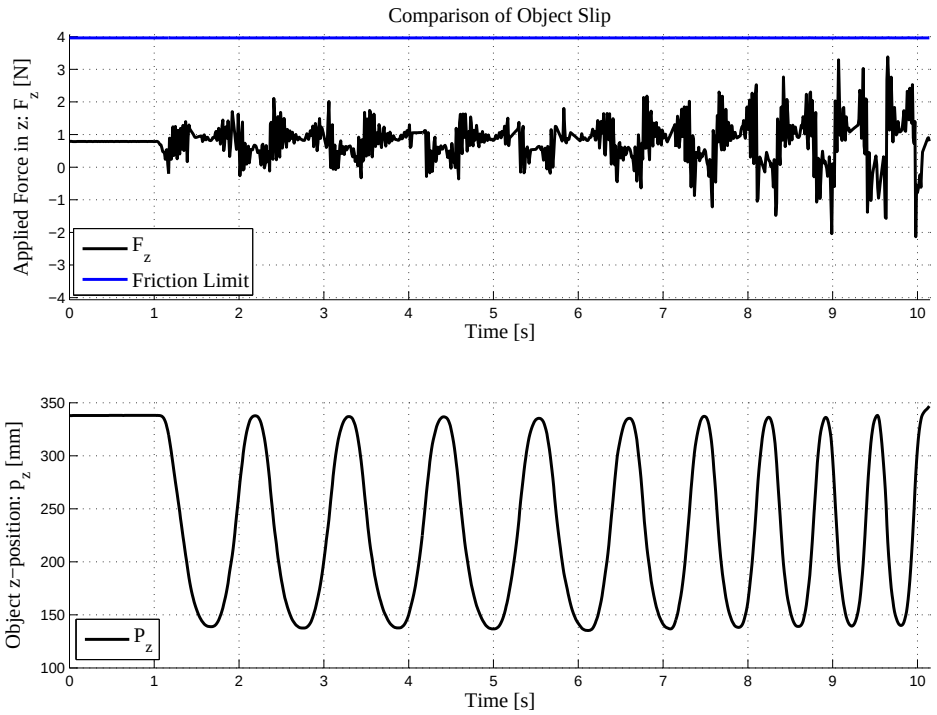

FIGURE A.10: Simulation plot of experiment UD-11.

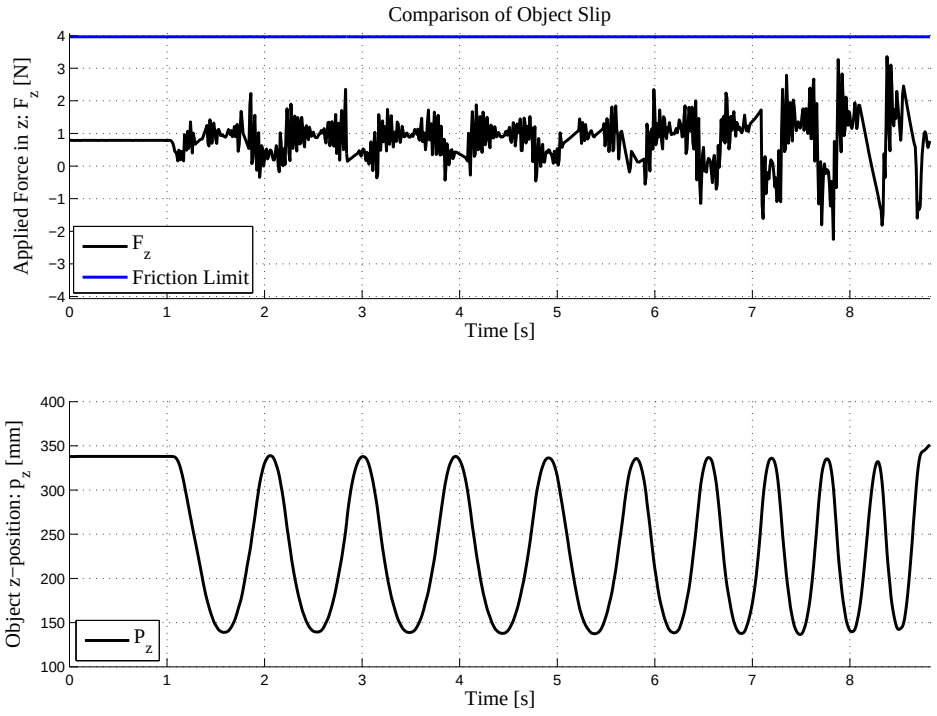

FIGURE A.11: Simulation plot of experiment UD-12.

A.2 Simulation: Throw Motion

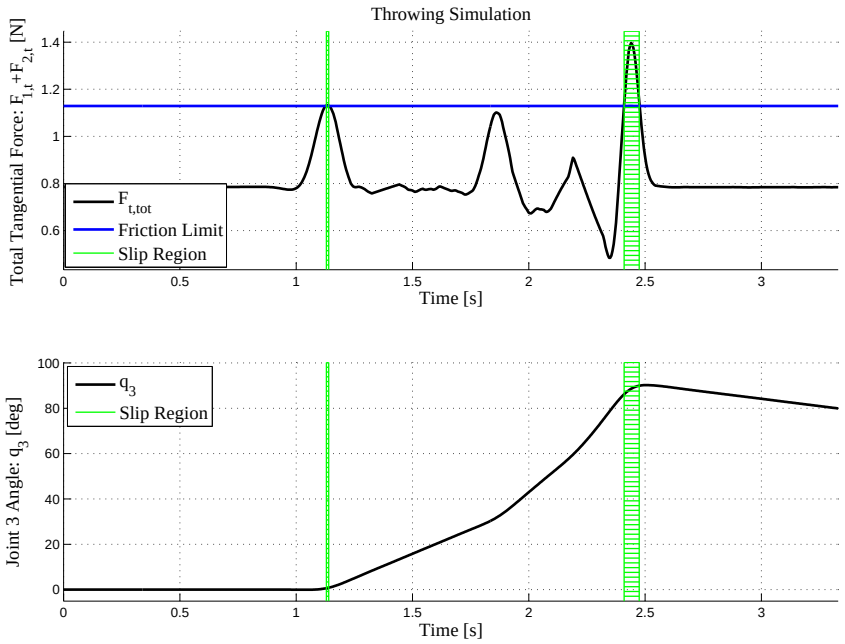

FIGURE A.12: Simulation plot of experiment T-1.

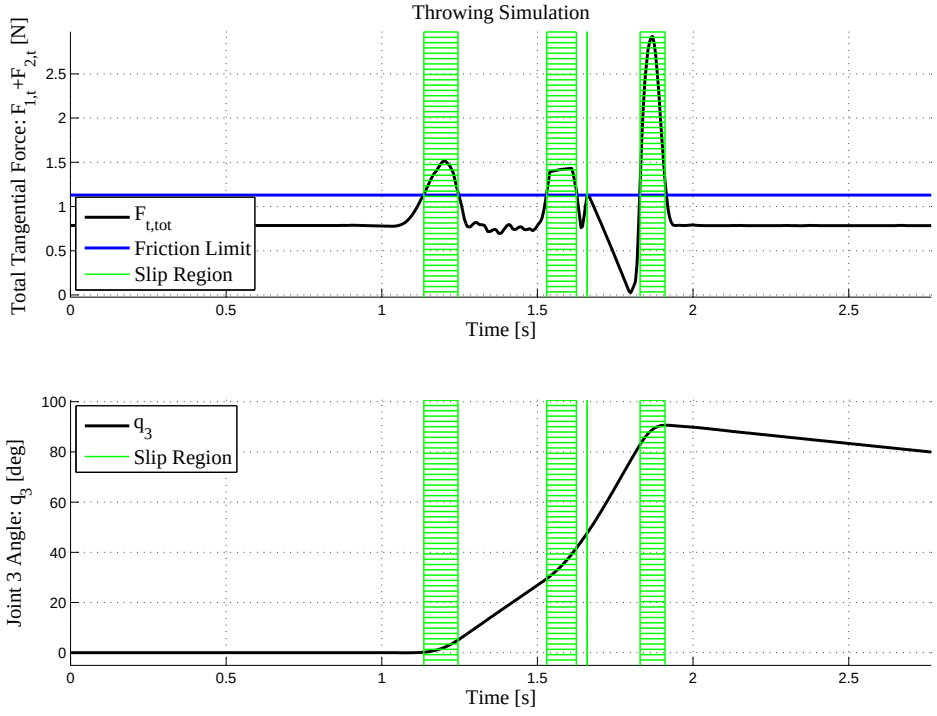

FIGURE A.13: Simulation plot of experiment T-2.

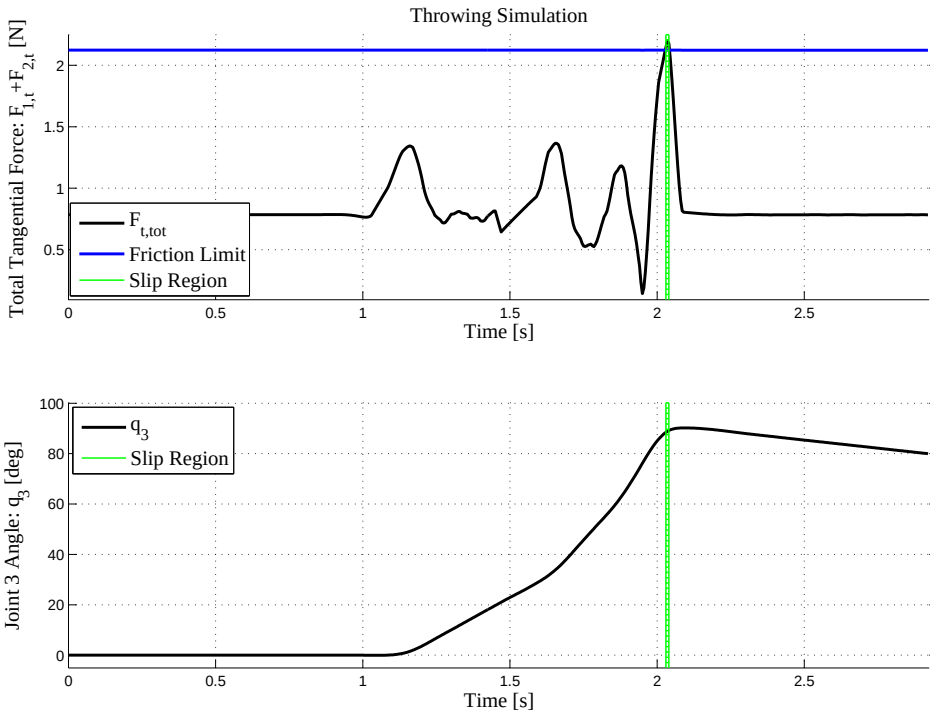

FIGURE A.14: Simulation plot of experiment T-3.

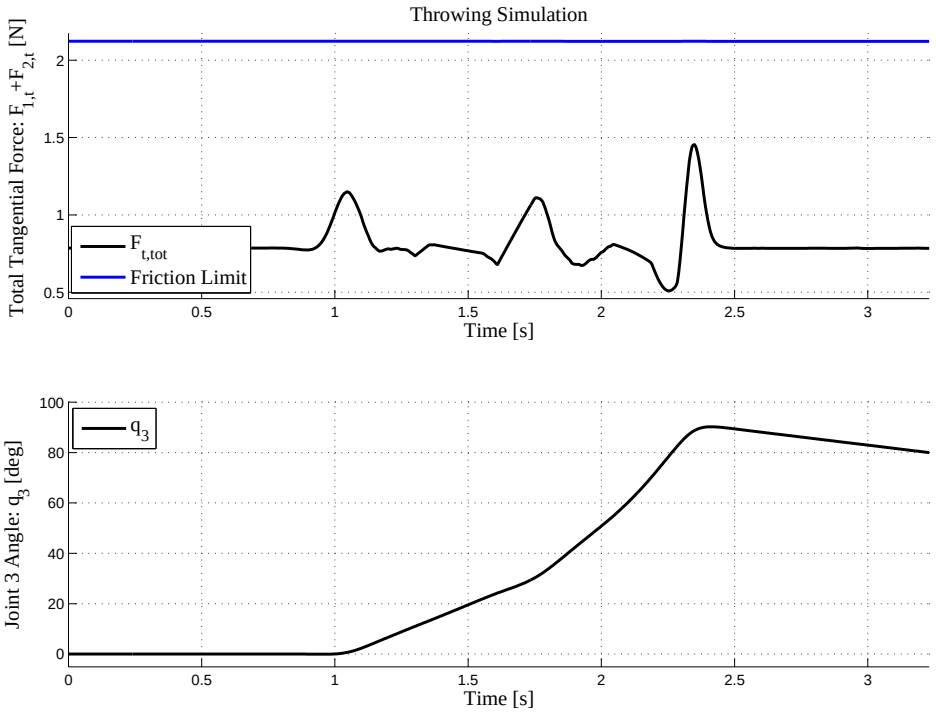

FIGURE A.15: Simulation plot of experiment T-4.

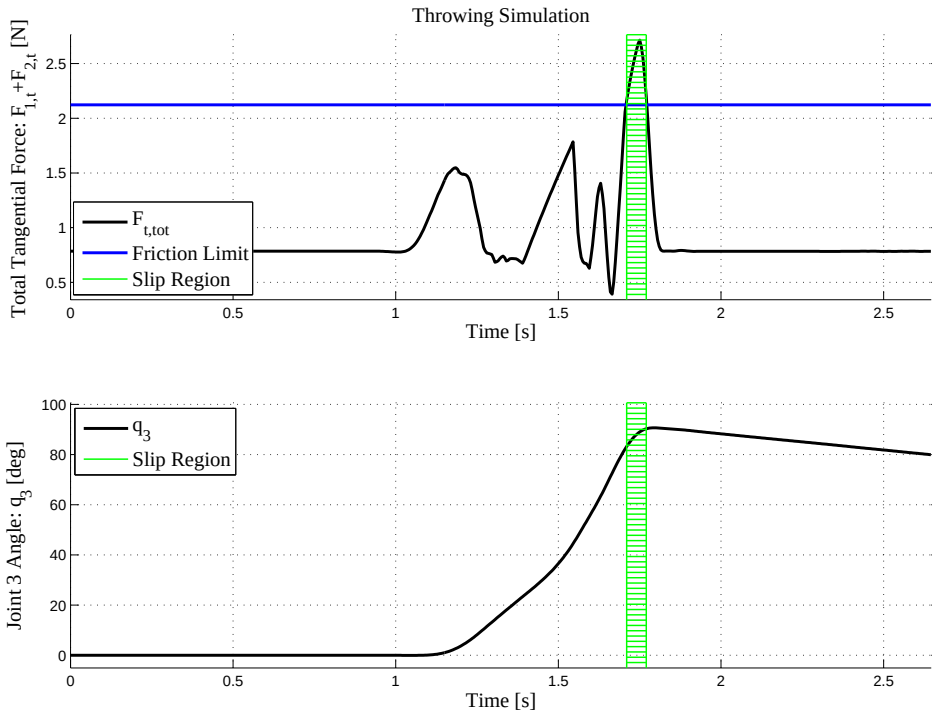

FIGURE A.16: Simulation plot of experiment T-5.

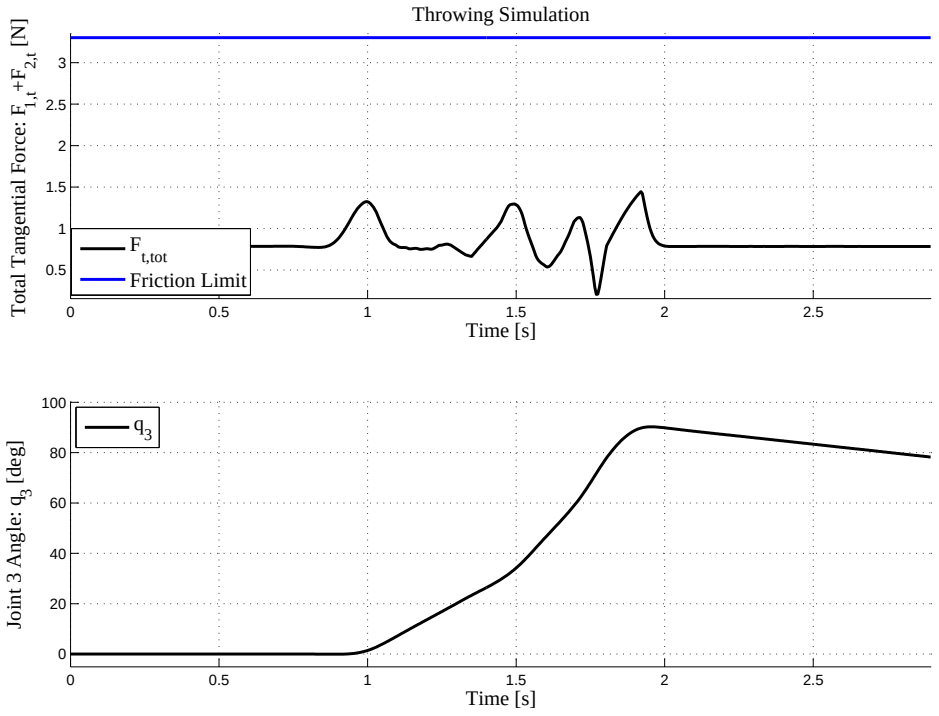

FIGURE A.17: Simulation plot of experiment T-6.

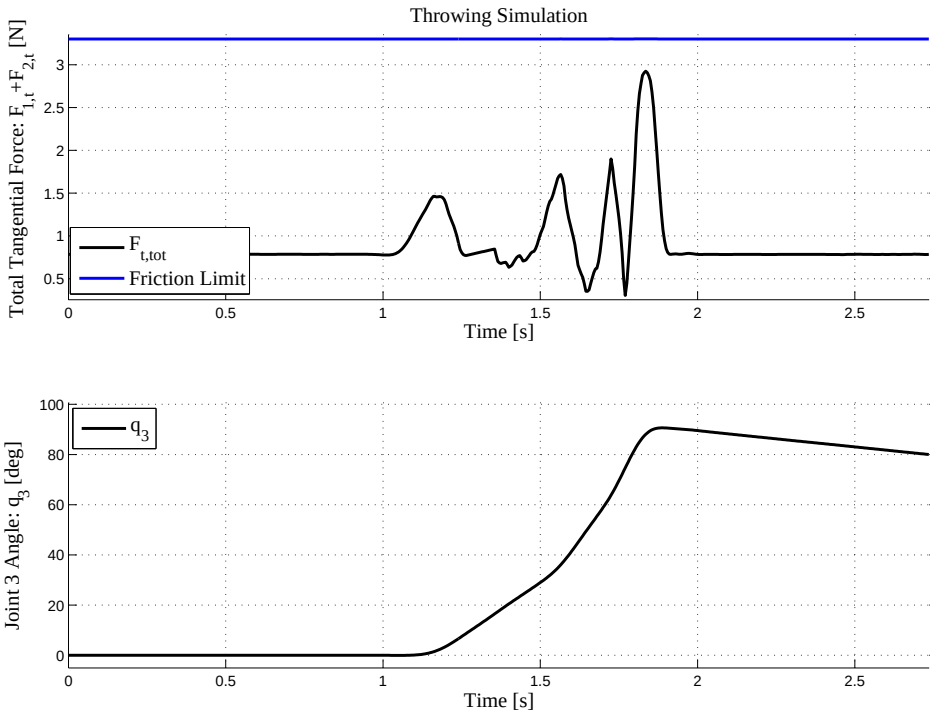

FIGURE A.18: Simulation plot of experiment T-7.

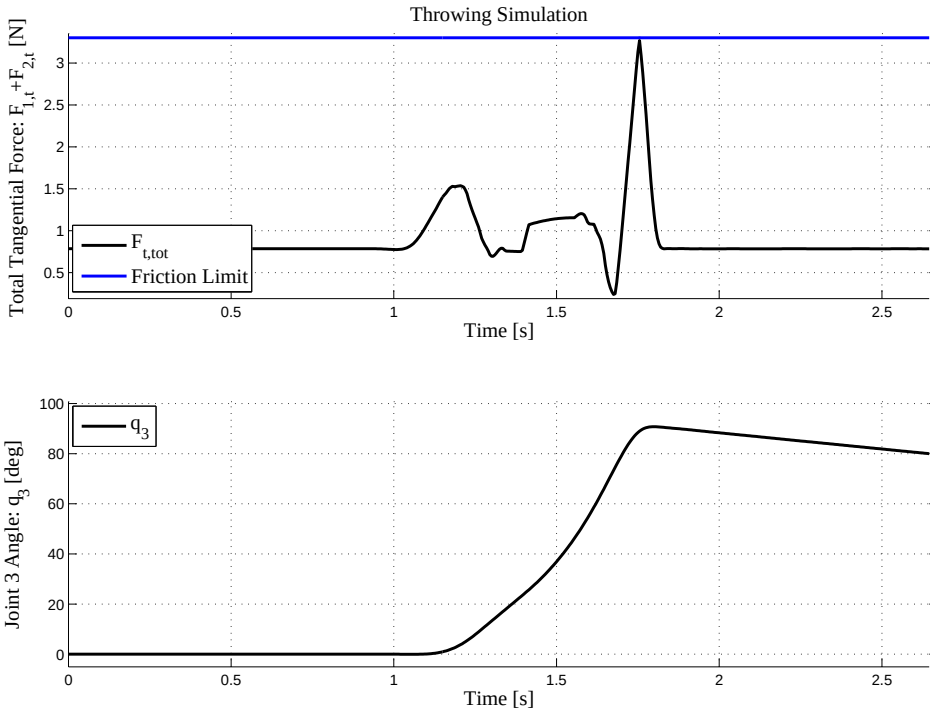

FIGURE A.19: Simulation plot of experiment T-8.

Appendix B

Attached Files

In addition to the thesis in PDF version in the root directory, there are three additional folders:

MATLAB:
All MATLAB files necessary for running simulations and animations. Also the measurement processing was done using MATLAB, so the scripts and raw data can be found within that folder.

Literature:
Relevant literature, most of which appear in the bibliography.

Experimental:
Videos from the experimental motions, RAPID code and pictures.

Bibliography

ABB (2014a). Irb 140 industrial robot. http://search.abb.com/library/Download.aspx?DocumentID=PR10031EN_R14&LanguageCode=en&DocumentPartId=&Action=Launch.

ABB (2014b). Robotstudio 5 - industrial software products. http://www05.abb.com/global/scot/scot241.nsf/veritydisplay/b755e615bec21b52c1257c32004fa70f/$file/PR10296EN_R3.pdf.

Barbagli, F., Frisoli, A., Salisbury, K., and Bergamasco, M. (2004). Simulating human fingers: a soft finger proxy model and algorithm. In *Haptic Interfaces for Virtual Environment and Teleoperator Systems, 2004. HAPTICS'04. Proceedings. 12th International Symposium on*, pages 9–17. IEEE.

Bicchi, A. (1994). On the problem of decomposing grasp and manipulation forces in multiple whole-limb manipulation. *Robotics and Autonomous Systems*, 13(2):127–147.

Bicchi, A. and Kumar, V. (2000). Robotic grasping and contact: A review. In *Robotics and Automation, 2000. Proceedings. ICRA'00. IEEE International Conference on*, volume 1, pages 348–353. IEEE.

Chasles, M. (1830). Note sur les propriétés génerales du système de deux corps semblables entr'eux et placés d'une manière quelconque dans l'espace; et sur le déplacement fini ou infiniment petit d'un corps solide libre [a note on the general properties of a system of two similar bodies arbitrarily positioned in space; and on the finite or infinitely small displacement of an unconstrained solid body]. *Bulletin des Sciences Mathématiques, Férussac*, 14:321–26.

Ciocarlie, M., Lackner, C., and Allen, P. K. (2007). Soft finger model with adaptive contact geometry for grasping and manipulation tasks. In *World Haptics 2007: Second Joint EuroHaptics Conference and Symposium on Haptic Interfaces for*

Virtual Environment and Teleoperator Systems: 22-24 March, 2007, Tsukuba, Japan, pages 219–224. IEEE.

Cline, M. B. (2002). *Rigid body simulation with contact and constraints*. PhD thesis, Citeseer.

De Wit, C. C., Olsson, H., Astrom, K. J., and Lischinsky, P. (1995). A new model for control of systems with friction. *Automatic Control, IEEE Transactions on*, 40(3):419–425.

Egeland, O. and Gravdahl, J. T. (2002). *Modeling and simulation for automatic control*, volume 76. Marine Cybernetics Trondheim, Norway.

Featherstone, R. (2008). *Rigid body dynamics algorithms*, volume 49. Springer New York.

FUTEK Advanced Sensor Technology, Inc. (2014). Lsb200 specification sheet. http://www.futek.com/files/pdf/Product%20Drawings/lsb200.pdf.

Hertz, H. (1882). On the contact of rigid elastic solids and on hardness, chapter 6: Assorted papers by h. hertz.

Howard, W. S. and Kumar, V. (1996). On the stability of grasped objects. *Robotics and Automation, IEEE Transactions on*, 12(6):904–917.

Howe, R. D. and Cutkosky, M. R. (1996). Practical force-motion models for sliding manipulation. *The International Journal of Robotics Research*, 15(6):557–572.

Howe, R. D., Kao, I., and Cutkosky, M. R. (1988). The sliding of robot fingers under combined torsion and shear loading. In *Robotics and Automation, 1988. Proceedings., 1988 IEEE International Conference on*, pages 103–105. IEEE.

Lanczos, C. (1970). *The variational principles of mechanics*, volume 4. Courier Dover Publications.

Lennart, L. (1999). System identification: theory for the user.

Li, Y. and Kao, I. (2001). A review of modeling of soft-contact fingers and stiffness control for dextrous manipulation in robotics. In *Robotics and Automation, 2001. Proceedings 2001 ICRA. IEEE International Conference on*, volume 3, pages 3055–3060. IEEE.

Mason, M. T. and Salisbury Jr, J. K. (1985). *Robot hands and the mechanics of manipulation*. MIT press.

Murray, R. M., Li, Z., Sastry, S. S., and Sastry, S. S. (1994). *A mathematical introduction to robotic manipulation*. CRC press.

National Instruments Corp. (2013). Benefits of programming graphically in ni labview. http://www.ni.com/white-paper/14556/en/pdf.

Robertson, P. (2013). B-spline approximations in an optimization framework. Technical report, Norwegian University of Science and Technology, Norway.

SCHUNK GmbH and Co. KG (2014). Universal gripper - data sheet. http://www.schunk.com/schunk_files/attachments/PG_70_EN.pdf.

Siciliano, B. and Khatib, O. (2008). *Springer handbook of robotics*. Springer.

Song, X., Liu, H., Bimbo, J., Althoefer, K., and Seneviratne, L. D. (2012). A novel dynamic slip prediction and compensation approach based on haptic surface exploration. In *Intelligent Robots and Systems (IROS), 2012 IEEE/RSJ International Conference on*, pages 4511–4516. IEEE.

Spong, M. W., Hutchinson, S., and Vidyasagar, M. (2006). *Robot modeling and control*. John Wiley & Sons New York.

Suárez, R., Cornella, J., and Garzón, M. R. (2006). *Grasp quality measures*. Institut d'Organització i Control de Sistemes Industrials.

The MathWorks, Inc. (2012). Matlab - the language of technical computing. http://www.mathworks.se/products/datasheets/pdf/matlab.pdf.

Wang, J., Ge, S., and Lee, T. (2001). Adaptive friction compensation for servo mechanisms. In *Adaptive control of nonsmooth dynamic systems*, pages 211–248. Springer.

Wright, S. and Nocedal, J. (1999). *Numerical optimization*, volume 2. Springer New York.

Xydas, N. and Kao, I. (1999). Modeling of contact mechanics and friction limit surfaces for soft fingers in robotics, with experimental results. *The International Journal of Robotics Research*, 18(9):941–950.